

國立交通大學
顯示科技研究所
碩士論文

高頻譜效率之正交分頻多工技術
應用於倍頻光載微波信號系統

High Spectral Efficiency OFDM Generation
for Radio-over-fiber System with Frequency
Multiplication

研 究 生：江 文 智

指 導 教 授：陳 智 弘 老 師

中 華 民 國 九 十 七 年 六 月

高頻譜效率之正交分頻多工技術
應用於倍頻光載微波信號系統
High Spectral Efficiency OFDM Generation
for Radio-over-fiber System with Frequency
Multiplication

研究生：江文智

Student : Wen-Jr Jiang

指導教授：陳智弘 博士

Advisor : Dr. Jyehong Chen



A Thesis

Submitted in Partial Fulfillment of the Requirements
For the Degree of Master in
Department of Photonics and Display Institute
College of Electrical Engineering and Computer Science
National Chiao-Tung University
HsinChu, Taiwan 300, R.O.C.

中華民國九十七年六月

Acknowledgements

在碩士班這兩年，首先感謝我的指導老師 陳智弘教授，提供良好的實驗環境以及無私的指導與照顧，讓我在碩士生涯中成長許多。實驗方面特別感謝林俊廷學長教導我許多實驗方法以及報告技巧，無私的指教與修正了我許多理論觀念，如果沒有學長如此的耐心指導下這篇論文無法如此順利的誕生，另外感謝施伯宗學長，彭鵬群學長提供我許多實驗技巧，還有林玉明學長，在程式方面提供了我不少的幫助。

接下來要謝謝實驗室的伙伴：非常感謝大鵬在實驗上的幫忙，感謝已經畢業的曹正、小彭及教練學長們，讓我碩一生活不孤單，另外謝謝小高、小P及易成陪伴我一起走過碩士班的生涯，還有學弟妹們，而咨、士愷、昱宏、漢昇、星宇在我實驗忙碌時，熱心地幫忙處理瑣事。還有謝謝高中到研究所的同學朋友們，你們的加油與鼓勵喔。

最後要感謝我的家人，媽媽的支持賦予我神奇的力量，爸爸的擔心，親戚的加油及照顧，因為你們我才能勇敢地克服困難，完成碩士學位。

帶著歡笑與淚水編織而成的回憶，邁向下個新奇的旅程，再會了交大。

江文智 于 風城 交大 民國九十七年六月


高頻譜效率之正交分頻多工技術 應用於倍頻光纖擷取系統

研究生: 江文智

指導教授: 陳智弘 博士

國立交通大學 電機資訊學院
顯示科技研究所

摘要



本篇論文提出一種新型的光調變技術，此種調變技術可以傳輸向量訊號並具有倍頻效果。利用單一驅動的光調變器產生載子抑制調變，驅動信號為 10-GHz 的正弦信號組合在 5-GHz 的 1.25-Gb/s 的開關鍵控，二相移相鍵控或四相移相鍵控信號，在光偵測器接受後，產生在 15-GHz 的倍頻微波信號。傳輸五十公里的單一模態光纖後，三種不同的信號靈敏度下降小於 0.2dB，四相移相鍵控較開關鍵控擁有兩倍的頻譜效益而且將近提升 2dB 的靈敏度。並且我們展示正交分頻多工調變的下傳信號與波段再利用得到的上傳信號，系統的上傳信號為 5-Gb/s 的 16QAM 正交分頻多工調變信號與透過反射半導體光放大器傳送 1.25-Gb/s 的 OOK 下傳信號。

High Spectrum Efficiency OFDM Generation for Radio-over-fiber System with Frequency Multiplication

Student: Wen-Jr Jiang

Advisor: Dr. Jyehong Chen

Department of Photonics and Display Institute,
National Chiao Tung University

ABSTRACT

This investigation presents a novel modulation approach for generating optical vector signals using frequency multiplication based on double sideband with carrier suppression. A single-electrode Mach-Zehnder modulator (MZM) is biased at null point with a driving signal consists of a 10-GHz sinusoidal signal and a 5-GHz sinusoidal signal modulated with 1.25-Gb/s on-off keying (OOK), 1.25-Gb/s binary phase shift keying (BPSK) data or 625-MSym/s quadruple phase shift keying (QPSK) data. After square-law photo detection, 1.25-Gb/s RF signal at a sum frequency of 15 GHz is generated. After transmission over 50-km single mode fiber (SMF), the power penalty of all three modulation formats is under 0.2 dB. QPSK format has twice the spectral efficiency and approximately 2 dB better receiving sensitivity than OOK format. And we also demonstrate OFDM signal with wavelength reuse for uplink signal. The 5-Gb/s 16QAM OFDM signal for ROF downstream link and 1.25-Gb/s OOK signal via RSOA for upstream link are demonstrated.

CONTENTS

Acknowledgements.....	i
Chinese Abstract.....	ii
English Abstract.....	iii
Contents.....	iv
List of Figures.....	vi
List of Tables.....	x
Chapter 1 Introduction.....	1
1.1 Review of Radio-over-fiber system	1
1.2 Basic modulation schemes	2
1.3 Motivation	4
Chapter 2 The Concept of New Optical Modulation System.....	5
2.1 Preface	5
2.2 Mach-Zehnder Modulator (MZM).....	5
2.3 Single-drive Mach-Zehnder modulator.....	6
2.4 The architecture of ROF system.....	6
2.4.1 Optical transmitter.....	6
2.4.2 Optical signal generations based on LiNbO ₃ MZM.....	7
2.4.3 Communication channel.....	9
2.4.4 Demodulation of optical millimeter-wave signal.....	10
2.5 The new proposed model of optical modulation system	12
Chapter 3 The theoretical calculations of Proposed system	15
3.1 Introduce MZM	15
3.2 Theoretical calculation of single drive MZM.....	18
3.2.1 Bias at maximum transmission point.....	18
3.2.2 Bias at quadrature point	19

3.2.3 Bias at null point	20
3.3 Theoretical calculations and simulation results	20
3.3.1 The generated optical signal.....	20
3.3.2 The generated electrical signal.....	26
3.3.3 Consider dispersion effect.....	30
3.4 The generated optical signal using optical filtering.....	35
3.4.1 Analysis of the generated signal.....	35
3.4.2 The effects of fiber dispersion.....	40
3.5 The optimal optical power ratio condition	45
3.5.1 Signal without optical filtering.....	45
3.5.2 When the LSB2 or LSB1 is filter out.....	48
Chapter 4 Experimental Demonstration of Proposed System.....	50
4.1 preface.....	50
4.2 Experimental results for optical signal without optical filtering ..	51
4.2.1 Experiment setup.....	51
4.3.2 Optimal condition for RF signal	53
4.3.3 Transmission results	60
4.4 Experimental setup for optical signal with optical filtering	62
4.4.1 Experiment setup.....	62
4.4.2 RF signals at sum frequency	63
4.4.4 RF signal at different modulation index.....	69
Chapter 5 Experimental Demonstration of OFDM Signal Generation..	73
5.1 Introduction OFDM generation system	73
5.2 Experimental Concept and Setup	74
5.3 Experimental Results and Discussions	79
Chapter 6 Conclusion	84

LIST OF FIGURES

Figure 1-1 Basic structure of microwave/millimeter-wave wireless system.	2
Figure 1-2 the Radio-over fiber system.	2
Figure 2-1 (a) and (b) are two schemes of transmitter and (c) is duty cycle of subcarrier biased at different points in the transfer function. (LO: local oscillator).....	7
Figure 2-2 Optical microwave/mm-wave modulation scheme by using MZM.....	9
Figure 2-3 The model of communication channel in a RoF system.	10
Figure 2-4 The model of receiver in a ROF system.....	11
Figure 2-5 The model of ROF system.	11
Figure 2-6 Concept of the proposed system. (LD: laser diode, MZM: Mach-Zehnder modulator, SMF: single mode fiber, C: circulator, FBG: fiber bragg grating, RSOA: reflective semiconductor optical amplifier).....	13
Figure 2-7 Simulation of RF performance fading versus SMF transmission length. ..	14
Figure 3-1 The principle diagram of the optical mm-wave generation using balanced MZM.....	18
Figure 3-2 The different order of Bessel functions vs. m.	19
Figure 3-3 The different order of Bessel functions vs. m.	23
Figure 3-4 Illustration of the optical spectrum at the output of the MZM. ($\omega_2 = 6\omega_1$)	25
Figure 3-5 Illustration of the optical spectrum at the output of the MZM.....	26
Figure 3-6 Illustration of the electrical spectrum of generated BTB mm-wave signals using MZM after square-law PD detection. ($\omega_2 = 6\omega_1$).....	28
Figure 3-7 The RF signal power ratio (RFPR, $P_{11,xy}$) as a function of MI.	29
Figure 3-8 shows the numerical and theoretical solution for RF signal fading issue	

after transmission.....	34
Figure 3-9 RF power vs. ω_1	34
Figure 3-10 shows the optical spectrum when the LSB1 is filter out.....	35
Figure 3-11 shows the optical spectrum when the LSB2 is filter out.....	35
Figure 3-12 Illustration of the electrical spectrum of generated BTB mm-wave signals when the LSB1 is filter out. ($\omega_2 = 6\omega_1$).....	39
Figure 3-13 Illustration of the electrical spectrum of generated BTB mm-wave signals when the LSB2 is filter out. ($\omega_2 = 6\omega_1$).....	39
Figure 3-14 shows the RF signal power vs. transmission length when the LSB1 is filter out.....	44
Figure 3-15 shows the RF signal power vs. transmission length when the LSB2 is filter out.....	44
Figure 3-16 shows optical spectrum without fiber grating filter out.....	47
Figure 3-17 the e-filed power for BPSK signal between zero and one.....	47
Figure 3-18 the e-filed power for OOK signal between zero and one.....	47
Figure 3-19 shows optical spectrum when the LSB2 is filter out.....	49
Figure 3-20 shows optical spectrum when the LSB1 is filter out.....	49
Figure 4-1 the optical spectrum for the fiber Bragg grating reflection and transmission.	50
Figure 4-2 shows the experimental setup to receive sum frequency.....	53
Figure 4-3 shows the optical spectrum for BPSK.....	54
Figure 4-4 shows the optical spectrum for OOK.....	55
Figure 4-5 the BER curves for BPSK at 5GHz.....	56
Figure 4-6 the BER curves for OOK at 5GHz.....	56
Figure 4-7 the BER curves for BPSK at 15GHz.....	57
Figure 4-8 the eye diagrams for BPSK at 15GHz.....	57

Figure 4-9 the BER curves for OOK at 15GHz.....	58
Figure 4-10 the eye diagrams for BPSK at 15GHz.....	58
Figure 4-11 measured receiving sensitivity at BER= 10^{-9} of OOK and BPSK signals versus SOPR.....	59
Figure 4-12 the simulation result of MER and Q factor for BPSK, OOK and QPSK.	59
Figure 4-13 the BER curves of OOK, BPSK and QPSK signals.....	60
Figure 4-14 the eye diagrams for BPSK signal w/o filtering.....	60
Figure 4-15 the eye diagrams for OOK signal w/o filtering.....	61
Figure 4-16 the constellations and I/Q eye diagram for QPSK signal.....	61
Figure 4-17 shows the experiment setup w/ optical filtering.....	63
Figure 4-18 the optical spectrum w/ filter out LSB2.	64
Figure 4-19 the simulation result of MER and Q factor for BPSK, OOK and QPSK.	65
Figure 4-20 measured receiving sensitivity at BER= 10^{-9} of OOK and BPSK signals versus SOPR.....	65
Figure 4-21 shows eye diagrams when the LSB2 is filter out.	66
Figure 4-22 the optical spectrum w/ filter out LSB1.	66
Figure 4-23 measured receiving sensitivity at BER= 10^{-9} of OOK and BPSK signals versus SOPR w/ filter out LSB1.....	67
Figure 4-24 shows eye diagrams when the LSB1 is filter out.	67
Figure 4-25 the BER curves of OOK, BPSK and QPSK signals.....	68
Figure 4-26 the constellations and I/Q eye diagram for QPSK signal w/ filter out LSB2.....	68
Figure 4-27 the constellations and I/Q eye diagram for QPSK signal w/ filter out LSB1.....	69
Figure 4-28 shows the optical spectrum for BPSK and OOK RF signal when the LSB2 is filter out.	70

Figure 4-29 shows the optical spectrum for BPSK and OOK RF signal when the LSB1 is filter out.	70
Figure 4-30 shows the BER curves for PSK signal in different MI when the LSB2 is filter out.	71
Figure 4-31 shows the BER curves for OOK signal in different MI when the LSB2 is filter out.	71
Figure 4-32 shows the BER curves for PSK signal in different MI when the LSB1 is filter out.	72
Figure 4-33 shows the BER curves for OOK signal in different MI when the LSB1 is filter out.	72
Figure 5-1 Conceptual diagram of generating optical OFDM-RoF signals.	77
Figure 5-2 Simulation of RF performance fading versus SMF transmission length. ..	77
Figure 5-3 Experimental setup of optical RF OFDM signal generation.....	78
Figure 5-4 Block diagrams of OFDM transmitter (a) and receiver (b).....	78
Figure 5-5 BER versus different OPRs.....	81
Figure 5-6 Optical spectra of RF signals.	81
Figure 5-7 Electrical spectra of OFDM signals.	82
Figure 5-8 Constellations of OFDM signal	83
Figure 5-9 BER curves of the downstream and the upstream signal.	83

LIST OF TABLES

Table 3-1 Measure the RF power without optical filtering.....	30
Table 3-2 Measure the RF power with optical filtering.....	38



Chapter 1

Introduction

1.1 Review of Radio-over-fiber system

There are many applications in the microwave band, such as 3G, WiFi (IEEE 80211 b/g/a), and WiMAX are very important for wireless network. When the growth of customers or increase data rate led to insufficient bandwidth in microwave band for the users. Hence, to develop higher frequency microwave, even millimeter-wave is a important issue in the future. Due to the higher frequency millimeter-wave signal has smaller coverage area. Hence, we need a lot of base stations to deliver millimeter-wave signal as shown in Fig. 1-1. In order to saving the system cost and less equipped base stations (BSs) along with a highly centralized central station (CS) equipped with optical and mm-wave components are very importance. Using fiber transmission medium is one of the best solutions because there are wider bandwidth and much less power loss in fiber. Therefore, Radio-over-fiber (ROF) systems are attracted and more interesting for potential use in the future. Broadband wireless communications are shown in Fig. 1-2. ROF technology is a promising solution to provide multi-gigabits/sec service because of using millimeter wave band, and it has wide converge and mobility. The combination of orthogonal frequency-division multiplexing (OFDM) and radio-over-fiber (ROF) systems (OFDM-ROF) is considerable attention for future gigabit broadband wireless communication [1-5]. The high peak to average power ratio (PAPR) and nonlinear distortion of optical transmitter are the main issues raised by OFDM and ROF systems, respectively.

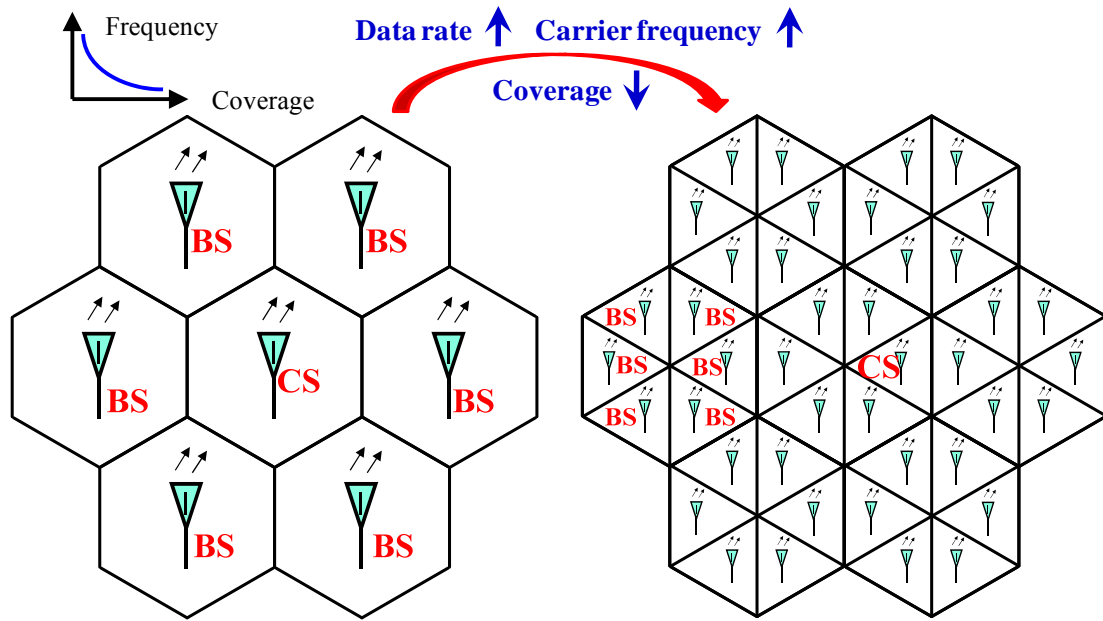


Figure 1-1 Basic structure of microwave/millimeter-wave wireless system.

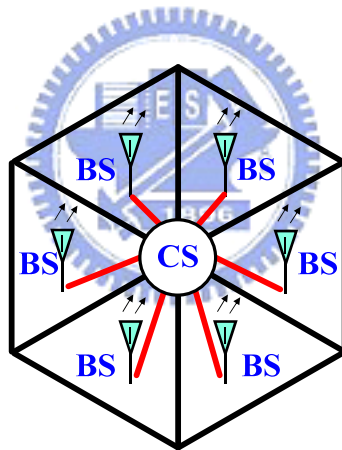


Figure 1-2 the Radio-over fiber system.

1.2 Basic modulation schemes

The optical radio frequency (RF) signal generation using an external Mach-Zehnder modulator (MZM) based on double-sideband (DSB), single-sideband (SSB), and double-sideband with optical carrier suppression (DSBCS) modulation schemes have been demonstrated [1,2,4-8]. Since the optical RF signals are weakly modulated because of the narrow linear region of

MZM, those that have undergone DSB and SSB modulation suffer from inferior sensitivities due to limited optical modulation index (OMI) [4-6,8]. Hence, an optical filter is needed to improve the performance [8]. Furthermore, the DSB signal experiences the problem of performance fading because of fiber dispersion [6]. Among these modulation schemes, DSBCS modulation has been demonstrated to be effective in the millimeter-wave range with excellent spectral efficiency, a low bandwidth requirement for electrical components, and superior receiver sensitivity following transmission over a long distance [6]. However, all of the proposed DSBCS schemes can only support on-off keying (OOK) format, and none can transmit vector modulation formats, such as phase shift keying (PSK), quadrature amplitude modulation (QAM), or OFDM signals, which are of utmost importance for wireless applications.

On the other hand, optical RF signal generations using remote heterodyne detection (RHD) have been also demonstrated [9-10]. The advantage of RHD systems is that the vector signal can be modulated at baseband. Therefore, the bandwidth requirement of the transmitter is low. However, the drawback is that phase noise and wavelength stability of the lasers at both transmitter and receiver should be carefully controlled.

This study proposes a novel method for generating optical direct-detection OFDM-RoF signals using a new DSBCS modulation scheme that can carry vector signals. A frequency multiplication scheme is employed to reduce the requirement of bandwidth of electronic components, which is an important issue at millimeter-wave RoF systems. Benchmarked against the OOK format, the 4-Gb/s 16-QAM OFDM format has the higher spectral efficiency with a sensitivity penalty of under 0.2-dB.

1.3 Motivation

Recently, the wireless communication is focused on millimeter-wave band around 60GHz. The millimeter-wave in this band has some properties for communication such as the short transmission length in the air and broadband bandwidth. It can provide safe communication and transmit high data rate information such as high definition television (HDTV) video signal. However, the electrical components are much more expensive when transmission RF signal is in higher frequency. Hence, the ROF system including frequency multiplication technique and supporting vector signals are required.



Chapter 2

The Concept of New Optical Modulation System

2.1 Preface

There are three parts in optical communication systems : optical transmitter, communication channel and optical receiver. Optical transmitter converts an electrical input signal into the corresponding optical signal and then launches it into the optical fiber serving as a communication channel. The role of an optical receiver is to convert the optical signal back into electrical form and recover the data transmitted through the lightwave system. In this chapter, we will do an introduction about the external Mach-Zehnder Modulator (MZM), constructing a model of new ROF system.

2.2 Mach-Zehnder Modulator (MZM)

Direct modulation and external modulation are two modulations of generated optical signal. When the bit rate of direct modulation signal is above 10 Gb/s, the frequency chirp imposed on signal becomes large enough. Hence, it is difficult to apply direct modulation to generate microwave/mm-wave. However, the bandwidth of signal generated by external modulator can exceed 10 Gb/s. Presently, most RoF systems are using external modulation with Mach-Zehnder modulator (MZM) or Electro-Absorption Modulator (EAM). The most commonly used MZM are based on LiNbO₃ (lithium niobate) technology. According to the applied electric field, there are two types of LiNbO₃ device : x-cut and z-cut. According to number of electrode, there are two types of LiNbO₃ device: dual-drive Mach-Zehnder modulator (DD-MZM) and single-drive Mach-Zehnder modulator (SD-MZM) [6].

2.3 Single-drive Mach-Zehnder modulator

The SD-MZM has two arms and an electrode. The optical phase in each arm can be controlled by changing the voltage applied on the electrode. When the lightwaves are in phase, the modulator is in “on” state. On the other hand, when the lightwaves are in opposite phase, the modulator is in “off” state, and the lightwave cannot propagate by waveguide for output.

2.4 The architecture of ROF system

2.4.1 Optical transmitter

Optical transmitter concludes optical source, optical modulator, RF signal, electrical mixer, electrical amplifier, etc.. Presently, most RoF systems are using laser as light source. The advantages of laser are compact size, high efficiency, good reliability small emissive area compatible with fiber core dimensions, and possibility of direct modulation at relatively high frequency. The modulator is used for converting electrical signal into optical form. Because the external integrated modulator was composed of MZMs, we select MZM as modulator to build the architecture of optical transmitter.

There are two schemes of optical transmitter generated optical signal. One scheme is used two MZM. First MZM generates optical carrier which carried the data. The output optical signal is BB signal. The other MZM generates optical subcarrier which carried the BB signal and then output the RF signal, as shown in Fig. 2-1 (a). The other scheme is used a mixer to get up-converted electrical signal and then send it into a MZM to generate the optical signal, as shown in Fig. 2-1 (b). Fig. 2-1 (c) shows the duty cycle of subcarrier biased at different points in the transfer function.

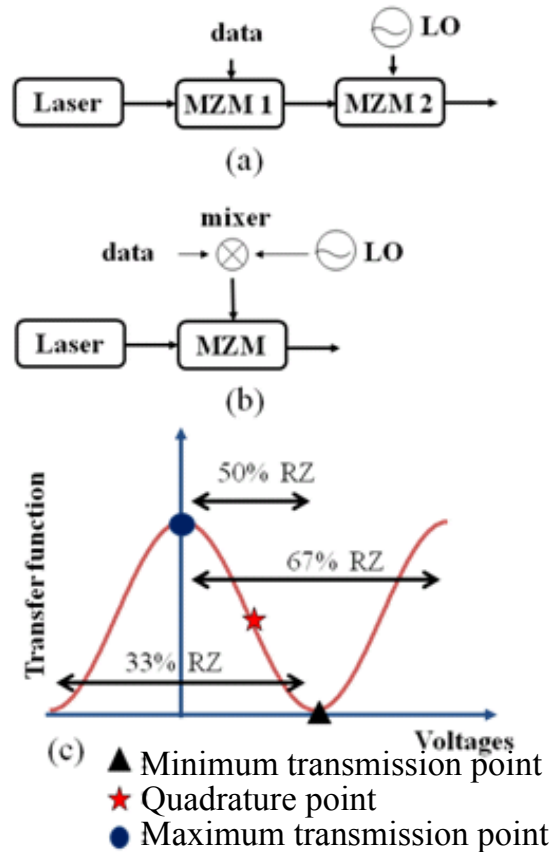


Figure 2-1 (a) and (b) are two schemes of transmitter and (c) is duty cycle of subcarrier biased at different points in the transfer function. (LO: local oscillator)

2.4.2 Optical signal generations based on LiNbO3 MZM

The microwave and mm-wave generations are key techniques in RoF systems. The optical mm-waves using external MZM based on double-sideband (DSB), single-sideband (SSB), and double-sideband with optical carrier suppression (DSBCS) modulation schemes have been demonstrated, as shown in Fig. 2-2. Generated optical signal by setting the bias voltage of MZM at quadrature point, the DSB modulation experiences performance fading problems due to fiber dispersion, resulting in degradation of the receiver sensitivity. When an optical signal is modulated by an electrical

RF signal, fiber chromatic dispersion causes the detected RF signal power to have a periodic fading characteristic. The DSB signals can be transmitted over several kilo-meters. Therefore, the SSB modulation scheme is proposed to overcome fiber dispersion effect. The SSB signal is generated when a phase difference of $\pi/2$ is applied between the two RF electrodes of the DD-MZM biased at quadrature point. Although the SSB modulation can reduce the impairment of fiber dispersion, it suffers worse receiver sensitivity due to limited optical modulation index (OMI). The DSBCS modulation is demonstrated optical mm-wave generation using DSBCS modulation. It has no performance fading problem and it also provides the best receiver sensitivity because the OMI is always equal to one. The other advantage is that the bandwidth requirement of the transmitter components is less than DSB and SSB modulation. However, the drawback of the DSBCS modulation is that it can't support vector signals, such as phase shift keying (PSK), quadrature amplitude modulation (QAM), or OFDM signals, which are of utmost importance in wireless applications.

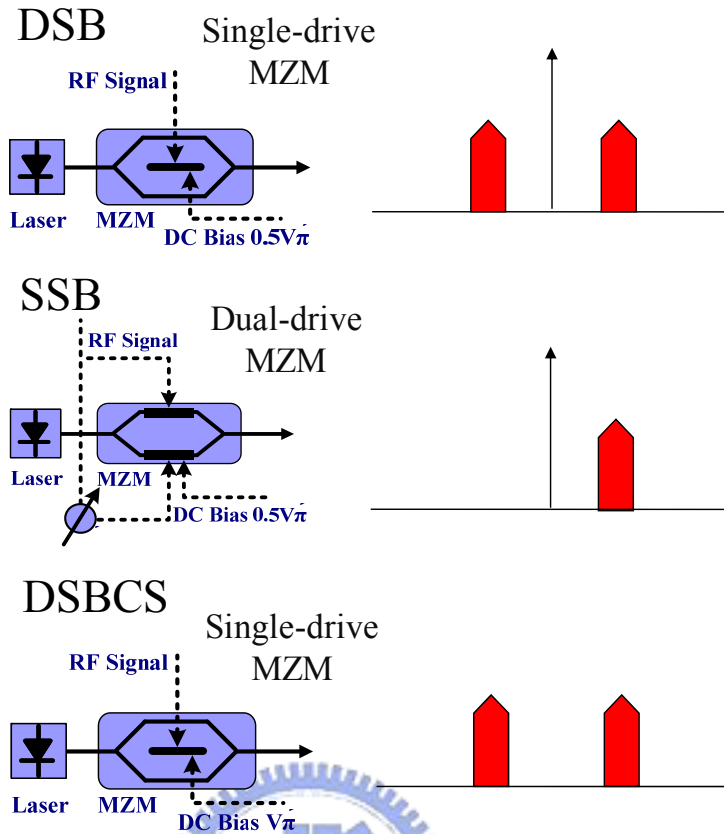


Figure 2-2 Optical microwave/mm-wave modulation scheme by using MZM.

2.4.3 Communication channel

Communication channel concludes fiber, optical amplifier, etc.. Presently, most RoF systems are using single-mode fiber (SMF) or dispersion compensated fiber (DCF) as the transmission medium. When the optical signal transmits in optical fiber, dispersion will be happened. DCF is use to compensate dispersion. The transmission distance of any fiber-optic communication system is eventually limited by fiber losses. For long-haul systems, the loss limitation has traditionally been overcome using regenerator with the optical signal is first converted into an electric current and then regenerated using a transmitter. Such regenerators become quite complex and expensive for WDM lightwave systems. An alternative approach to loss

management makes use of optical amplifiers, which amplify the optical signal directly without requiring its conversion to the electric domain [14]. Presently, most RoF systems are using erbium-doped fiber amplifier (EDFA). An optical band-pass filter (OBPF) is necessary to filter out the ASE noise. The model of communication channel is shown in Fig. 2-3.

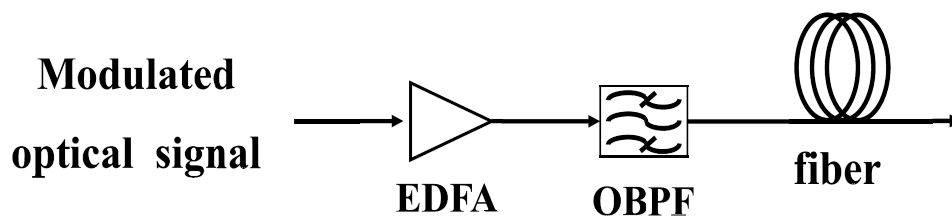


Figure 2-3 The model of communication channel in a RoF system.

2.4.4 Demodulation of optical millimeter-wave signal

Optical receiver concludes photo-detector (PD), demodulator, etc.. PD usually consists of the photo diode and the trans-impedance amplifier (TIA). In the microwave or the mm-wave system, the PIN diode is usually used because it has lower transit time. The function of TIA is to convert photo-current to output voltage.

The BB and RF signals are identical after square-law photo detection. We can get RF signal by using a mixer to drop down RF signal to baseband then filtered by low-pass filter (LPF).

After getting down-converted signal, it will be sent into a signal tester to test the quality, just like bit-error-rate (BER) tester or oscilloscope, as shown in Fig. 2-4.

Combining the transmitter with communication channel and receiver, that is the model of ROF system, as shown in Fig. 2-5. We select the scheme of Fig. 2-3 (b) to become the transmitter in the model of ROF system.

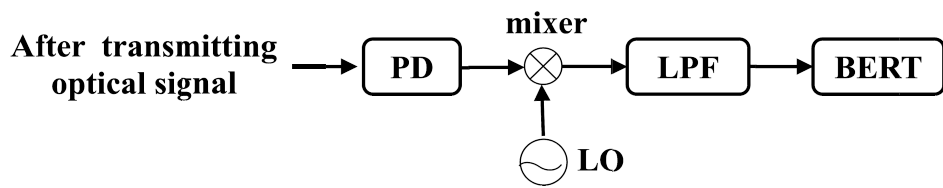


Figure 2-4 The model of receiver in a ROF system.

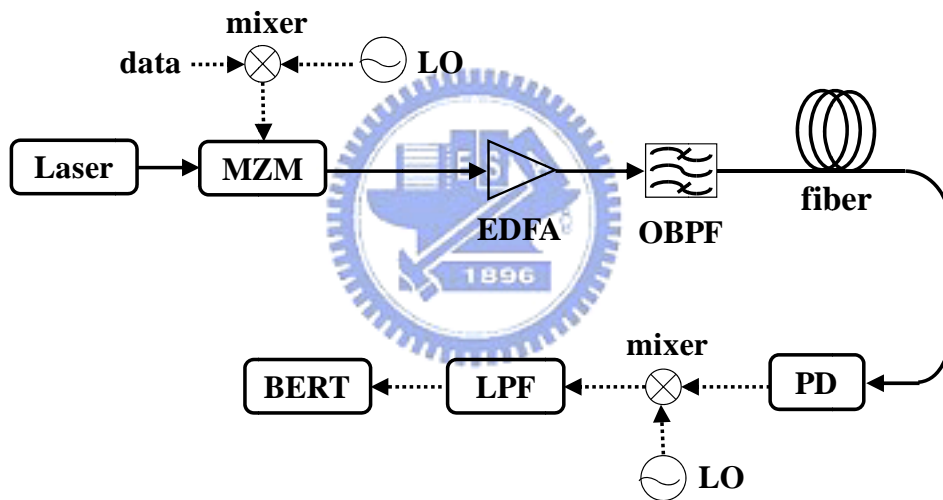


Figure 2-5 The model of ROF system.

2.5 The new proposed model of optical modulation system

In section 2.3.2, there is an introduction of three traditional modulation schemes to generate optical RF signal. In this work, we propose a new modulation approach to generate optical vector signals by frequency multiplication based on a DSBCS scheme and only using a single-electrode MZM. Fig. 2-6 schematically depicts the optical vector signal generation system. The single-electrode MZM driving signals consist of a sinusoidal signal of frequency f_1 modulated with a RF signal and a sinusoidal signal of frequency f_2 , as indicated in insets (a) and (b) of Fig. 2-6, respectively. To realize the DSBCS modulation scheme, the MZM is biased at the null point. Inset (d) in Fig. 2-6 presents the generated optical spectrum that has two upper-wavelength sidebands (USB1, USB2) and two lower-wavelength sidebands (LSB1, LSB2) with carrier suppression.

At the base station, the LSB2 subcarrier is filtered out for the upstream data link (inset (f)), and the rest of the signal is sent to local users. After square-law photo detection, the cross term of USB2 and USB1 generates the RF signal at the difference frequency (f_2-f_1). Concurrently, the cross term of LSB1 and USB2 yields the RF signal at the sum frequency (f_2+f_1). Here we only consider the RF signal at the sum frequency and a frequency multiplication of optical RF signal can be achieved by proper choosing the frequencies of vector signal and sinusoidal signal. The filtering out of LSB2 subcarrier not only provides an upstream light source but also eliminates performance fading. As presented in Fig. 2-7, a two-tone RF signal at frequencies of 5 GHz and 10 GHz is used to simulate the performance fading. After square-law photo detection, the generated RF signals at difference and

sum frequencies of 5 GHz and 15 GHz suffer performance fading before filtering. If an optical filter is utilized to remove anyone of the four optical subcarriers, the fading of both 5-GHz and 15-GHz RF signals can be readily eliminated. Notably, a frequency multiplication (1.5 times after square-law photo detection) scheme is adopted to reduce the cost of the electronic components, especially for RF signals in the millimeter-wave range.

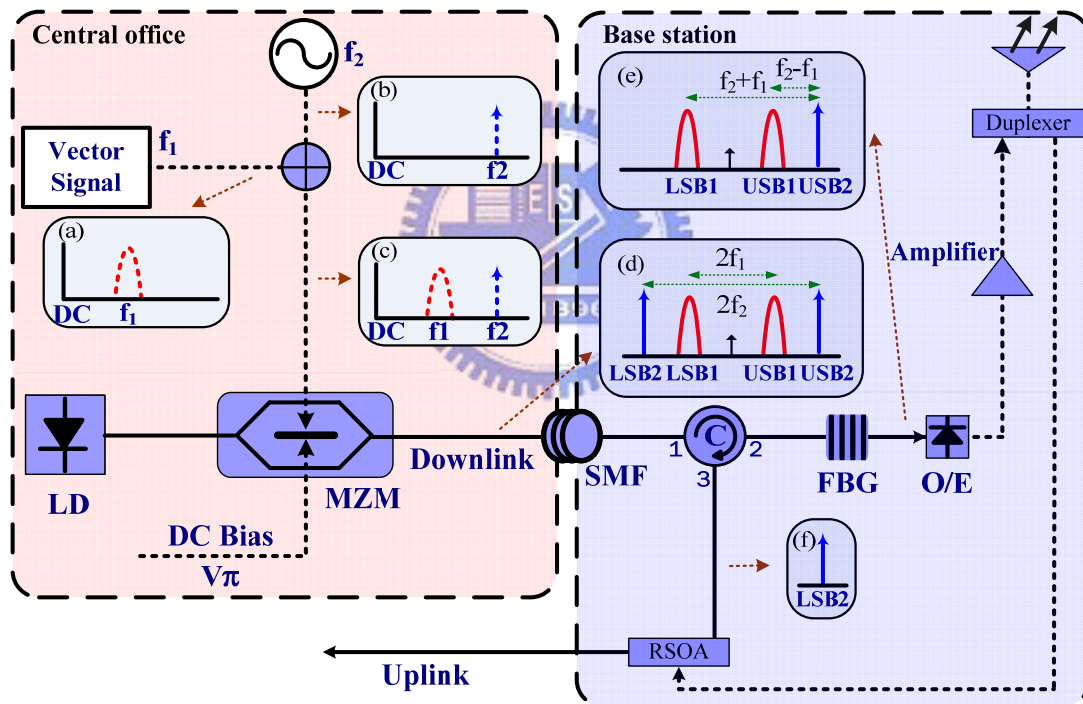


Figure 2-6 Concept of the proposed system. (LD: laser diode, MZM: Mach-Zehnder modulator, SMF: single mode fiber, C: circulator, FBG: fiber bragg grating, RSOA: reflective semiconductor optical amplifier)

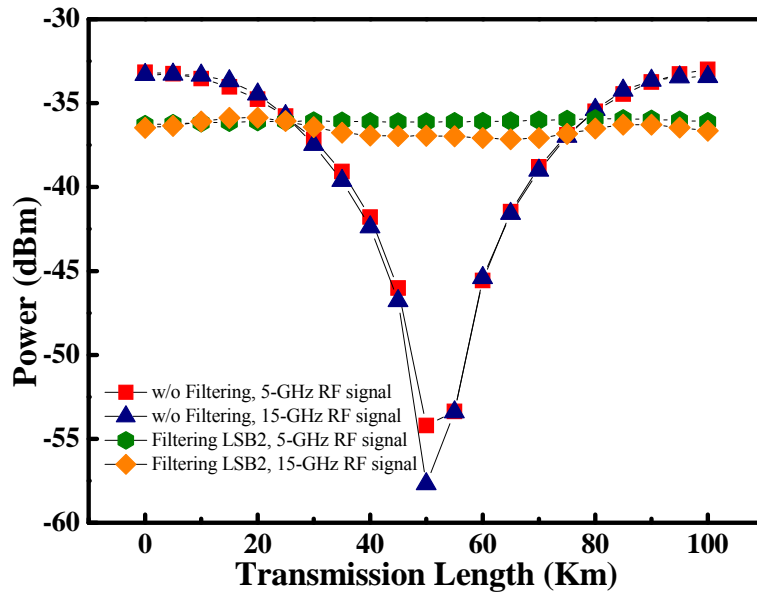


Figure 2-7 Simulation of RF performance fading versus SMF transmission length.



Chapter 3

The theoretical calculations of proposed system

3.1 Introduce MZM

For MZM with configuration as Fig. 3-1, the output E-field for upper arm is

$$E_U = E_0 \cdot a \cdot e^{j\Delta\phi_1} \quad (1)$$

$$\Delta\phi_1 \triangleq \frac{v_1}{v_\pi} \cdot \pi \quad (2)$$

$\Delta\phi_1$ is the optical carrier phase difference that is induced by v_1 , where a is the power splitting ratio.

The output E-field for upper arm is

$$E_L = E_0 \cdot \sqrt{1 - a^2} \cdot e^{j\Delta\phi_2} \quad (3)$$

$\Delta\phi_2$ is the optical carrier phase difference that is induced by v_2

$$\Delta\phi_2 \triangleq \frac{v_2}{v_\pi} \cdot \pi \quad (4)$$

The output E-field for MZM is

$$E_T = E_0 \cdot \{a \cdot b \cdot e^{j\Delta\phi_1} + \sqrt{1 - a^2} \cdot \sqrt{1 - b^2} \cdot e^{j\Delta\phi_2}\} \quad (5)$$

where a and b are the power splitting ratios of the first and second Y-splitters in MZM, respectively. The power splitting ratio of two arms of a balanced MZM is 0.5. The electrical field at the output of the MZM is given by

$$E_T = \frac{1}{2} \cdot E_0 \cdot \{e^{j\Delta\phi_1} + e^{j\Delta\phi_2}\} \quad (6)$$

$$E_T = E_0 \cdot \cos\left(\frac{\Delta\phi_1 - \Delta\phi_2}{2}\right) \cdot \exp\left(j \frac{\Delta\phi_1 + \Delta\phi_2}{2}\right) \quad (7)$$

For single electro x-cut MZM. The electrical field at the output is given by

$$E_{OUT} = E_0 \cdot \cos\left(\frac{\Delta\phi - (-\Delta\phi)}{2}\right) \cdot \exp\left(j \frac{\Delta\phi + (-\Delta\phi)}{2}\right) \quad (8)$$

Add time component, the electrical field is

$$E_{OUT} = E_0 \cdot \cos(\Delta\phi) \cdot \cos(\omega_0 t) \quad (9)$$

where E_0 and ω_c denote the amplitude and angular frequency of the input optical carrier, respectively; $V(t)$ is the applied driving voltage, and $\Delta\phi$ is the optical carrier phase difference that is induced by $V(t)$ between the two arms of the MZM. The loss of MZM is neglected. $V(t)$ consisting of an electrical sinusoidal signal and a dc biased voltage can be written as,

$$V(t) = V_{bias} + V_m \cos(\omega t) \quad (10)$$

where V_{bias} is the dc biased voltage, V_m and ω_{RF} are the amplitude and the angular frequency of the electrical driving signal, respectively. The optical carrier phase difference induced by $V(t)$ is given by

$$\Delta\phi = \frac{V(t)}{2V_\pi} = \frac{V_{bias} + V_m \cos(\omega t)}{V_\pi} \cdot \frac{\pi}{2} \quad (11)$$

Eq. (10) can be written as:

$$\begin{aligned} E_{OUT} &= E_0 \cdot \cos \left[\frac{V_{bias} + V_m \cos(\omega t)}{V_\pi} \cdot \frac{\pi}{2} \right] \cdot \cos(\omega_0 t) \\ &= E_0 \cdot \cos [b + m \cdot \cos(\omega_{RF} t)] \cdot \cos(\omega_0 t) \\ &= E_0 \cdot \cos(\omega_0 t) \cdot \{ \cos(b) \cdot \cos[m \cdot \cos(\omega_{RF} t)] \\ &\quad - \sin(b) \cdot \sin[m \cdot \cos(\omega_{RF} t)] \} \end{aligned} \quad (12)$$

where $b \triangleq \frac{V_{bias}}{2V_\pi} \pi$ is a constant phase shift that is induced by the dc biased

voltage, and $m \triangleq \frac{V_m}{2V_\pi} \pi$ is the phase modulation index.

$$\begin{cases} \cos(x \sin \theta) = J_0(x) + 2 \sum_{n=1}^{\infty} J_{2n}(x) \cos(2n\theta) \\ \sin(x \sin \theta) = 2 \sum_{n=1}^{\infty} J_{2n-1}(x) \sin[(2n-1)\theta] \end{cases}$$

$$\begin{cases} \cos(x \cos \theta) = J_0(x) + 2 \sum_{n=1}^{\infty} (-1)^n J_{2n}(x) \cos(2n\theta) \\ \sin(x \cos \theta) = 2 \sum_{n=1}^{\infty} (-1)^n J_{2n-1}(x) \cos[(2n-1)\theta] \end{cases} \quad (13)$$

Expanding Eq. (12) using Bessel functions, as detailed in Eq. (13). The electrical field at the output of the MZM can be written as:

$$\begin{aligned} E_{\text{OUT}} = E_0 \cdot \cos(\omega_0 t) \cdot \\ \{ \cos(b) \cdot [J_0(m) + 2 \cdot \sum_{i=1}^{\infty} (-1)^i \cdot J_{2i}(m) \cdot \cos(2i\omega_{RF}t)] \\ - \sin(b) \cdot [2 \cdot \sum_{i=1}^{\infty} (-1)^i \cdot J_{2i-1}(m) \cdot \cos[(2i-1)\omega_{RF}t]] \} \end{aligned} \quad (14)$$

where J_n is the Bessel function of the first kind of order n . the electrical field of the mm-wave signal can be written as

$$\begin{aligned} E_{\text{OUT}} = E_0 \cdot \cos(b) \cdot J_0(m) \cdot \cos(\omega_0 t) \\ + E_0 \cdot \cos(b) \cdot \sum_{i=1}^{\infty} J_{2i}(m) \cdot \cos[(\omega_0 - 2i\omega_{RF})t + n\pi] \\ + E_0 \cdot \cos(b) \cdot \sum_{i=1}^{\infty} J_{2i}(m) \cdot \cos[(\omega_0 + 2i\omega_{RF})t + n\pi] \\ - E_0 \cdot \sin(b) \cdot \sum_{i=1}^{\infty} J_{2i-1}(m) \cdot \cos[\omega_0 - (2i-1)\omega_{RF}t + n\pi] \\ - E_0 \cdot \sin(b) \cdot \sum_{i=1}^{\infty} J_{2i-1}(m) \cdot \cos[\omega_0 + (2i-1)\omega_{RF}t + n\pi] \end{aligned} \quad (15)$$

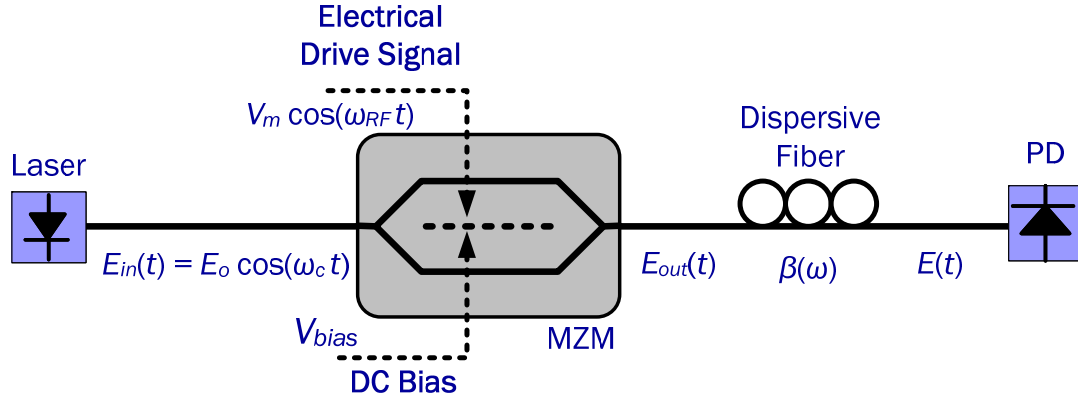


Figure 3-1 The principle diagram of the optical mm-wave generation using balanced MZM.

3.2 Theoretical calculation of single drive MZM

3.2.1 Bias at maximum transmission point

When the MZM is biased at the maximum transmission point, the bias voltage is set at $V_{bias} = 0$, and $\cos b = 1$ and $\sin b = 0$. Consequently, the electrical field of the mm-wave signal can be written as

$$\begin{aligned}
 E_{OUT}(t) &= E_0 \cdot J_0(m) \cdot \cos(\omega_0 t) \\
 &+ E_0 \cdot \sum_{n=1}^{\infty} J_{2n}(m) \cdot \cos[(\omega_0 - 2n\omega_{RF})t + n\pi] \\
 &+ E_0 \cdot \sum_{n=1}^{\infty} J_{2n}(m) \cdot \cos[(\omega_0 + 2n\omega_{RF})t + n\pi]
 \end{aligned} \tag{16}$$

The amplitudes of the generated optical sidebands are proportional to those of the corresponding Bessel functions associated with the phase modulation index m . With the amplitude of the electrical driving signal V_m equal to V_π , the

maximum m is $\frac{\pi}{2}$. As $0 < m < \frac{\pi}{2}$, the Bessel function J_n for $n \geq 1$ decreases and increases with the order of Bessel function and m , respectively, as shown in Figure 3-2. $J_1\left(\frac{\pi}{2}\right)$, $J_2\left(\frac{\pi}{2}\right)$, $J_3\left(\frac{\pi}{2}\right)$, and $J_4\left(\frac{\pi}{2}\right)$ are 0.5668, 0.2497, 0.069, and 0.014, respectively. Therefore, the optical sidebands with the Bessel function higher than $J_3(m)$ can be ignored, and Eq. (14) can be further simplified to

$$\begin{aligned}
 E_{OUT} = & E_0 \cdot J_0(m) \cdot \cos(\omega_0 t) \\
 & + E_0 \cdot J_2(m) \cdot \cos[(\omega_0 - 2\omega_{RF})t + \pi] \\
 & + E_0 \cdot J_2(m) \cdot \cos[(\omega_0 + 2\omega_{RF})t + \pi] \\
 & + E_0 \cdot J_4(m) \cdot \cos[(\omega_0 - 4\omega_{RF})t] \\
 & + E_0 \cdot J_4(m) \cdot \cos[(\omega_0 + 4\omega_{RF})t]
 \end{aligned} \tag{17}$$

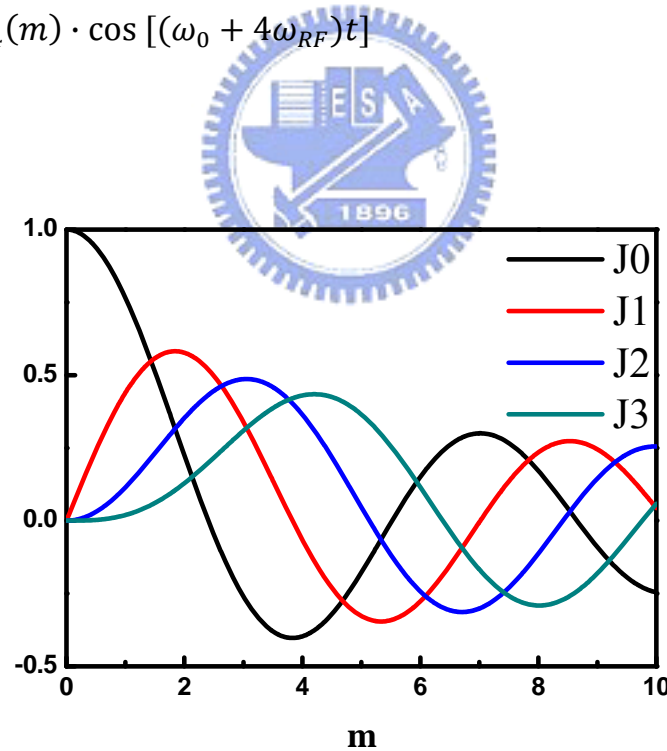


Figure 3-2 The different order of Bessel functions vs. m .

3.2.2 Bias at quadrature point

When the MZM is biased at the quadrature point, the bias voltage is set at

$V_{bias} = \frac{V_{\pi}}{2}$, and $\cos b = \frac{\sqrt{2}}{2}$ and $\sin b = \frac{\sqrt{2}}{2}$. Consequently, the electrical field of the mm-wave signal can be written as

$$\begin{aligned}
E_{OUT} = & \frac{1}{\sqrt{2}} \cdot E_0 \cdot J_0(m) \cdot \cos(\omega_0 t) \\
& + \frac{1}{\sqrt{2}} \cdot E_0 \cdot J_1(m) \cdot \cos [(\omega_0 - \omega_{RF})t] \\
& + \frac{1}{\sqrt{2}} \cdot E_0 \cdot J_1(m) \cdot \cos [(\omega_0 + \omega_{RF})t] \\
& + \frac{1}{\sqrt{2}} \cdot E_0 \cdot J_2(m) \cdot \cos [(\omega_0 - 2\omega_{RF})t + \pi] \\
& + \frac{1}{\sqrt{2}} \cdot E_0 \cdot J_2(m) \cdot \cos [(\omega_0 + 2\omega_{RF})t + \pi] \\
& + \frac{1}{\sqrt{2}} \cdot E_0 \cdot J_3(m) \cdot \cos [(\omega_0 - 3\omega_{RF})t + \pi] \\
& + \frac{1}{\sqrt{2}} \cdot E_0 \cdot J_3(m) \cdot \cos [(\omega_0 + 3\omega_{RF})t + \pi]
\end{aligned} \tag{18}$$

3.2.3 Bias at null point

When the MZM is biased at the null point, the bias voltage is set at $V_{bias} = V_{\pi}$, and $\cos b = 0$ and $\sin b = 1$. Consequently, the electrical field of the mm-wave signal using DSBCS modulation can be written as

$$\begin{aligned}
E_{OUT} = & E_0 \cdot J_1(m) \cdot \cos [(\omega_0 - \omega_{RF})t] \\
& + E_0 \cdot J_1(m) \cdot \cos [(\omega_0 + \omega_{RF})t] \\
& + E_0 \cdot J_3(m) \cdot \cos [(\omega_0 - 3\omega_{RF})t + \pi] \\
& + E_0 \cdot J_3(m) \cdot \cos [(\omega_0 + 3\omega_{RF})t + \pi] \\
& + E_0 \cdot J_5(m) \cdot \cos [(\omega_0 - 5\omega_{RF})t] \\
& + E_0 \cdot J_5(m) \cdot \cos [(\omega_0 + 5\omega_{RF})t]
\end{aligned} \tag{19}$$

3.3 Theoretical calculations and simulation results

3.3.1 The generated optical signal

The theoretical calculations of proposed system, the driving RF signal $V(t)$ consisting of an electrical sinusoidal signal and a dc biased voltage can be written as

$$V(t) = V_{bias} + V_1 \cos \omega_1 t + V_2 \cos \omega_2 t \quad (20)$$

where V_{bias} is the dc biased voltage, V_1, V_2 and ω_1, ω_2 are the amplitude and the angular frequency of the electrical driving signals, respectively. The optical carrier phase difference induced by $V(t)$ is given by

$$E_{OUT} = E_0 \cdot \cos \left[\frac{\pi}{2V_\pi} (V_{bias} + V_1 \cos \omega_1 t + V_2 \cos \omega_2 t) \right]$$

$$E_{OUT} = E_0 \cdot \cos [b + m_1 \cos \omega_1 t + m_2 \cos \omega_2 t] \quad (21)$$

where $b \triangleq \frac{V_{bias}\pi}{2V_\pi}$ is a constant phase shift that is induced by the dc biased voltage, and $m_1 = \frac{V_1\pi}{2V_\pi}, m_2 = \frac{V_2\pi}{2V_\pi}$ is the phase modulation index.

$$E_{OUT} = E_0 \cdot \cos b \cdot \cos(m_1 \cos \omega_1 t + m_2 \cos \omega_2 t)$$

$$- E_0 \cdot \sin b \cdot \sin(m_1 \cos \omega_1 t + m_2 \cos \omega_2 t)$$

$$E_{OUT} = E_0 \cdot \cos b \{ \cos(m_1 \cos \omega_1 t) \cos(m_2 \cos \omega_2 t)$$

$$- \sin(m_1 \cos \omega_1 t) \sin(m_2 \cos \omega_2 t) \}$$

$$- E_0 \cdot \sin b \{ \sin(m_1 \cos \omega_1 t) \cos(m_2 \cos \omega_2 t)$$

$$+ \cos(m_1 \cos \omega_1 t) \sin(m_2 \cos \omega_2 t) \} \quad (22)$$

When the MZM is biased at the null point, the bias voltage is set at $V_{bias} = V_\pi$, and $\cos b = 0$ and $\sin b = 1$. Consequently, the electrical field of the mm-wave signal using DSBCS modulation can be written as

$$E_{OUT} = -E_0 \{ \sin(m_1 \cos \omega_1 t) \cos(m_2 \cos \omega_2 t)$$

$$+ \cos(m_1 \cos \omega_1 t) \sin(m_2 \cos \omega_2 t) \} \quad (23)$$

First, to expand equation $\sin(m_1 \cos \omega_1 t) \cos(m_2 \cos \omega_2 t)$

$$\begin{aligned}
& \sin(m_1 \cos \omega_1 t) \cos(m_2 \cos \omega_2 t) \\
&= \left\{ 2 \sum_{n=1}^{\infty} (-1)^n J_{2n-1}(m_1) \cos[(2n-1)\omega_1 t] \right\} \\
&\quad \cdot \left\{ J_0(m_2) + 2 \sum_{n=1}^{\infty} (-1)^n J_{2n}(m_2) \cos(2n\omega_2 t) \right\} \\
&= \{-2J_1(m_1) \cos(\omega_1 t) + 2J_3(m_1) \cos(3\omega_1 t) - \dots\} \\
&\quad \cdot \{J_0(m_2) - 2J_2(m_2) \cos(2\omega_2 t) + 2J_4(m_2) \cos(4\omega_2 t) - \dots\} \tag{24}
\end{aligned}$$

The optical sidebands with the Bessel function higher than $J_3(m)$ can be ignored. Consequently, the electrical field can be written as

$$\begin{aligned}
& \sin(m_1 \cos \omega_1 t) \cos(m_2 \cos \omega_2 t) \\
&\approx -2J_0(m_2)J_1(m_1) \cos \omega_1 t \\
&\quad + 2J_0(m_2)J_3(m_1) \cos(3\omega_1 t) \\
&\quad + 4J_1(m_1)J_2(m_2) \cdot \frac{1}{2} [\cos(\omega_1 + 2\omega_2)t + \cos(\omega_1 - 2\omega_2)t] \\
&\quad - 4J_2(m_2)J_3(m_1) \cdot \frac{1}{2} [\cos(3\omega_1 + 2\omega_2)t + \cos(3\omega_1 - 2\omega_2)t] \tag{25}
\end{aligned}$$

Add time component $\cos \omega_c t$

$$\begin{aligned}
& \sin(m_1 \cos \omega_1 t) \cos(m_2 \cos \omega_2 t) \cos \omega_c t \\
&= -2J_0(m_2)J_1(m_1) \cos \omega_1 t \cos \omega_c t \\
&\quad + 2J_0(m_2)J_3(m_1) \cos(3\omega_1 t) \cos \omega_c t \\
&\quad + 4J_1(m_1)J_2(m_2) \cdot \frac{1}{2} [\cos(\omega_1 + 2\omega_2)t + \cos(\omega_1 - 2\omega_2)t] \cos \omega_c t \\
&\quad - 4J_2(m_2)J_3(m_1) \cdot \frac{1}{2} [\cos(3\omega_1 + 2\omega_2)t + \cos(3\omega_1 - 2\omega_2)t] \cos \omega_c t \tag{26}
\end{aligned}$$

$J_0(m_2)J_1(m_1)$, $2J_0(m_2)J_3(m_1)$, $4J_1(m_1)J_2(m_2)$, and $4J_2(m_2)J_3(m_1)$ are shown in Figure 3-3. Therefore, the optical sidebands with the Bessel function

$4J_2(m_2)J_3(m_1)$ can be ignored, and Eq. (14) can be further simplified to

$$\begin{aligned}
 & \sin(m_1 \cos \omega_1 t) \cos(m_2 \cos \omega_2 t) \cos \omega_c t \\
 &= -J_0(m_2)J_1(m_1)[\cos(\omega_c + \omega_1)t + \cos(\omega_c - \omega_1)t] \\
 & \quad + J_0(m_2)J_3(m_1)[\cos(\omega_c + 3\omega_1)t + \cos(\omega_c - 3\omega_1)t] \\
 & \quad + J_1(m_1)J_2(m_2)[\cos(\omega_c + \omega_1 + 2\omega_2)t + \cos(\omega_c - \omega_1 - 2\omega_2)t] \\
 & \quad + J_1(m_1)J_2(m_2)[\cos(\omega_c + \omega_1 - 2\omega_2)t + \cos(\omega_c - \omega_1 + 2\omega_2)t]
 \end{aligned} \tag{27}$$

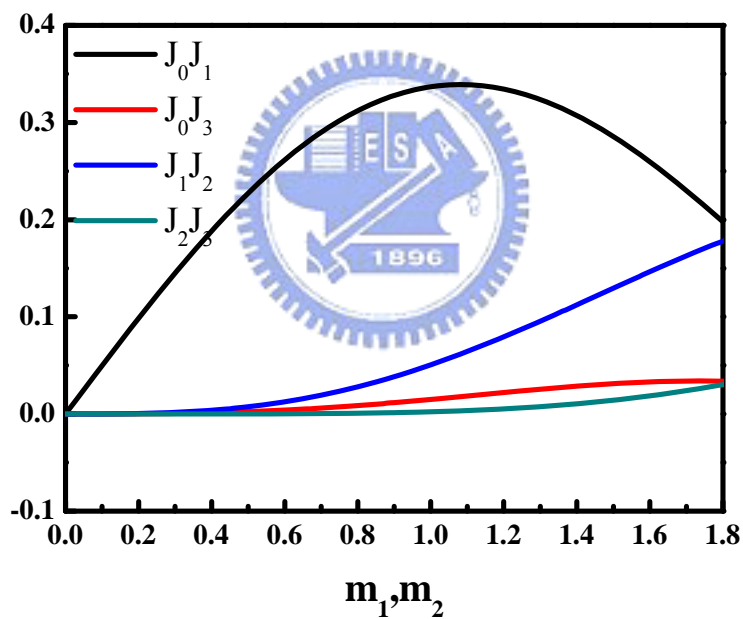


Figure 3-3 The different order of Bessel functions vs. m.

Second: To expand equation $\cos(m_1 \cos \omega_1 t) \sin(m_2 \cos \omega_2 t)$

$$\begin{aligned}
& \cos(m_1 \cos \omega_1 t) \sin(m_2 \cos \omega_2 t) \\
&= \left\{ J_0(m_1) + 2 \sum_{n=1}^{\infty} (-1)^n J_{2n}(m_1) \cos(2n \omega_1 t) \right\} \\
&\quad \cdot \left\{ 2 \sum_{n=1}^{\infty} (-1)^n J_{2n-1}(m_2) \cos[(2n-1) \omega_2 t] \right\} \\
&= \{ J_0(m_1) - 2J_2(m_1) \cos(2\omega_1 t) + 2J_4(m_1) \cos(4\omega_1 t) - \dots \} \\
&\quad \cdot \{ -2J_1(m_2) \cos(\omega_2 t) + 2J_3(m_2) \cos(3\omega_2 t) - \dots \} \\
&\approx -2J_0(m_1)J_1(m_2) \cos \omega_2 t \\
&\quad + 2J_0(m_1)J_3(m_2) \cos(3\omega_2 t) \\
&\quad + 4J_1(m_2)J_2(m_1) \cdot \frac{1}{2} [\cos(\omega_2 + 2\omega_1) t + \cos(\omega_2 - 2\omega_1) t] \\
&\quad - 4J_2(m_1)J_3(m_2) \cdot \frac{1}{2} [\cos(3\omega_2 + 2\omega_1) t + \cos(3\omega_2 - 2\omega_1) t]
\end{aligned} \tag{28}$$

Add time component $\cos \omega_c t$

$$\begin{aligned}
& \cos(m_1 \cos \omega_1 t) \sin(m_2 \cos \omega_2 t) \cos \omega_c t \\
&= -2J_0(m_1)J_1(m_2) \cos \omega_2 t \cos \omega_c t \\
&\quad + 2J_0(m_1)J_3(m_2) \cos(3\omega_2 t) \cos \omega_c t \\
&\quad + 4J_1(m_2)J_2(m_1) \cdot \frac{1}{2} [\cos(\omega_2 + 2\omega_1) t + \cos(\omega_2 - 2\omega_1) t] \cos \omega_c t \\
&\quad - 4J_2(m_1)J_3(m_2) \cdot \frac{1}{2} [\cos(3\omega_2 + 2\omega_1) t + \cos(3\omega_2 - 2\omega_1) t] \cos \omega_c t \\
&= -J_0(m_1)J_1(m_2) [\cos(\omega_c + \omega_2) t + \cos(\omega_c - \omega_2) t] \\
&\quad + J_0(m_1)J_3(m_2) [\cos(\omega_c + 3\omega_2) t + \cos(\omega_c - 3\omega_2) t] \\
&\quad + J_1(m_2)J_2(m_1) [\cos(\omega_c + \omega_2 + 2\omega_1) t + \cos(\omega_c - \omega_2 - 2\omega_1) t] \\
&\quad + J_1(m_2)J_2(m_1) [\cos(\omega_c + \omega_2 - 2\omega_1) t + \cos(\omega_c - \omega_2 + 2\omega_1) t]
\end{aligned} \tag{29}$$

The output electrical field can be rewritten as

$$E_{OUT}(t) = E_0 \cos \omega_c t \{ \sin(m_1 \cos \omega_1 t) \cos(m_2 \cos \omega_2 t) \}$$

$$+ \cos(m_1 \cos \omega_1 t) \sin(m_2 \cos \omega_2 t) \}$$

$$E_{OUT}(t) = E_0 \cdot$$

$$\begin{aligned} & \{ J_0(m_2) J_1(m_1) [\cos(\omega_c + \omega_1)t + \cos(\omega_c - \omega_1)t] \\ & - J_0(m_2) J_3(m_1) [\cos(\omega_c + 3\omega_1)t + \cos(\omega_c - 3\omega_1)t] \\ & - J_1(m_1) J_2(m_2) [\cos(\omega_c + \omega_1 + 2\omega_2)t + \cos(\omega_c - \omega_1 - 2\omega_2)t] \\ & - J_1(m_1) J_2(m_2) [\cos(\omega_c + \omega_1 - 2\omega_2)t + \cos(\omega_c - \omega_1 + 2\omega_2)t] \\ & + J_0(m_1) J_1(m_2) [\cos(\omega_c + \omega_2)t + \cos(\omega_c - \omega_2)t] \\ & - J_0(m_1) J_3(m_2) [\cos(\omega_c + 3\omega_2)t + \cos(\omega_c - 3\omega_2)t] \\ & - J_1(m_2) J_2(m_1) [\cos(\omega_c + \omega_2 + 2\omega_1)t + \cos(\omega_c - \omega_2 - 2\omega_1)t] \\ & - J_1(m_2) J_2(m_1) [\cos(\omega_c + \omega_2 - 2\omega_1)t + \cos(\omega_c - \omega_2 + 2\omega_1)t] \} \end{aligned}$$

(30)

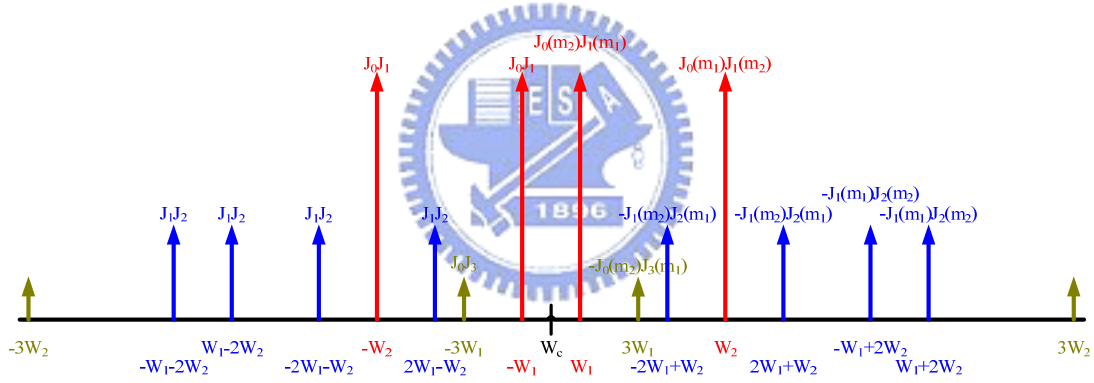


Figure 3-4 Illustration of the optical spectrum at the output of the MZM.

$$(\omega_2 = 6\omega_1)$$

The commercial software, VPI WDM-TransmissionMaker[®] 5.0, is used to simulate numerically the power ratio. Fig. 3-5 shows the optical power ratio (OPR, $P_{10,xy}$) as a function of MI. The $P_{10,xy}$ is defined as

$$P_{10,xy} = \frac{P_{10}}{P_{xy}}$$

(31)

where P_{10} and P_{xy} are the optical powers of the sideband frequency at $\omega_c \pm (1 \cdot \omega_1 + 0 \cdot \omega_2)$ and the sideband frequency at $\omega_c \pm (x \cdot \omega_1 + y \cdot \omega_2)$,

respectively. As MI falls from one to zero, the optical power ratios are improved.

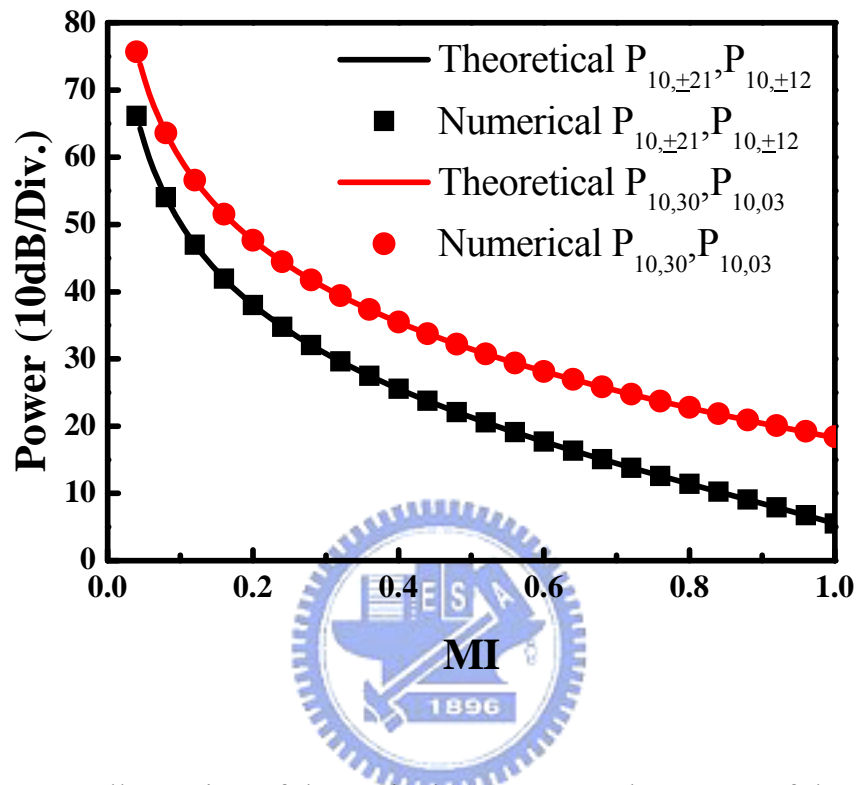


Figure 3-5 Illustration of the optical spectrum at the output of the MZM.

3.3.2 The generated electrical signal

After square-law detection using an ideal PD with responsivity R , the photocurrent can be expressed as

$$i(t) = R \cdot |E(t)|^2 \quad (32)$$

The RF signal is

$$i(t) = RE_0^2 \cdot \{DC$$

$$\begin{aligned}
& + [J_0^2(m_2)J_1^2(m_1) - 2J_0^2(m_2)J_1(m_1)J_3(m_1) + 2J_1^2(m_1)J_2^2(m_2) \\
& - 4J_0(m_1)J_1^2(m_2)J_2(m_1)] \\
& \cdot \cos(2\omega_1 t) \\
& + [2J_0(m_1)J_0(m_2)J_1(m_1)J_1(m_2) - 2J_0(m_2)J_1(m_1)J_1(m_2)J_2(m_1) \\
& - 2J_0(m_1)J_1(m_1)J_1(m_2)J_2(m_2) + 2J_1(m_1)J_1(m_2)J_2(m_1)J_2(m_2)] \\
& + 2J_0(m_1)J_1(m_1)J_2(m_2)J_3(m_2) + 2J_0(m_2)J_1(m_2)J_2(m_1)J_3(m_1)] \\
& \cdot \{\cos[(\omega_2 - \omega_1)t] + \cos[(\omega_2 + \omega_1)t]\} \\
& + [J_0^2(m_1)J_1^2(m_2) - 2J_0^2(m_1)J_1(m_2)J_3(m_2) + 2J_1^2(m_2)J_2^2(m_1) \\
& - 4J_0(m_2)J_1^2(m_1)J_2(m_2)] \\
& \cdot \cos(2\omega_2 t) \\
& + [-2J_0(m_2)J_1(m_1)J_1(m_2)J_2(m_1) - 2J_0(m_1)J_0(m_2)J_1(m_2)J_3(m_1) \\
& + 2J_1(m_1)J_1(m_2)J_2(m_1)J_2(m_2)] \\
& \cdot \{\cos[(\omega_2 - 3\omega_1)t + \cos[(\omega_2 + 3\omega_1)t]]\} \\
& + [-2J_0(m_1)J_1^2(m_2)J_2(m_1) - 2J_0(m_2)J_1^2(m_1)J_2(m_2) \\
& + 2J_0(m_2)J_1(m_1)J_2(m_2)J_3(m_1) + 2J_0(m_1)J_1(m_2)J_2(m_1)J_3(m_2)] \\
& \cdot \cos[(2\omega_2 - 2\omega_1)t] \\
& + [-2J_0^2(m_2)J_1(m_1)J_3(m_1) + 2J_1^2(m_2)J_2^2(m_1)] \\
& \cdot \cos(4\omega_1 t) \\
& + [J_1^2(m_2)J_2^2(m_1) + 2J_0(m_2)J_1(m_1)J_2(m_2)J_3(m_1)] \\
& \cdot \cos[(2\omega_2 - 4\omega_1)t] \\
& + 2J_0(m_2)J_1(m_2)J_2(m_1)J_3(m_1) \\
& \cdot \cos[(\omega_2 - 5\omega_1)t + \text{RF}]
\end{aligned}$$

(33)

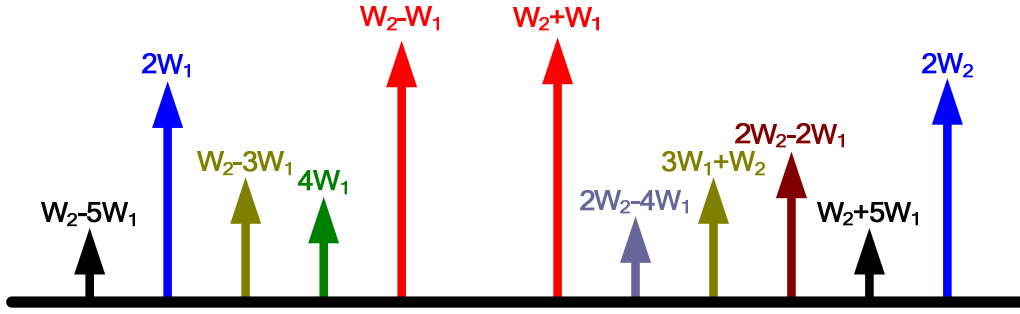


Figure 3-6 Illustration of the electrical spectrum of generated BTB mm-wave signals using MZM after square-law PD detection. ($\omega_2 = 6\omega_1$)

Fig. 3-7 shows the RF signal power ratio (RFPR, $P_{11,xy}$) as a function of MI.

The $P_{11,xy}$ is defined as

$$P_{10,xy} = \frac{P_{11}}{P_{xy}}$$



(34)

where P_{11} and P_{xy} are the RF signal powers of the frequency at $1 \cdot \omega_1 + 1 \cdot \omega_2$ and the frequency at $x \cdot \omega_1 + y \cdot \omega_2$, respectively. The RF signal power at sum and subtract frequencies are the same, so do not consider the $P_{11,-11}$ term.

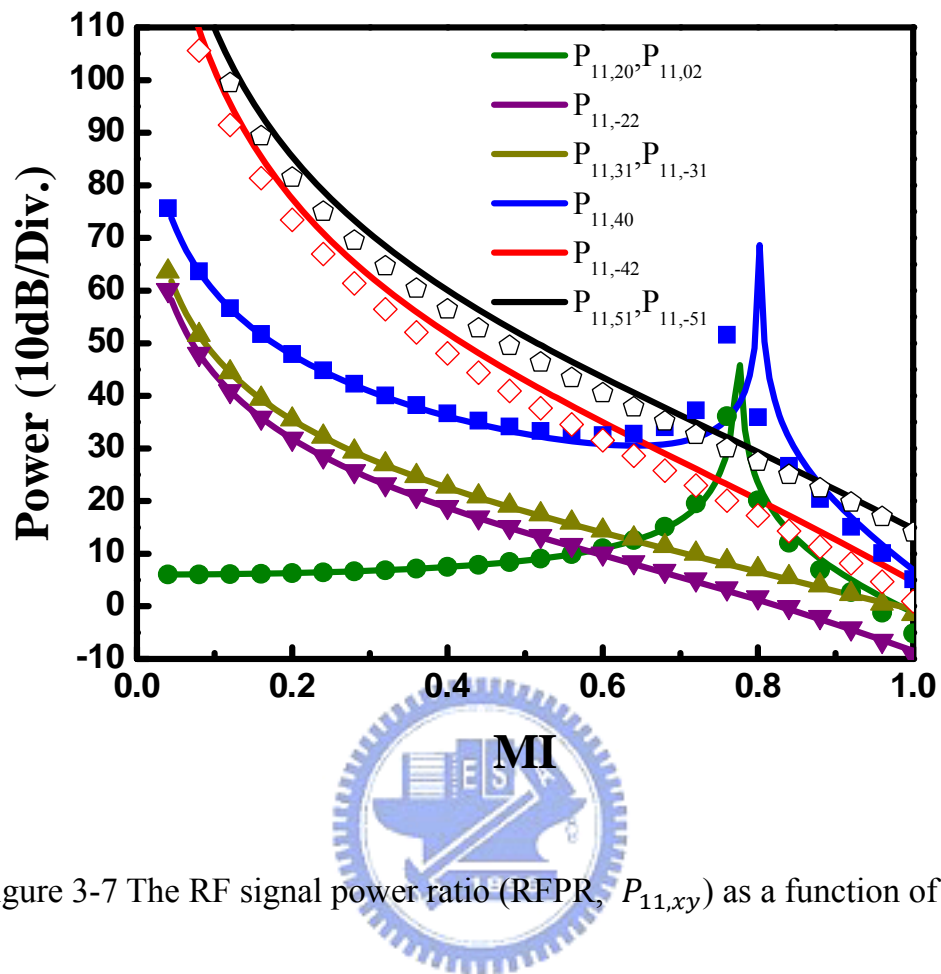


Figure 3-7 The RF signal power ratio (RFPR, $P_{11,xy}$) as a function of MI.

Table 3-1 Measure the RF power without optical filtering

Frequency	Amplitude
$2\omega_1$	$+J_0^2(m_2)J_1^2(m_1) - 2J_0^2(m_2)J_1(m_1)J_3(m_1) + 2J_1^2(m_1)J_2^2(m_2)$ $-4J_0(m_1)J_1^2(m_2)J_2(m_1)$
$\omega_2 - \omega_1, \omega_2 + \omega_1$	$+2J_0(m_1)J_0(m_2)J_1(m_1)J_1(m_2) - 2J_0(m_2)J_1(m_1)J_1(m_2)J_2(m_1)$ $-2J_0(m_1)J_1(m_1)J_1(m_2)J_2(m_2) + 2J_1(m_1)J_1(m_2)J_2(m_1)J_2(m_2)$ $+2J_0(m_1)J_1(m_1)J_2(m_2)J_3(m_2) + 2J_0(m_2)J_1(m_2)J_2(m_1)J_3(m_1)$
$2\omega_2$	$+J_0^2(m_1)J_1^2(m_2) - 2J_0^2(m_1)J_1(m_2)J_3(m_2) + 2J_1^2(m_2)J_2^2(m_1)$ $-4J_0(m_2)J_1^2(m_1)J_2(m_2)$
$\omega_2 - 3\omega_1, \omega_2 + 3\omega_1$	$-2J_0(m_2)J_1(m_1)J_1(m_2)J_2(m_1) - 2J_0(m_1)J_0(m_2)J_1(m_2)J_3(m_1)$ $+2J_1(m_1)J_1(m_2)J_2(m_1)J_2(m_2)$
$2\omega_2 - 2\omega_1$	$-2J_0(m_1)J_1^2(m_2)J_2(m_1) - 2J_0(m_2)J_1^2(m_1)J_2(m_2)$ $+2J_0(m_2)J_1(m_1)J_2(m_2)J_3(m_1) + 2J_0(m_1)J_1(m_2)J_2(m_1)J_3(m_2)$
$4\omega_1$	$-2J_0^2(m_2)J_1(m_1)J_3(m_1) + 2J_1^2(m_2)J_2^2(m_1)$
$2\omega_2 - 4\omega_1$	$+J_1^2(m_2)J_2^2(m_1) + 2J_0(m_2)J_1(m_1)J_2(m_2)J_3(m_1)$
$\omega_2 - 5\omega_1, \omega_2 + 5\omega_1$	$+2J_0(m_2)J_1(m_2)J_2(m_1)J_3(m_1)$

3.3.3 Consider dispersion effect

When optical RF signals are transmitted over a single-mode fiber with dispersion, a phase shift to each optical sideband relative to optical carrier is induced. The propagation constant of the dispersion fiber $\beta(\omega)$ can be expressed as

$$\begin{aligned}\beta(\omega) &= n(\omega) \frac{\omega}{c} \\ &= \beta_0 + \beta_1(\omega - \omega_c) + \frac{1}{2}\beta_2(\omega - \omega_c)^2 + \dots\end{aligned}\quad (35)$$

where $\beta_m = \left. \frac{d^m \beta}{d\omega^m} \right|_{\omega=\omega_c}$ is the derivative of the propagation constant

evaluated at $\omega = \omega_c$. The effect of high order fiber dispersion at 1550-nm band is neglected. For carrier tones with central frequency at $\omega = \omega_c \pm n\omega_{RF}$, we have

$$\beta(\omega_c \pm n\omega_{RF}) \cong \beta_0 \pm n\beta_1(\omega_c)\omega_{RF} + \frac{1}{2}n^2\beta_2(\omega_c)\omega_{RF}^2 \quad (36)$$

and

$$\beta_2(\omega_c) = -\frac{c}{2\pi f_c^2} \cdot D(\omega_c) \quad (37)$$

where c is light speed in free space, D is the chromatic dispersion parameter, and f_c is the frequency of the optical carrier. For a standard single-mode fiber, D is 17-ps/(nm.km). The fiber loss is ignored. Therefore, after transmission over a single-mode fiber of length z , the electrical field can be written as

$$\begin{aligned} E_{OUT}(t) = E_0 \cdot \{ & J_0(m_2)J_1(m_1)\cos [(\omega_c + \omega_1)t - \beta_0 z - \beta_1\omega_1 z - \frac{1}{2}\beta_2\omega_1^2 z] \\ & + J_0(m_2)J_1(m_1)\cos [(\omega_c - \omega_1)t - \beta_0 z + \beta_1\omega_1 z - \frac{1}{2}\beta_2\omega_1^2 z] \\ & + J_0(m_1)J_1(m_2)\cos [(\omega_c + \omega_2)t - \beta_0 z - \beta_1\omega_2 z - \frac{1}{2}\beta_2\omega_2^2 z] \\ & + J_0(m_1)J_1(m_2)\cos [(\omega_c - \omega_2)t - \beta_0 z + \beta_1\omega_2 z - \frac{1}{2}\beta_2\omega_2^2 z] + \dots \} \end{aligned} \quad (38)$$

After square-law photo detection, the RF signal can be expressed as

$$\begin{aligned} i(t) = RE_0^2 \cdot \{ & \text{DC} + \text{RF} \\ & + 2J_0(m_1)J_0(m_2)J_1(m_1)J_1(m_2) \cdot \cos [(\omega_c + \omega_1)t - \beta_0 z - \beta_1\omega_1 z - \frac{1}{2}\beta_2\omega_1^2 z] \\ & \cdot \cos [(\omega_c + \omega_2)t - \beta_0 z - \beta_1\omega_2 z - \frac{1}{2}\beta_2\omega_2^2 z] \end{aligned}$$

$$\begin{aligned}
& +2J_0(m_1)J_0(m_2)J_1(m_1)J_1(m_2) \cdot \cos [(\omega_c - \omega_1)t - \beta_0z + \beta_1\omega_1z - \frac{1}{2}\beta_2\omega_1^2z] \\
& \quad \cdot \cos [(\omega_c - \omega_2)t - \beta_0z + \beta_1\omega_2z - \frac{1}{2}\beta_2\omega_2^2z] \\
& +2J_0(m_1)J_0(m_2)J_1(m_1)J_1(m_2) \cdot \cos [(\omega_c + \omega_1)t - \beta_0z - \beta_1\omega_1z - \frac{1}{2}\beta_2\omega_1^2z] \\
& \quad \cdot \cos [(\omega_c - \omega_2)t - \beta_0z + \beta_1\omega_2z - \frac{1}{2}\beta_2\omega_2^2z] \\
& +2J_0(m_1)J_0(m_2)J_1(m_1)J_1(m_2) \cdot \cos [(\omega_c - \omega_1)t - \beta_0z + \beta_1\omega_1z - \frac{1}{2}\beta_2\omega_1^2z] \\
& \quad \cdot \cos [(\omega_c + \omega_2)t - \beta_0z - \beta_1\omega_2z - \frac{1}{2}\beta_2\omega_2^2z] \}
\end{aligned} \tag{39}$$

The RF signal at the substrate frequency $\omega_2 - \omega_1$:

$$\begin{aligned}
I_{\omega_2-\omega_1} &= J_0(m_1)J_0(m_2)J_1(m_1)J_1(m_2) \cdot \\
& \quad \{ \cos [(\omega_2 - \omega_1)t - \beta_1\omega_2z - \frac{1}{2}\beta_2\omega_2^2z + \beta_1\omega_1z + \frac{1}{2}\beta_2\omega_1^2z] \\
& \quad + \cos [(\omega_2 - \omega_1)t + \beta_1\omega_1z - \frac{1}{2}\beta_2\omega_1^2z + \beta_1\omega_2z + \frac{1}{2}\beta_2\omega_2^2z] \}
\end{aligned} \tag{40}$$

Define

$$\begin{cases} c = (\omega_2 - \omega_1)t + \beta_1\omega_1z - \beta_2\omega_2z \\ d = \frac{1}{2}\beta_2\omega_1^2z - \frac{1}{2}\beta_2\omega_2^2z = \frac{1}{2}\beta_2z(\omega_1^2 - \omega_2^2) \end{cases} \tag{41}$$

The RF signal at the substrate frequency can be written as

$$\begin{aligned}
I_{\omega_2-\omega_1} &= J_0(m_1)J_0(m_2)J_1(m_1)J_1(m_2) \cdot [\cos(c + d) + \cos(c - d)] \\
I_{\omega_2-\omega_1} &= 2J_0(m_1)J_0(m_2)J_1(m_1)J_1(m_2) \cdot \cos(c) \cos(d) \\
&= 2J_0(m_1)J_0(m_2)J_1(m_1)J_1(m_2) \cdot \cos[\frac{1}{2}\beta_2z(\omega_2^2 - \omega_1^2)] \\
& \quad \cdot \cos[(\omega_2 - \omega_1)t + \beta_1\omega_1z - \beta_2\omega_1z]
\end{aligned} \tag{42}$$

The RF signal at the sum frequency $\omega_2 + \omega_1$:

$$I_{\omega_2+\omega_1} = J_0(m_1)J_0(m_2)J_1(m_1)J_1(m_2) \cdot \left\{ \begin{aligned} &\cos[(\omega_1 + \omega_2)t - \beta_1\omega_1z - \frac{1}{2}\beta_2\omega_1^2z - \beta_1\omega_2z + \frac{1}{2}\beta_2\omega_2^2z] \\ &+ \cos[(\omega_1 + \omega_2)t - \beta_1\omega_2z - \frac{1}{2}\beta_2\omega_2^2z - \beta_1\omega_1z + \frac{1}{2}\beta_2\omega_1^2z] \end{aligned} \right\} \quad (43)$$

Define

$$\begin{cases} e = (\omega_1 + \omega_2)t - \beta_1\omega_1z - \beta_1\omega_2z \\ f = \frac{1}{2}\beta_2\omega_2^2z - \frac{1}{2}\beta_2\omega_1^2z = \frac{1}{2}\beta_2z(\omega_2^2 - \omega_1^2) \end{cases} \quad (44)$$

The RF signal at the sum frequency can be written as

$$\begin{aligned} I_{\omega_2+\omega_1} &= J_0(m_1)J_0(m_2)J_1(m_1)J_1(m_2) \cdot [\cos(e + f) + \cos(e - f)] \\ I_{\omega_2+\omega_1} &= 2J_0(m_1)J_0(m_2)J_1(m_1)J_1(m_2) \cdot \cos(e) \cos(f) \\ &= 2J_0(m_1)J_0(m_2)J_1(m_1)J_1(m_2) \cdot \cos\left[\frac{1}{2}\beta_2z(\omega_2^2 - \omega_1^2)\right] \\ &\quad \cdot \cos[(\omega_1 + \omega_2)t - \beta_1\omega_1z - \beta_2\omega_1z] \end{aligned} \quad (45)$$

Fig. 3-8 and Fig. 3-9 show the numerical simulation and theoretical solutions, the RF fading problem with the same results. Fig. 3-8 RF signal is driving 5 GHz and 30 GHz sinusoidal. Fig. 3-9 shows the results after 50km SMF transmission.

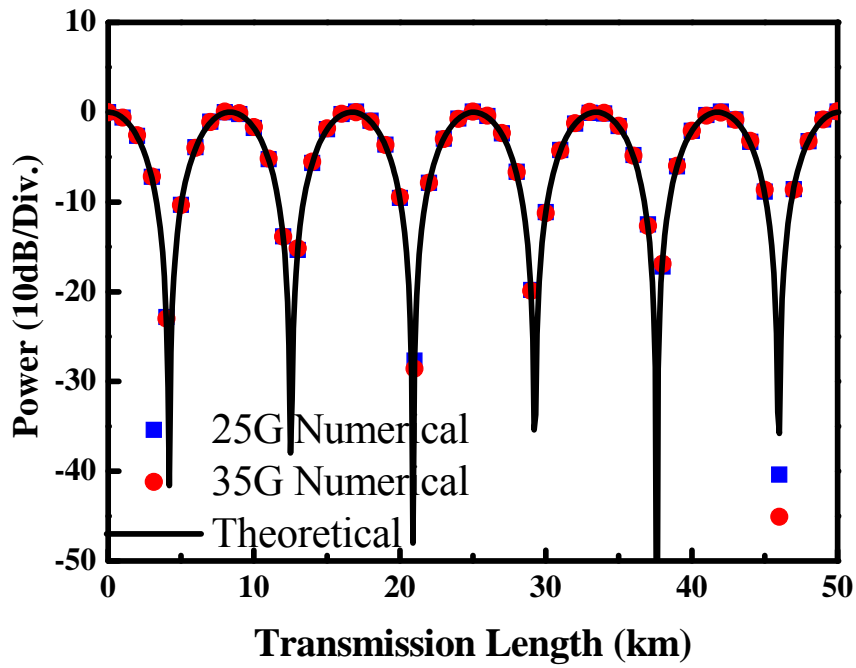


Figure 3-8 shows the numerical and theoretical solution for RF signal fading issue after transmission.

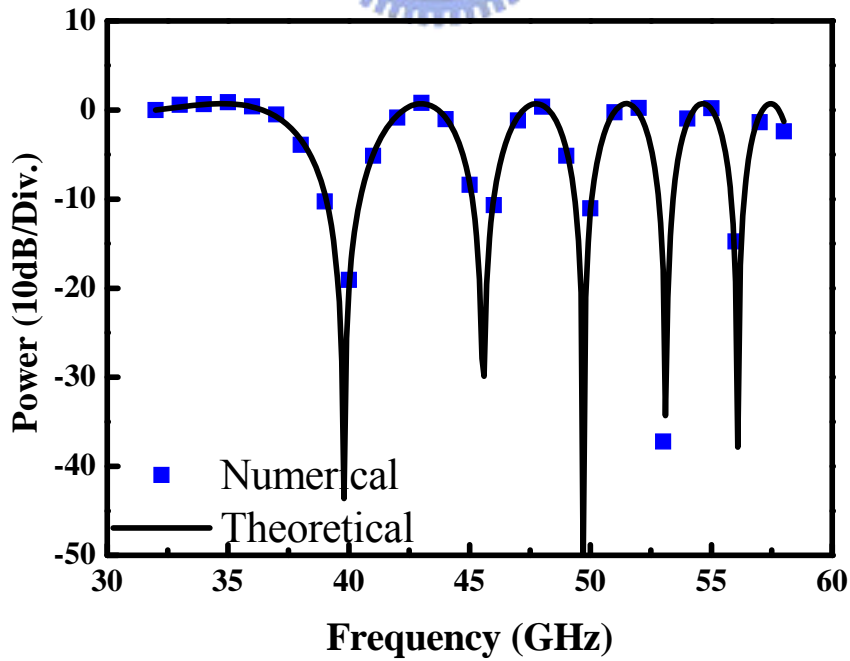


Figure 3-9 RF power vs. ω_1 .

3.4 The generated optical signal using optical filtering

3.4.1 Analysis of the generated signal

When we use fiber grating, the equation for the optical spectrum is

$$E_{OUT} = E_0 \cdot$$

$$\begin{aligned} & \{J_0(m_2)J_1(m_1)[k_1 \cdot \cos(\omega_c + \omega_1)t + \cos(\omega_c - \omega_1)t] \\ & -J_0(m_2)J_3(m_1)[\cos(\omega_c + 3\omega_1)t + \cos(\omega_c - 3\omega_1)t] \\ & -J_1(m_1)J_2(m_2)[\cos(\omega_c + \omega_1 + 2\omega_2)t + \cos(\omega_c - \omega_1 - 2\omega_2)t] \\ & -J_1(m_1)J_2(m_2)[\cos(\omega_c + \omega_1 - 2\omega_2)t + \cos(\omega_c - \omega_1 + 2\omega_2)t] \\ & +J_0(m_1)J_1(m_2)[k_2 \cdot \cos(\omega_c + \omega_2)t + \cos(\omega_c - \omega_2)t] \\ & -J_0(m_1)J_3(m_2)[\cos(\omega_c + 3\omega_2)t + \cos(\omega_c - 3\omega_2)t] \\ & -J_1(m_2)J_2(m_1)[\cos(\omega_c + \omega_2 + 2\omega_1)t + \cos(\omega_c - \omega_2 - 2\omega_1)t] \\ & -J_1(m_2)J_2(m_1)[\cos(\omega_c + \omega_2 - 2\omega_1)t + \cos(\omega_c - \omega_2 + 2\omega_1)t] \} \quad (46) \end{aligned}$$

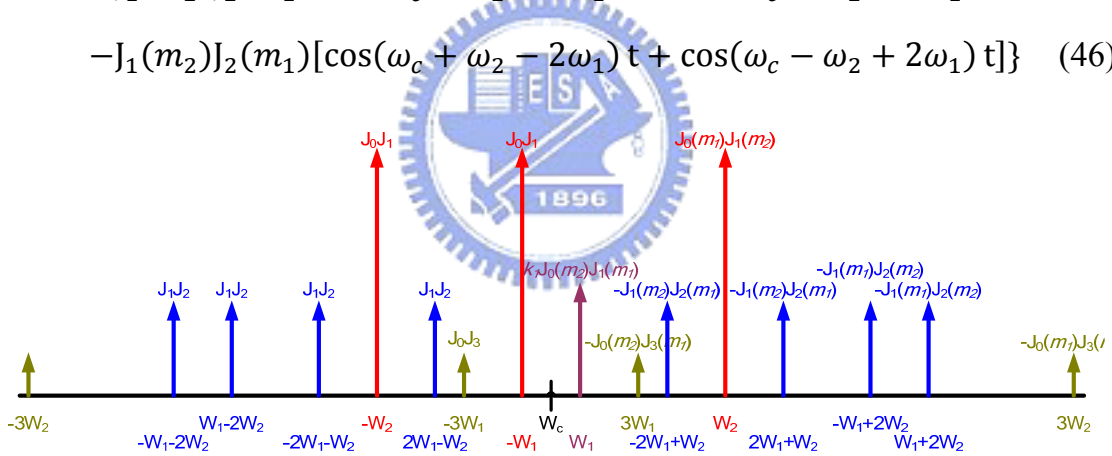


Figure 3-10 shows the optical spectrum when the LSB1 is filter out.

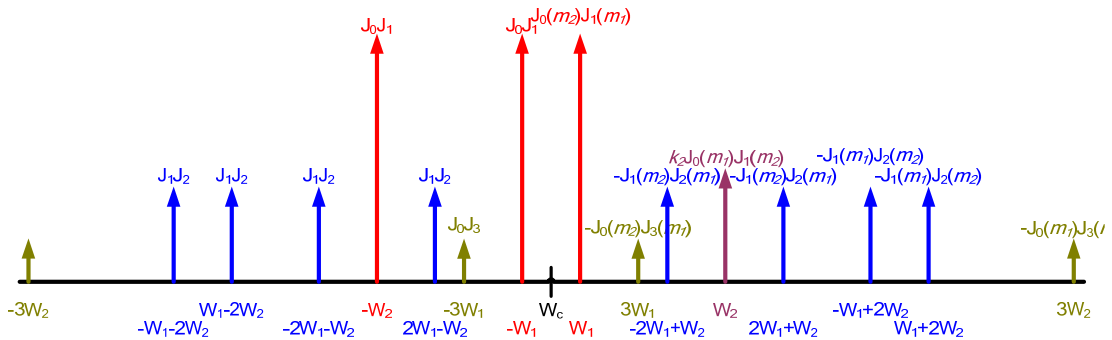


Figure 3-11 shows the optical spectrum when the LSB2 is filter out.

After square-law detection, the photocurrent can be expressed as

$$\begin{aligned}
i(t) = RE_0^2 \cdot \{DC \\
& + [k_1 \cdot J_0^2(m_2)J_1^2(m_1) - (1 + k_1) \cdot J_0^2(m_2)J_1(m_1)J_3(m_1) \\
& + 2J_1^2(m_1)J_2^2(m_2) - (2k_2 + 2) \cdot J_0(m_1)J_1^2(m_2)J_2(m_1)] \\
& \cdot \cos(2\omega_1 t) \\
& + [(1 + k_1 k_2) \cdot J_0(m_1)J_0(m_2)J_1(m_1)J_1(m_2) \\
& - (1 + k_1) \cdot J_0(m_2)J_1(m_1)J_1(m_2)J_2(m_1) \\
& - (1 + k_2) \cdot J_0(m_1)J_1(m_1)J_1(m_2)J_2(m_2) \\
& + 2J_1(m_1)J_1(m_2)J_2(m_1)J_2(m_2) \\
& + 2J_0(m_1)J_1(m_1)J_2(m_2)J_3(m_2) + 2J_0(m_2)J_1(m_2)J_2(m_1)J_3(m_1)] \\
& \cdot \cos[(\omega_2 - \omega_1)t] \\
& + [(k_1 + k_2) \cdot J_0(m_1)J_0(m_2)J_1(m_1)J_1(m_2) \\
& - (1 + k_1) \cdot J_0(m_2)J_1(m_1)J_1(m_2)J_2(m_1) \\
& - (1 + k_2) \cdot J_0(m_1)J_1(m_1)J_1(m_2)J_2(m_2) \\
& + 2J_1(m_1)J_1(m_2)J_2(m_1)J_2(m_2) \\
& + 2J_0(m_1)J_1(m_1)J_2(m_2)J_3(m_2) + 2J_0(m_2)J_1(m_2)J_2(m_1)J_3(m_1)] \\
& \cdot \cos[(\omega_2 + \omega_1)t] \\
& + [k_2 \cdot J_0^2(m_1)J_1^2(m_2) - (1 + k_2) \cdot J_0^2(m_1)J_1(m_2)J_3(m_2) \\
& + 2J_1^2(m_2)J_2^2(m_1) - (2k_1 + 2) \cdot J_0(m_2)J_1^2(m_1)J_2(m_2)] \\
& \cdot \cos(2\omega_2 t) \\
& + [-(1 + k_1) \cdot J_0(m_2)J_1(m_1)J_1(m_2)J_2(m_1) \\
& - (1 + k_2) \cdot J_0(m_1)J_0(m_2)J_1(m_2)J_3(m_1) \\
& + 2J_1(m_1)J_1(m_2)J_2(m_1)J_2(m_2)] \\
& \cdot \{\cos[(\omega_2 - 3\omega_1)t + \cos[(\omega_2 + 3\omega_1)t]]\}
\end{aligned}$$

$$\begin{aligned}
& +[-(1 + k_2) \cdot J_0(m_1)J_1^2(m_2)J_2(m_1) \\
& -(1 + k_1) \cdot J_0(m_2)J_1^2(m_1)J_2(m_2) \\
& + 2J_0(m_2)J_1(m_1)J_2(m_2)J_3(m_1) + 2J_0(m_1)J_1(m_2)J_2(m_1)J_3(m_2)] \\
& \cdot \cos [(2\omega_2 - 2\omega_1)t] \\
& +[-(1 + k_1) \cdot J_0^2(m_2)J_1(m_1)J_3(m_1) + 2J_1^2(m_2)J_2^2(m_1)] \\
& \cdot \cos (4\omega_1 t) \\
& +[J_1^2(m_2)J_2^2(m_1) + 2J_0(m_2)J_1(m_1)J_2(m_2)J_3(m_1)] \\
& \cdot \cos [(2\omega_2 - 4\omega_1)t] \\
& + 2J_0(m_2)J_1(m_2)J_2(m_1)J_3(m_1) \\
& \cdot \cos [(\omega_2 - 5\omega_1)t] + \text{RF} \}
\end{aligned}$$

(47)



Table 3-2 Measure the RF power with optical filtering

Frequency	Amplitude
$2\omega_1$	$+k_1 \cdot J_0^2(m_2)J_1^2(m_1) - (1 + k_1) \cdot J_0^2(m_2)J_1(m_1)J_3(m_1)$ $+2J_1^2(m_1)J_2^2(m_2) - (2k_2 + 2) \cdot J_0(m_1)J_1^2(m_2)J_2(m_1)$
$\omega_2 - \omega_1$	$+(1 + k_1k_2) \cdot J_0(m_1)J_0(m_2)J_1(m_1)J_1(m_2)$ $-(1 + k_1) \cdot J_0(m_2)J_1(m_1)J_1(m_2)J_2(m_1)$ $-(1 + k_2) \cdot J_0(m_1)J_1(m_1)J_1(m_2)J_2(m_2)$ $+2J_1(m_1)J_1(m_2)J_2(m_1)J_2(m_2)$ $+2J_0(m_1)J_1(m_1)J_2(m_2)J_3(m_2)$ $+2J_0(m_2)J_1(m_2)J_2(m_1)J_3(m_1)$
$\omega_2 + \omega_1$	$+(k_1 + k_2) \cdot J_0(m_1)J_0(m_2)J_1(m_1)J_1(m_2)$ $-(1 + k_1) \cdot J_0(m_2)J_1(m_1)J_1(m_2)J_2(m_1)$ $-(1 + k_2) \cdot J_0(m_1)J_1(m_1)J_1(m_2)J_2(m_2)$ $+2J_1(m_1)J_1(m_2)J_2(m_1)J_2(m_2)$ $+2J_0(m_1)J_1(m_1)J_2(m_2)J_3(m_2)$ $+2J_0(m_2)J_1(m_2)J_2(m_1)J_3(m_1)$
$2\omega_2$	$+k_2 \cdot J_0^2(m_1)J_1^2(m_2) - (1 + k_2) \cdot J_0^2(m_1)J_1(m_2)J_3(m_2)$ $+2J_1^2(m_2)J_2^2(m_1) - (2k_1 + 2) \cdot J_0(m_2)J_1^2(m_1)J_2(m_2)$
$\omega_2 - 3\omega_1, \omega_2 + 3\omega_1$	$-(1 + k_1) \cdot J_0(m_2)J_1(m_1)J_1(m_2)J_2(m_1)$ $-(1 + k_2) \cdot J_0(m_1)J_0(m_2)J_1(m_2)J_3(m_1)$ $+2J_1(m_1)J_1(m_2)J_2(m_1)J_2(m_2)$
$2\omega_2 - 2\omega_1$	$-(1 + k_2) \cdot J_0(m_1)J_1^2(m_2)J_2(m_1)$ $-(1 + k_1) \cdot J_0(m_2)J_1^2(m_1)J_2(m_2)$ $+2J_0(m_2)J_1(m_1)J_2(m_2)J_3(m_1)$ $+2J_0(m_1)J_1(m_2)J_2(m_1)J_3(m_2)$
$4\omega_1$	$-(1 + k_1) \cdot J_0^2(m_2)J_1(m_1)J_3(m_1) + 2J_1^2(m_2)J_2^2(m_1)$
$2\omega_2 - 4\omega_1$	$+J_1^2(m_2)J_2^2(m_1) + 2J_0(m_2)J_1(m_1)J_2(m_2)J_3(m_1)$
$\omega_2 - 5\omega_1$	$+2J_0(m_2)J_1(m_2)J_2(m_1)J_3(m_1)$

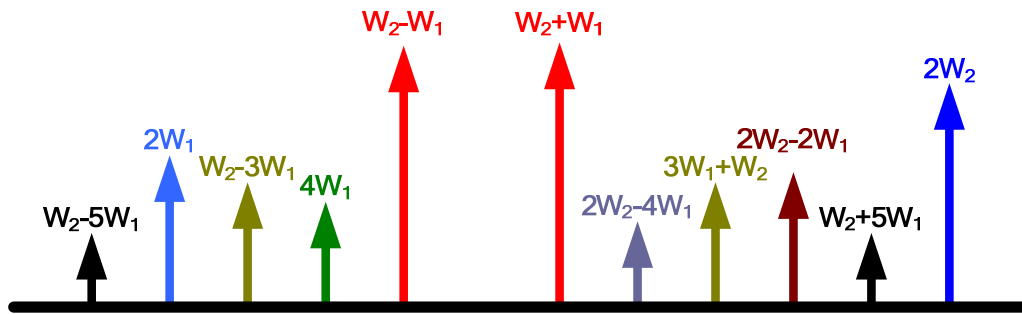


Figure 3-12 Illustration of the electrical spectrum of generated BTB mm-wave signals when the LSB1 is filter out. ($\omega_2 = 6\omega_1$)

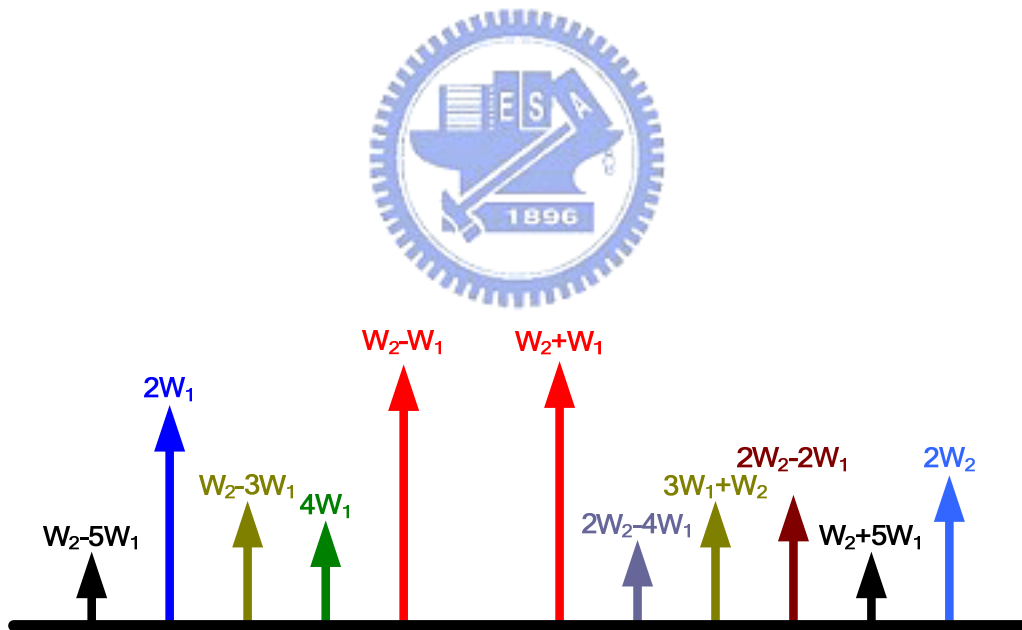


Figure 3-13 Illustration of the electrical spectrum of generated BTB mm-wave signals when the LSB2 is filter out. ($\omega_2 = 6\omega_1$)

3.4.2 The effects of fiber dispersion

Consider fiber dispersion effect, the electrical field can be written as

$$\begin{aligned}
 E_{OUT} = E_0 \cdot \{ & k_1 \cdot J_0(m_2)J_1(m_1)\cos [(\omega_c + \omega_1)t - \beta_0z - \beta_1\omega_1z - \frac{1}{2}\beta_2\omega_1^2z] \\
 & + J_0(m_2)J_1(m_1)\cos [(\omega_c - \omega_1)t - \beta_0z + \beta_1\omega_1z - \frac{1}{2}\beta_2\omega_1^2z] \\
 & + k_2 \cdot J_0(m_1)J_1(m_2)\cos [(\omega_c + \omega_2)t - \beta_0z - \beta_1\omega_2z - \frac{1}{2}\beta_2\omega_2^2z] \\
 & + J_0(m_1)J_1(m_2)\cos [(\omega_c - \omega_2)t - \beta_0z + \beta_1\omega_2z - \frac{1}{2}\beta_2\omega_2^2z] + \dots \}
 \end{aligned} \tag{48}$$

After square-law photo detection, the RF signal can be expressed as

$$\begin{aligned}
 i(t) = RE_0^2 \cdot \{ & \text{DC} + \text{RF} \\
 & + 2J_0(m_1)J_0(m_2)J_1(m_1)J_1(m_2) \\
 & \cdot k_1 \cdot \cos [(\omega_c + \omega_1)t - \beta_0z - \beta_1\omega_1z - \frac{1}{2}\beta_2\omega_1^2z] \\
 & \cdot k_2 \cdot \cos [(\omega_c + \omega_2)t - \beta_0z - \beta_1\omega_2z - \frac{1}{2}\beta_2\omega_2^2z] \\
 & + 2J_0(m_1)J_0(m_2)J_1(m_1)J_1(m_2) \\
 & \cdot \cos [(\omega_c - \omega_1)t - \beta_0z + \beta_1\omega_1z - \frac{1}{2}\beta_2\omega_1^2z] \\
 & \cdot \cos [(\omega_c - \omega_2)t - \beta_0z + \beta_1\omega_2z - \frac{1}{2}\beta_2\omega_2^2z] \\
 & + 2J_0(m_1)J_0(m_2)J_1(m_1)J_1(m_2) \\
 & \cdot k_1 \cdot \cos [(\omega_c + \omega_1)t - \beta_0z - \beta_1\omega_1z - \frac{1}{2}\beta_2\omega_1^2z] \\
 & \cdot \cos [(\omega_c - \omega_2)t - \beta_0z + \beta_1\omega_2z - \frac{1}{2}\beta_2\omega_2^2z] \\
 & + 2J_0(m_1)J_0(m_2)J_1(m_1)J_1(m_2) \\
 & \cdot \cos [(\omega_c - \omega_1)t - \beta_0z + \beta_1\omega_1z - \frac{1}{2}\beta_2\omega_1^2z] \\
 & \cdot k_2 \cdot \cos [(\omega_c + \omega_2)t - \beta_0z - \beta_1\omega_2z - \frac{1}{2}\beta_2\omega_2^2z] \}
 \end{aligned} \tag{49}$$

The RF signal at the substrate frequency $\omega_2 - \omega_1$:

$$I_{\omega_2 - \omega_1} = J_0(m_1)J_0(m_2)J_1(m_1)J_1(m_2) \cdot \{k_1k_2 \cdot \cos[(\omega_2 - \omega_1)t - \beta_1\omega_2z - \frac{1}{2}\beta_2\omega_2^2z + \beta_1\omega_1z + \frac{1}{2}\beta_2\omega_1^2z] + \cos[(\omega_2 - \omega_1)t + \beta_1\omega_1z - \frac{1}{2}\beta_2\omega_1^2z + \beta_1\omega_2z + \frac{1}{2}\beta_2\omega_2^2z]\} \quad (50)$$

Define

$$\begin{cases} a = (\omega_2 - \omega_1)t + \beta_1\omega_1z - \beta_2\omega_2z \\ b = \frac{1}{2}\beta_2\omega_1^2z - \frac{1}{2}\beta_2\omega_2^2z = \frac{1}{2}\beta_2z(\omega_1^2 - \omega_2^2) \end{cases} \quad (51)$$

The RF signal at the substrate frequency can be written as

$$\begin{aligned} I_{\omega_2 - \omega_1} &= J_0(m_1)J_0(m_2)J_1(m_1)J_1(m_2) \\ &\cdot [k_1k_2 \cdot \cos(a + b) + k_1k_2 \cdot \cos(a - b) + (1 - k_1k_2) \cdot \cos(a - b)] \\ I_{\omega_2 - \omega_1} &= J_0(m_1)J_0(m_2)J_1(m_1)J_1(m_2) \\ &\cdot [2k_1k_2 \cos(a) \cos(b) + (1 - k_1k_2) \cdot \cos(a - b)] \\ &= J_0(m_1)J_0(m_2)J_1(m_1)J_1(m_2) \\ &\cdot \{2k_1k_2 \cos[\frac{1}{2}\beta_2z(\omega_2^2 - \omega_1^2)] \cdot \cos[(\omega_2 - \omega_1)t + \beta_1\omega_1z - \beta_2\omega_1z] \\ &+ (1 - k_1k_2) \cos[(\omega_2 - \omega_1)t + \beta_1\omega_1z - \beta_2\omega_2z - \frac{1}{2}\beta_2z(\omega_1^2 - \omega_2^2)]\} \end{aligned} \quad (52)$$

The RF signal power at the substrate frequency can be written as

$$\begin{aligned} P_{\omega_2 - \omega_1} &= [J_0(m_1)J_0(m_2)J_1(m_1)J_1(m_2)]^2 \cdot \{A^2 + B^2 + 2AB \cdot \cos(\theta_2)\} \\ &= [J_0(m_1)J_0(m_2)J_1(m_1)J_1(m_2)]^2 \\ &\cdot \{[2k_1k_2 \cos[\frac{1}{2}\beta_2z(\omega_2^2 - \omega_1^2)]]^2 + [(1 - k_1k_2)]^2 \\ &+ 2 [2k_1k_2 \cos[\frac{1}{2}\beta_2z(\omega_2^2 - \omega_1^2)]] \cdot (1 - k_1k_2) \cdot \cos(\theta_2)\} \end{aligned} \quad (53)$$

The RF signal at the sum frequency $\omega_2 + \omega_1$

$$I_{\omega_2+\omega_1} = J_0(m_1)J_0(m_2)J_1(m_1)J_1(m_2) \cdot \left\{ k_1 \cos[(\omega_1 + \omega_2)t - \beta_1\omega_1z - \frac{1}{2}\beta_2\omega_1^2z - \beta_1\omega_2z + \frac{1}{2}\beta_2\omega_2^2z] + k_2 \cos[(\omega_1 + \omega_2)t - \beta_1\omega_2z - \frac{1}{2}\beta_2\omega_2^2z - \beta_1\omega_1z + \frac{1}{2}\beta_2\omega_1^2z] \right\} \quad (54)$$

Define

$$\begin{cases} a = (\omega_1 + \omega_2)t - \beta_1\omega_1z - \beta_1\omega_2z \\ b = \frac{1}{2}\beta_2\omega_2^2z - \frac{1}{2}\beta_2\omega_1^2z = \frac{1}{2}\beta_2z(\omega_2^2 - \omega_1^2) \end{cases}$$

The RF signal at the sum frequency can be written as

$$I_{\omega_2+\omega_1} = J_0(m_1)J_0(m_2)J_1(m_1)J_1(m_2) \cdot [k_1 \cos(a + b) + k_1 \cos(a - b) + (k_2 - k_1) \cos(a - b)]$$

$$I_{\omega_2+\omega_1} = J_0(m_1)J_0(m_2)J_1(m_1)J_1(m_2) \cdot [2k_1 \cos(a) \cos(b) + (k_2 - k_1) \cos(a - b)]$$

$$= J_0(m_1)J_0(m_2)J_1(m_1)J_1(m_2) \cdot \left\{ 2k_1 \cos\left[\frac{1}{2}\beta_2z(\omega_2^2 - \omega_1^2)\right] \cdot \cos[(\omega_1 + \omega_2)t - \beta_1\omega_1z - \beta_2\omega_1z] + (k_2 - k_1) \cos[(\omega_2 + \omega_1)t - \beta_1\omega_1z - \beta_2\omega_2z - \frac{1}{2}\beta_2z(\omega_2^2 - \omega_1^2)] \right\} \quad (55)$$

Or

$$I_{\omega_2+\omega_1} = J_0(m_1)J_0(m_2)J_1(m_1)J_1(m_2) \cdot [k_2 \cos(a + b) + k_2 \cos(a - b) + (k_1 - k_2) \cos(a - b)]$$

$$I_{\omega_2+\omega_1} = J_0(m_1)J_0(m_2)J_1(m_1)J_1(m_2) \cdot \left\{ 2k_2 \cos\left[\frac{1}{2}\beta_2z(\omega_2^2 - \omega_1^2)\right] \cdot \cos[(\omega_1 + \omega_2)t - \beta_1\omega_1z - \beta_2\omega_1z] + (k_1 - k_2) \cos[(\omega_2 + \omega_1)t - \beta_1\omega_1z - \beta_2\omega_2z - \frac{1}{2}\beta_2z(\omega_2^2 - \omega_1^2)] \right\}$$

$$= A \cdot \cos[(\omega_1 + \omega_2)t + \theta_1] + B \cdot \cos[(\omega_1 + \omega_2)t + \theta_1 + \theta_2] \quad (56)$$

The RF signal power at the sum frequency can be written as

$$\begin{aligned}
P_{\omega_2+\omega_1} &= [J_0(m_1)J_0(m_2)J_1(m_1)J_1(m_2)]^2 \cdot \{A^2 + B^2 + 2AB \cdot \cos(\theta_2)\} \\
&= [J_0(m_1)J_0(m_2)J_1(m_1)J_1(m_2)]^2 \\
&\quad \cdot \{[2k_2 \cos[\frac{1}{2}\beta_2 z(\omega_2^2 - \omega_1^2)]]^2 + [(k_1 - k_2)]^2 \\
&\quad + 2[2k_2 \cos[\frac{1}{2}\beta_2 z(\omega_2^2 - \omega_1^2)]] \cdot (k_1 - k_2) \cdot \cos(\theta_2)\}
\end{aligned} \tag{57}$$

Or

$$\begin{aligned}
P_{\omega_2+\omega_1} &= [J_0(m_1)J_0(m_2)J_1(m_1)J_1(m_2)]^2 \cdot \{A^2 + B^2 + 2AB \cdot \cos(\theta_2)\} \\
&= [J_0(m_1)J_0(m_2)J_1(m_1)J_1(m_2)]^2 \\
&\quad \cdot \{[2k_1 \cos[\frac{1}{2}\beta_2 z(\omega_2^2 - \omega_1^2)]]^2 + [(k_2 - k_1)]^2 \\
&\quad + 2[2k_1 \cos[\frac{1}{2}\beta_2 z(\omega_2^2 - \omega_1^2)]] \cdot (k_2 - k_1) \cdot \cos(\theta_2)\}
\end{aligned} \tag{58}$$

Because grating only filter out LSB1 or LSB2 at the same time, so the equation of the RF signal power at the sum and substrate frequency are the same. The RF signal power can be written as

$$\begin{aligned}
P_{\omega_2+\omega_1} &= P_{\omega_2-\omega_1} \\
&= [J_0(m_1)J_0(m_2)J_1(m_1)J_1(m_2)]^2 \\
&\quad \cdot \{[2k_1 k_2 \cos[\frac{1}{2}\beta_2 z(\omega_2^2 - \omega_1^2)]]^2 + [(1 - k_1 k_2)]^2 \\
&\quad + 2[2k_1 k_2 \cos[\frac{1}{2}\beta_2 z(\omega_2^2 - \omega_1^2)]] \cdot (1 - k_1 k_2) \cdot \cos(\theta_2)\}
\end{aligned} \tag{59}$$

If grating is filter out 28dB, $20\text{Log}(k_1 \text{ or } k_2) = -28$, $k_1 \text{ or } k_2 = 0.04$.

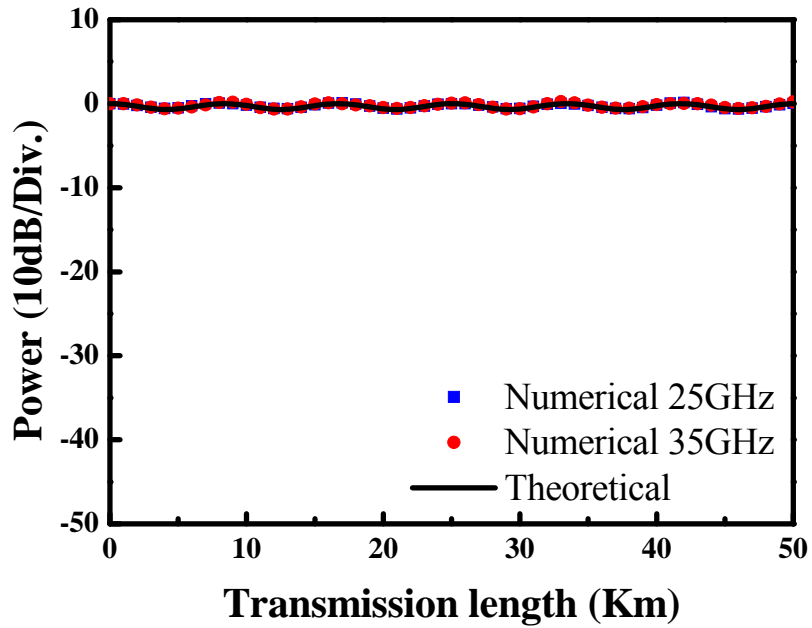


Figure 3-14 shows the RF signal power vs. transmission length when the LSB1 is filter out.

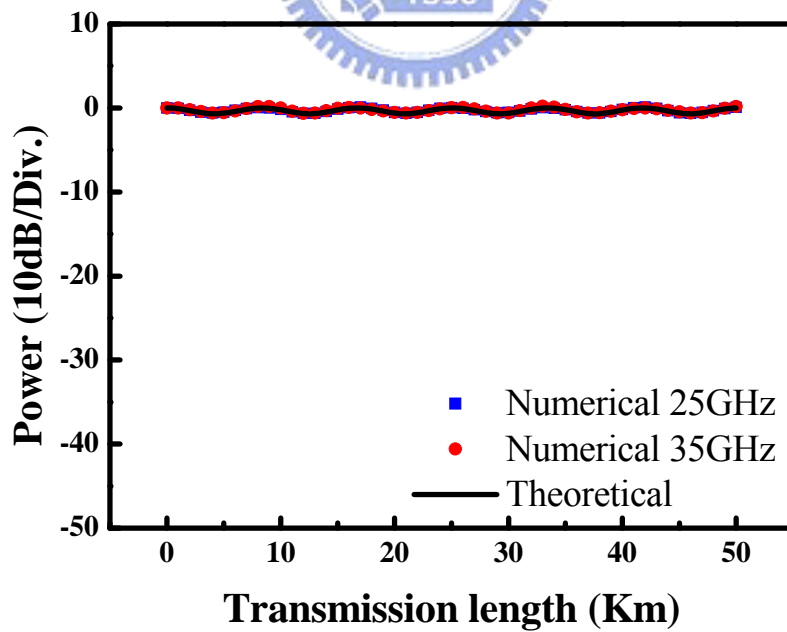


Figure 3-15 shows the RF signal power vs. transmission length when the LSB2 is filter out.

3.5 The optimal optical power ratio condition

3.5.1 Signal without optical filtering

We assume the output e-field of LSB2, LSB1, RSB1 and RSB2 are E_1, E_2, E_3 and E_4 respectively. When we use single drive MZM and set the bias point of MZM at V_π and then the e-field is

$$E_1 = E_4, E_2 = E_3 \quad (60)$$

For the PSK signal that the total power can be written as

$$\begin{aligned} E_1^2 + E_2^2 + E_3^2 + E_4^2 &= P \\ 2E_1^2 + 2E_2^2 &= P \end{aligned} \quad (61)$$

The optical field is then detected using an ideal square-law photodetector, and the RF signals generated are mathematically evaluated as follows:

$$\begin{aligned} &2E_1^2 + 2E_2^2 + E_1 \cdot E_2 + E_3 \cdot E_4 + E_1 \cdot E_3 + E_2 \cdot E_4 \\ \text{The } f_1 + f_2 \text{ RF signal term is} \\ &E_1 \cdot E_3 + E_2 \cdot E_4 = 2E_1 \cdot E_2 \end{aligned} \quad (62)$$

Where $E_2 = \sqrt{\frac{P}{2} - E_1^2}$ for PSK signal

The RF signal become

$$2E_1 \cdot \sqrt{\frac{P}{2} - E_1^2} \quad (63)$$

The maximum of RF signal power originates from

$$\left(2E_1 \cdot \sqrt{\frac{P}{2} - E_1^2} \right)' = 0 \quad (64)$$

To solve the differential equation we would get the e-field

$$\begin{aligned} E_1 &= \sqrt{P}/2, E_2 = \sqrt{P}/2 \\ E_1 : E_2 : E_3 : E_4 &= 1 : 1 : 1 : 1 \end{aligned} \quad (65)$$

The optical powers are

$$I_1 = I_2 = I_3 = I_4 = P/4, I_1 : I_2 : I_3 : I_4 = 1 : 1 : 1 : 1 \quad (66)$$

For the OOK signal that the total power can be written as

$$2E_1^2 + E_2^2 + E_3^2 + 2E_4^2 = P$$

$$4E_1^2 + 2E_2^2 = P \quad (67)$$

The $f_1 + f_2$ RF signal term is

$$E_1 \cdot E_3 + E_2 \cdot E_4 = 2E_1 \cdot E_2 \quad (68)$$

Where $E_1 = \sqrt{\frac{P}{4} - \frac{E_2^2}{2}}$ for OOK signal

The RF signal become

$$2E_2 \cdot \sqrt{\frac{P}{4} - \frac{E_2^2}{2}} \quad (69)$$

The maximum of RF signal power is happened in

$$\left(2E_2 \cdot \sqrt{\frac{P}{4} - \frac{E_2^2}{2}} \right)' = 0 \quad (70)$$

To solve the differential equation we would get the e-filed

$$E_2 = \sqrt{P}/2, E_1 = \sqrt{P}/8$$

and

$$E_1 : E_2 : E_3 : E_4 = 1 : \sqrt{2} : \sqrt{2} : 1 \quad (71)$$

The optical powers are

$$I_1 = I_4 = 2E_1^2 = P/4$$

$$I_2 = I_3 = E_2^2 = P/4 \quad (72)$$

and

$$I_1 : I_2 : I_3 : I_4 = 1 : 1 : 1 : 1 \quad (73)$$

When the optical signal without filtering, the optimal SOPR of both PSK and OOK RF signals is 0-dB.

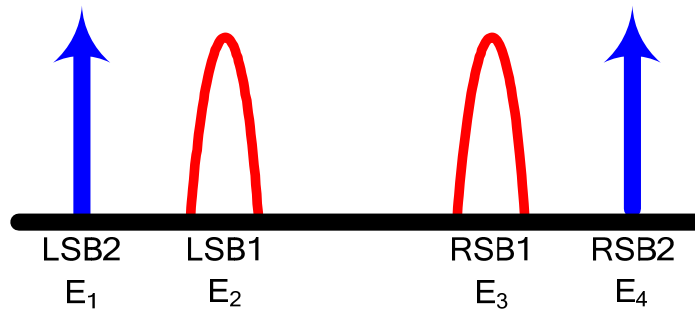


Figure 3-16 shows optical spectrum without fiber grating filter out.

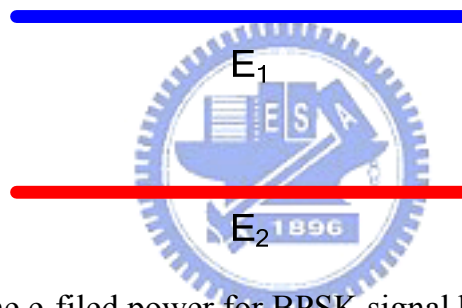


Figure 3-17 the e-filed power for BPSK signal between zero and one.

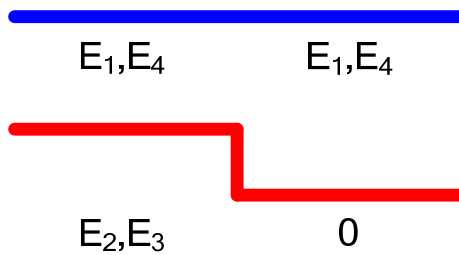


Figure 3-18 the e-filed power for OOK signal between zero and one.

3.5.2 When the LSB2 or LSB1 is filter out

Using fiber grating to remove LSB1 and getting maximum output RF signal condition for PSK signal is

$$E_2 : E_3 : E_4 = 1 : 1 : \sqrt{2} \quad (74)$$

The optical power equal

$$I_2 : I_3 : I_4 = 1 : 1 : 2 \quad (75)$$

and for OOK signal

$$E_2 : E_3 : E_4 = 1 : 1 : 1 \quad (76)$$

The optical power equal

$$I_2 : I_3 : I_4 = 1 : 1 : 2 \quad (77)$$

The optimal SOPR of both PSK and OOK RF signals is 3-dB when the LSB2 with filtering.



Using fiber grating to remove LSB1 and getting maximum output RF signal condition for PSK signal is

$$E_1 : E_3 : E_4 = 1 : \sqrt{2} : 1 \quad (78)$$

The optical power equal

$$I_1 : I_3 : I_4 = 1 : 2 : 1 \quad (79)$$

And for OOK signal

$$E_1 : E_3 : E_4 = 1 : 2 : 1 \quad (80)$$

The optical power equal

$$I_2 : I_3 : I_4 = 1 : 2 : 1 \quad (81)$$

The optimal SOPR of both PSK and OOK RF signals is -3-dB when the LSB1 with filtering.

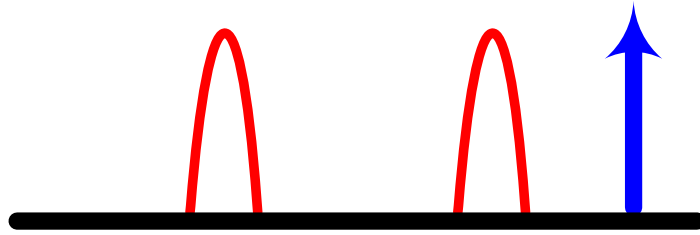


Figure 3-19 shows optical spectrum when the LSB2 is filter out.

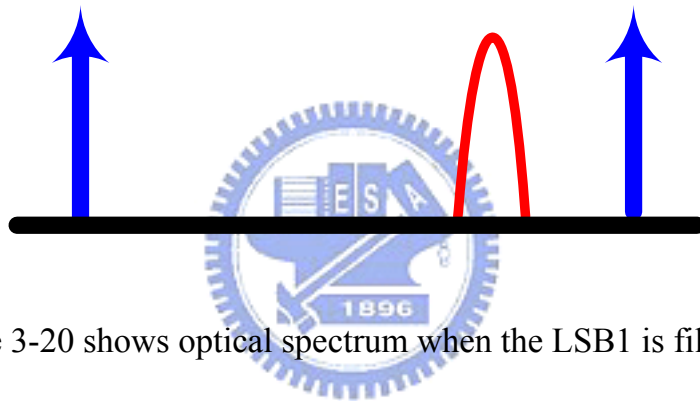


Figure 3-20 shows optical spectrum when the LSB1 is filter out.

Chapter 4

Experimental demonstration of the proposed system

4.1 preface

In chapter 3, we provide the theoretical and numerical results for the concept of proposed system. Therefore, the result can be tried to apply to the radio-over-fiber system. In this chapter, we will build the experimental setup for the propose system based on DSBCS modulation. Figure 4-1 shows the optical spectrum for the fiber Bragg grating reflection and transmission.

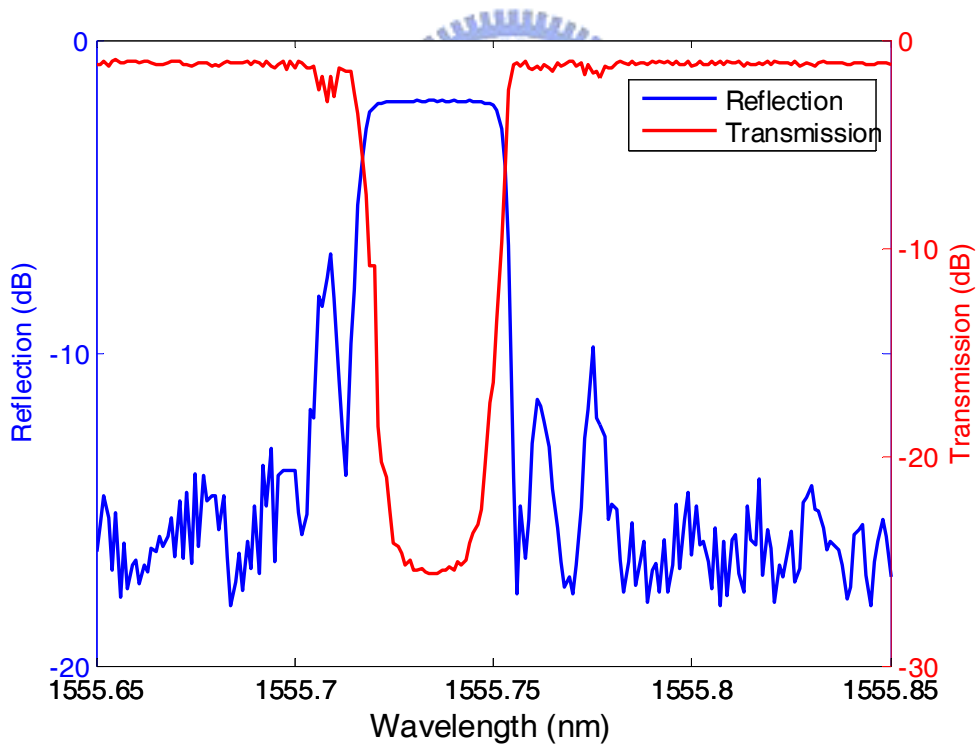


Figure 4-1 the optical spectrum for the fiber Bragg grating reflection and transmission.

4.2 Experimental results for optical signal without optical filtering

4.2.1 Experiment setup

Figure 4-2 displays the experimental setup for optical vector signal generation and transmission using a single-electrode MZM. The continue wave laser source about 1550nm is generation using tunable laser. The laser source is then passed through a polarization controller to achieve output optical power is a maximum when the MZM is biased at full point. The OOK/BPSK signal is a 1.25-Gb/s pseudo random binary sequence (PRBS) signal with a word length of $2^{31}-1$ and is up-converted using a 5-GHz sinusoidal signal (f1). The 625-MSym/s QPSK signal at 5-GHz is generated using an arbitrary waveform generator. Then the RF OOK/BPSK/QPSK signals are combined with a 10-GHz sinusoidal signal (f2). This combined RF signal is fed into single-electrode MZM and the MZM is bias the null point. The generated optical spectrum that has two upper-wavelength sidebands (USB1, USB2) and two lower- wavelength sidebands (LSB1, LSB2) with carrier suppression. The generated optical signal is amplified by EDFA and then filtered by an optical tunable filter with a bandwidth of 38GHz. The input EDFA optical power is fixed -20dBm. The power of optical RF signal which entered fiber is set to less than 0 dBm to reduce the effect of both fiber nonlinearity and dispersion changing the duty cycle of optical microwaves. After transmitted over standard single mode fiber (SSMF), the transmitted optical microwave signal is converted into an electrical microwave signal by a PIN PD with a 3 dB bandwidth of 38 GHz, and the converted electrical signal is amplified by an electrical amplifier. If we would measure the RF signal at the subtract frequency, the RF signal is then passed through the electrical bandpass filter at

5GHz. The center frequency of bandpass filter is 15GHz when we would measure the RF signal at the sum frequency. After the photo receiver, the optical signal generates two RF signals with a subtract frequency of 5 GHz (f_2-f_1) and a sum frequency of 15 GHz (f_1+f_2), respectively. Insets (i) and (ii) of Figure 4-2 show the receiver architectures of RF OOK/BPSK and QPSK signals, respectively. The RF OOK/BPSK signal is down-converted to baseband signal and directly tested by a BER tester. The RF QPSK signal is down-converted to 5 GHz by a 10 GHz oscillator and a mixer to realize intermediate frequency (IF) demodulation. A digital real-time oscilloscope (Tektronix DPO71254) stores the waveform and an off-line digital signal processing (DSP) program using Matlab is employed to demodulate the QPSK signal. For QPSK signal, the bit error rate (BER) performance is calculated from the measured modulation error ratio (MER). The MER is defined as $MER = \frac{I_r^2 + Q_r^2}{(I_r - I_o)^2 + (Q_r - Q_o)^2}$, where I_r and Q_r represent the demodulated in-phase and quadrature-phase symbols, and I_o and Q_o are the ideal normalized in-phase and quadrature-phase QPSK symbols. The optical intensity of the data-modulated subcarriers (5 GHz) relative to that of the sinusoidal subcarrier (10 GHz) can be easily tuned by adjusting the input electrical power to optimize the performance of the optical RF signals.

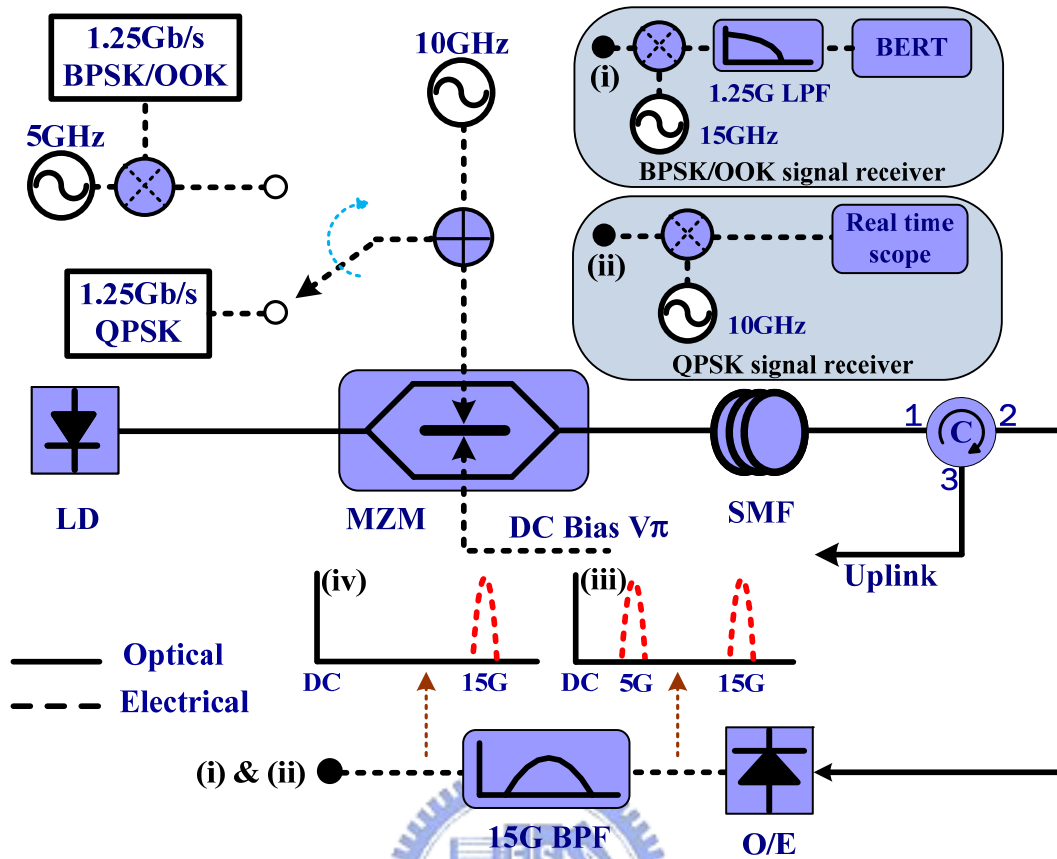


Figure 4-2 shows the experimental setup to receive sum frequency.

4.3.2 Optimal condition for RF signal

Fig. 4-3 and Fig. 4-4 show the optical spectrums in different SOPR (SOPR = P_s/P_d , P_s and P_d are the optical powers of the 10-GHz subcarrier and the 5-GHz data-modulated subcarrier, respectively.) for BPSK and OOK signal. The BER curves of BPSK and OOK signal at substrate frequency shown in Fig. 4-5 and Fig. 4-6. When we consider the RF signal at sum frequency. The BER curves and eye diagrams of BPSK are shown in Fig 4-7 and Fig. 4-8. For OOK signal are shown in Fig. 4-9 and Fig. 4-10. Fig. 4-11 and Fig. 4-12 present the measured receiver sensitivity at a bit error rate (BER) of 10^{-9} and simulated Q-factor or MER of BPSK and OOK or QPSK RF signals as function of the ratio of the sinusoidal subcarrier power to the data-modulated subcarriers

power The modulated index of the 10-GHz sinusoidal signal ($MI=V_{p-p}/2V_{II}$) is set to 0.1 and adjusted SOPR to 0dB by changing the electrical power of the 5-GHz data. And then is adjusted the electrical power of 10-GHz sinusoidal signal to changing SOPR. For RF signal generation without filtering, the optimal SOPR of both BPSK and OOK RF signals is 0 dB.

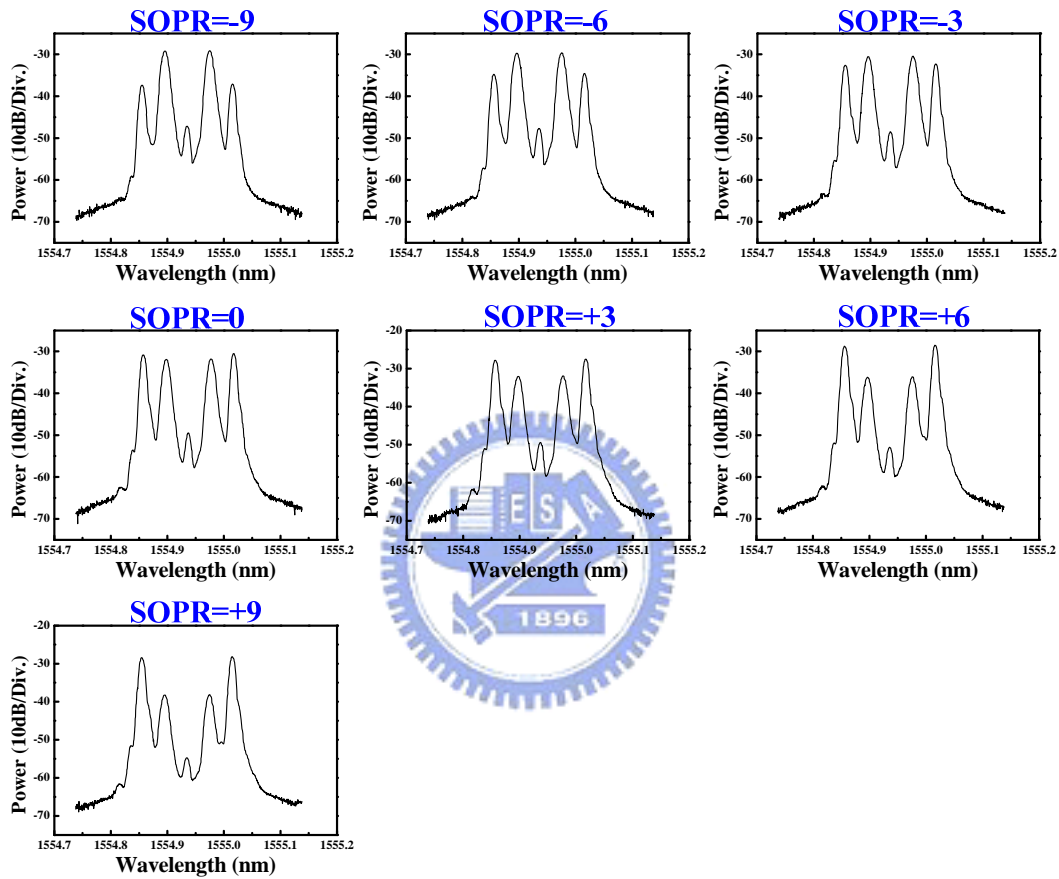


Figure 4-3 shows the optical spectrum for BPSK.

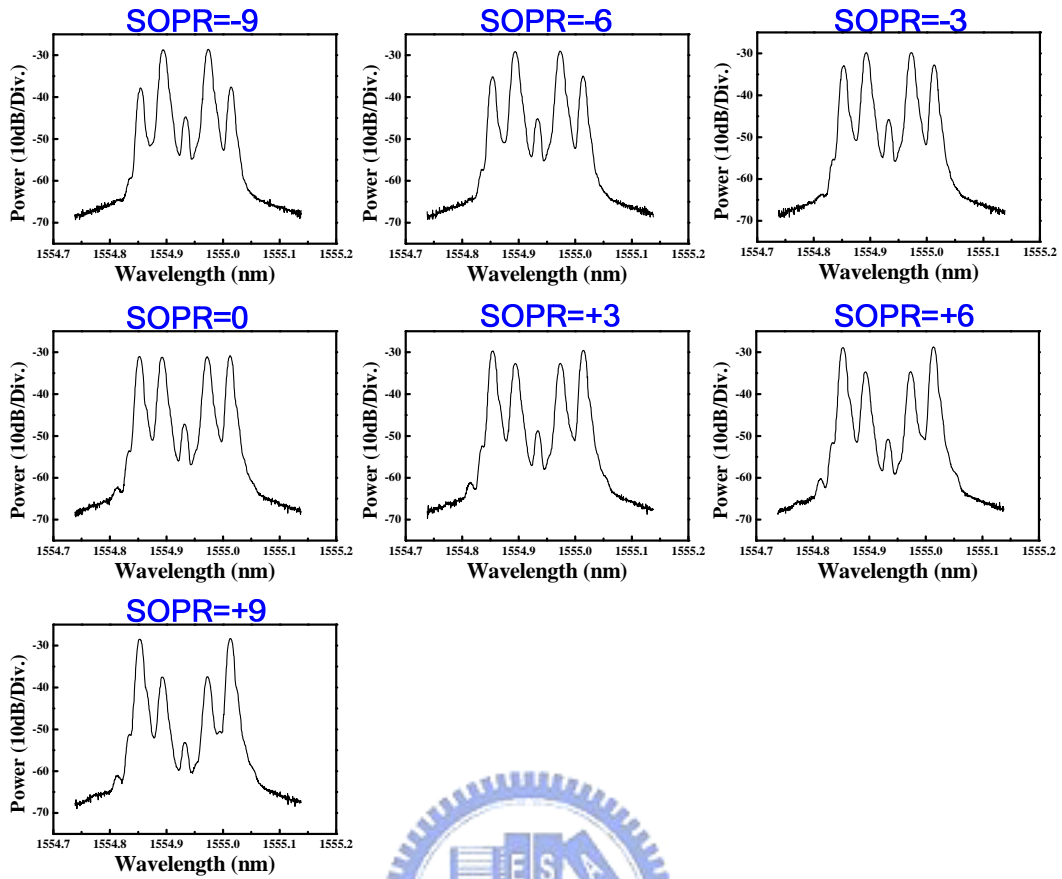
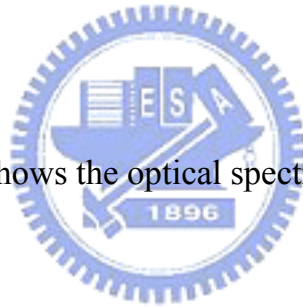


Figure 4-4 shows the optical spectrum for OOK.



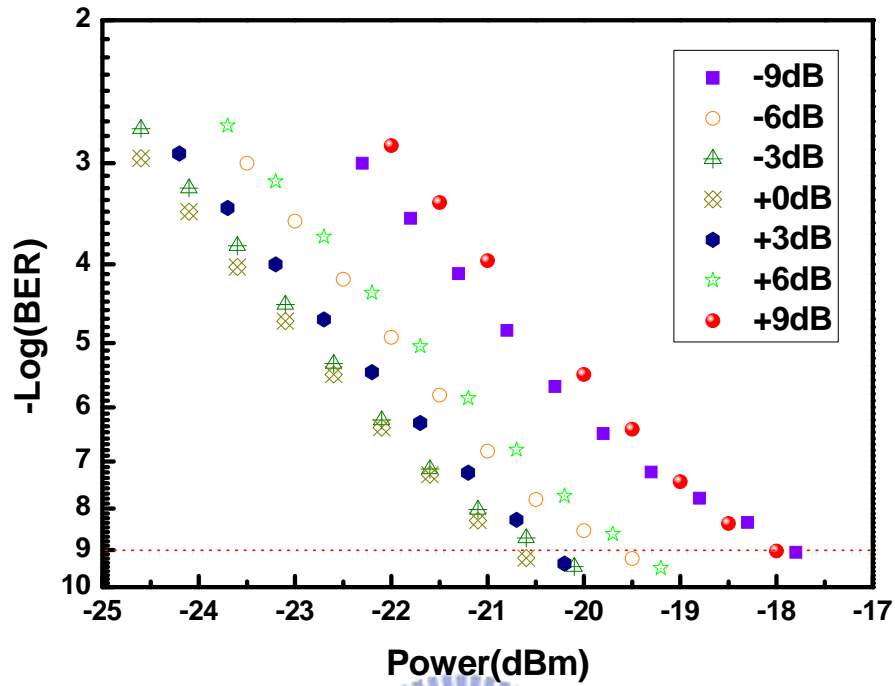


Figure 4-5 the BER curves for BPSK at 5GHz.

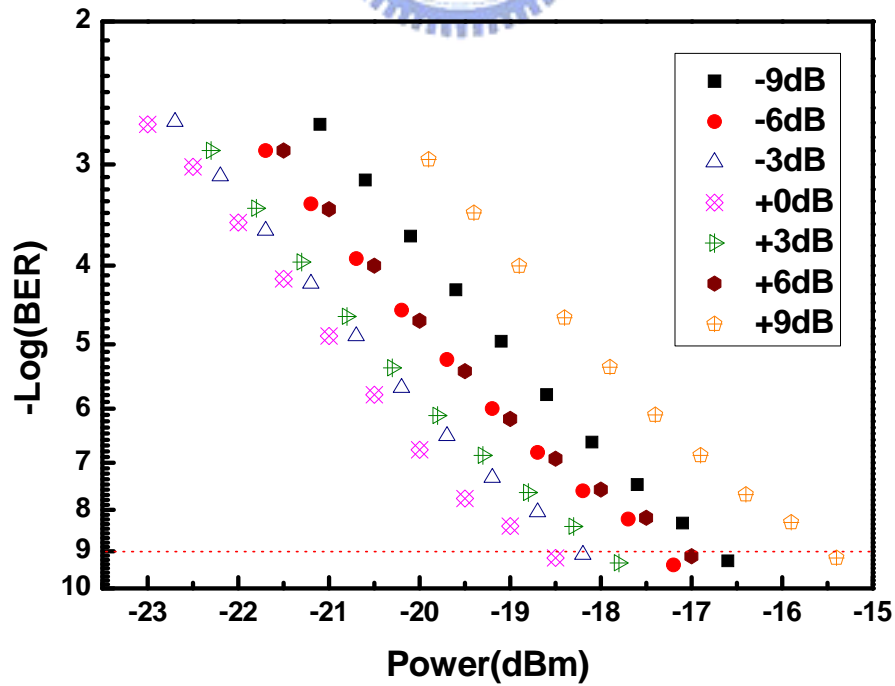


Figure 4-6 the BER curves for OOK at 5GHz.

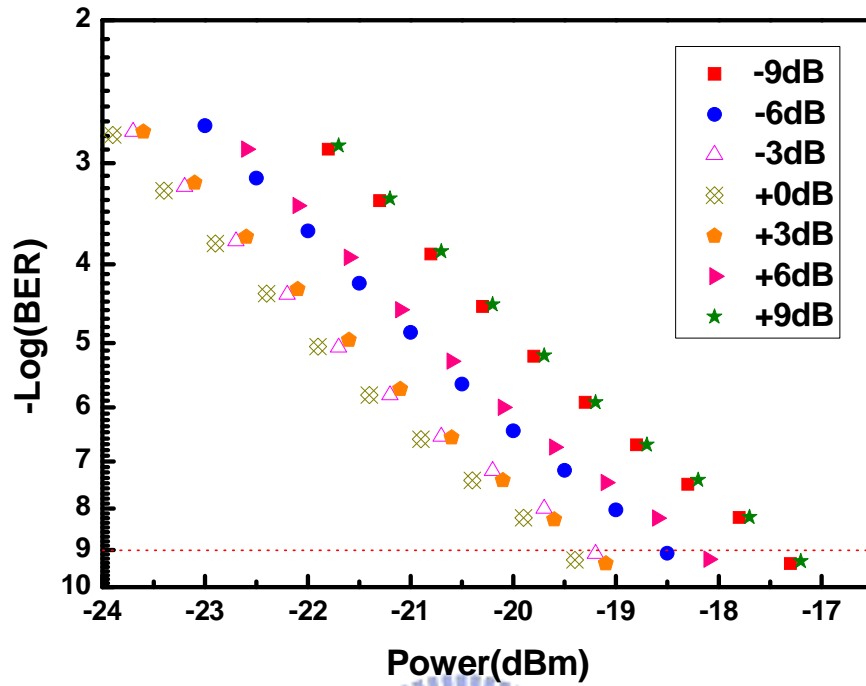


Figure 4-7 the BER curves for BPSK at 15GHz.

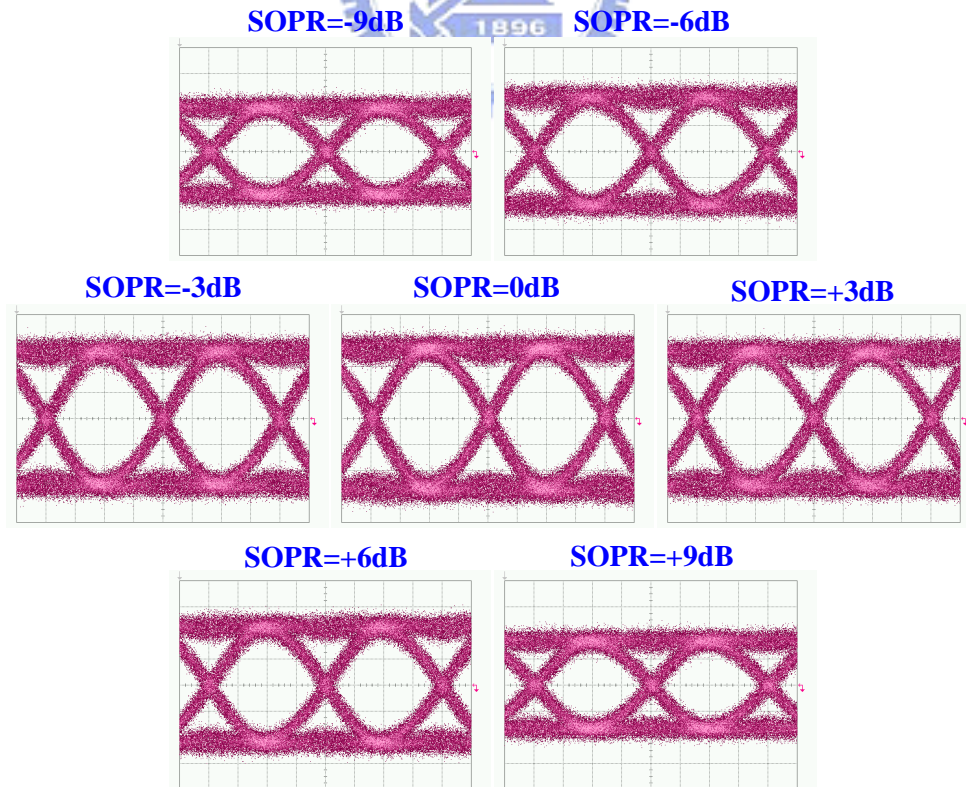


Figure 4-8 the eye diagrams for BPSK at 15GHz.

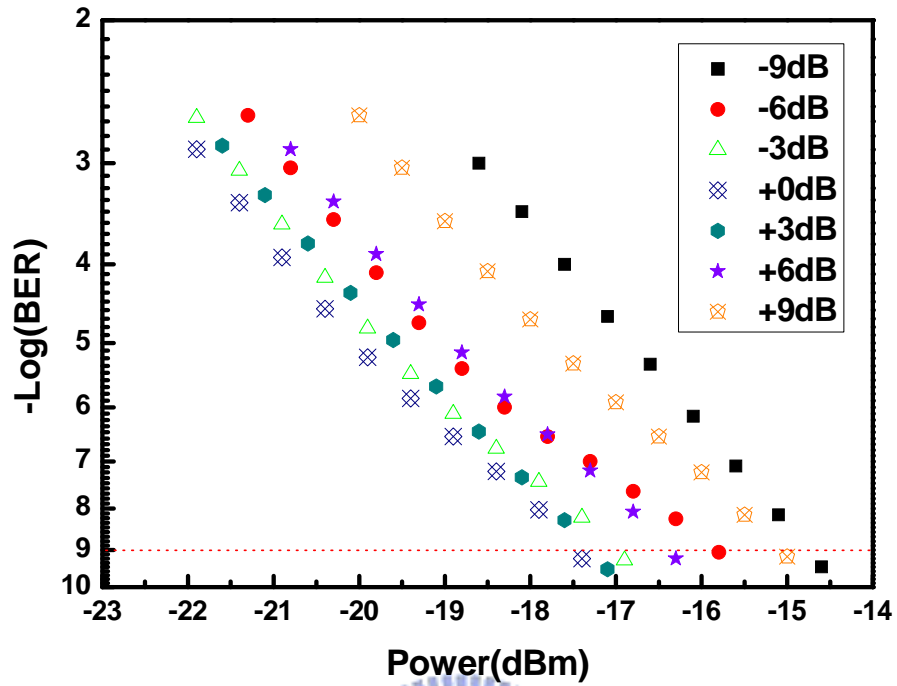


Figure 4-9 the BER curves for OOK at 15GHz

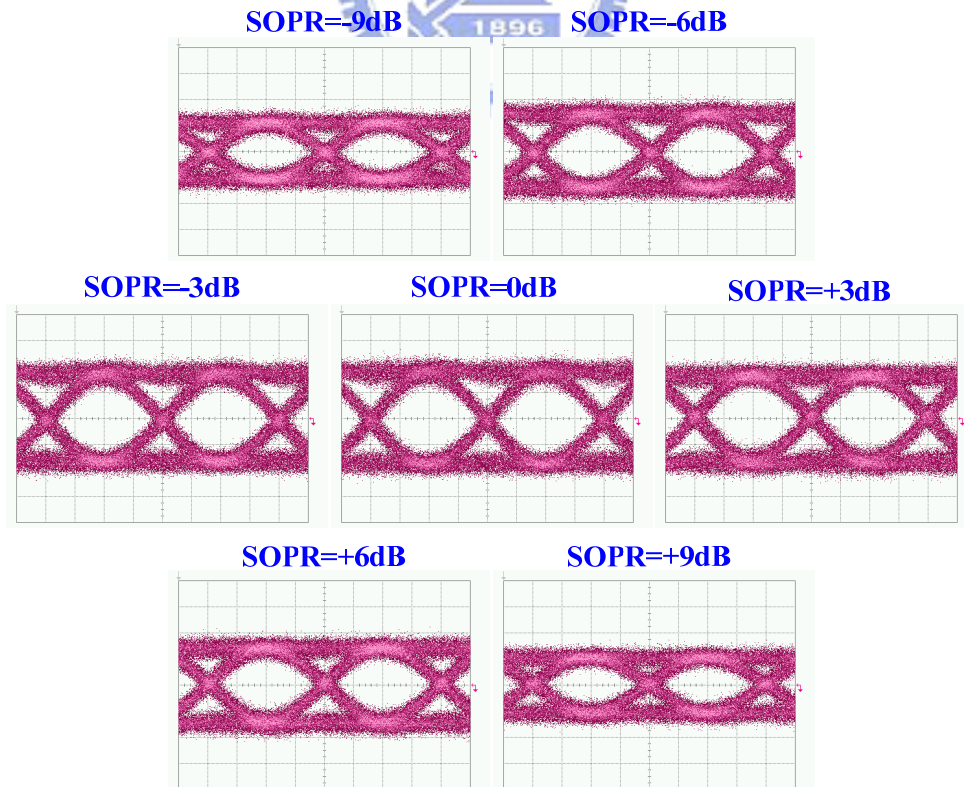


Figure 4-10 the eye diagrams for BPSK at 15GHz.

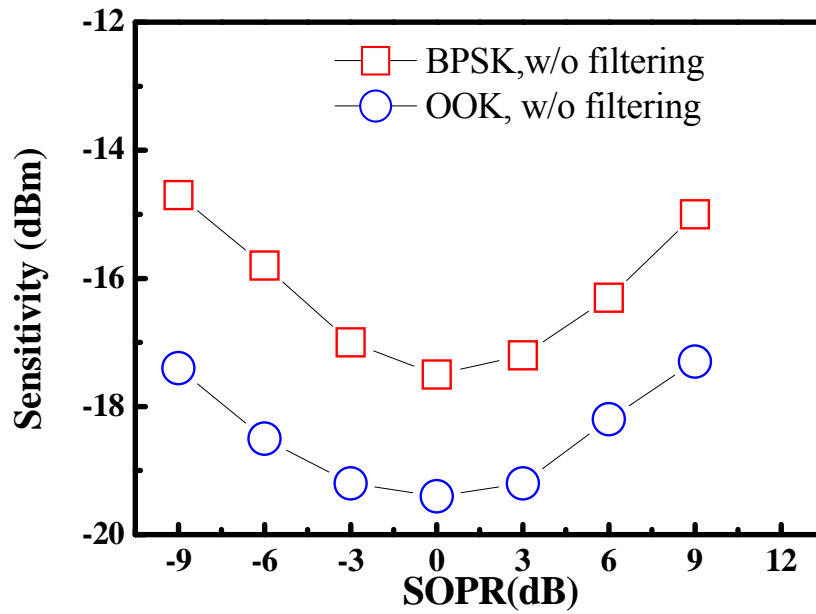


Figure 4-11 measured receiving sensitivity at BER=10⁻⁹ of OOK and BPSK signals versus SOPR.

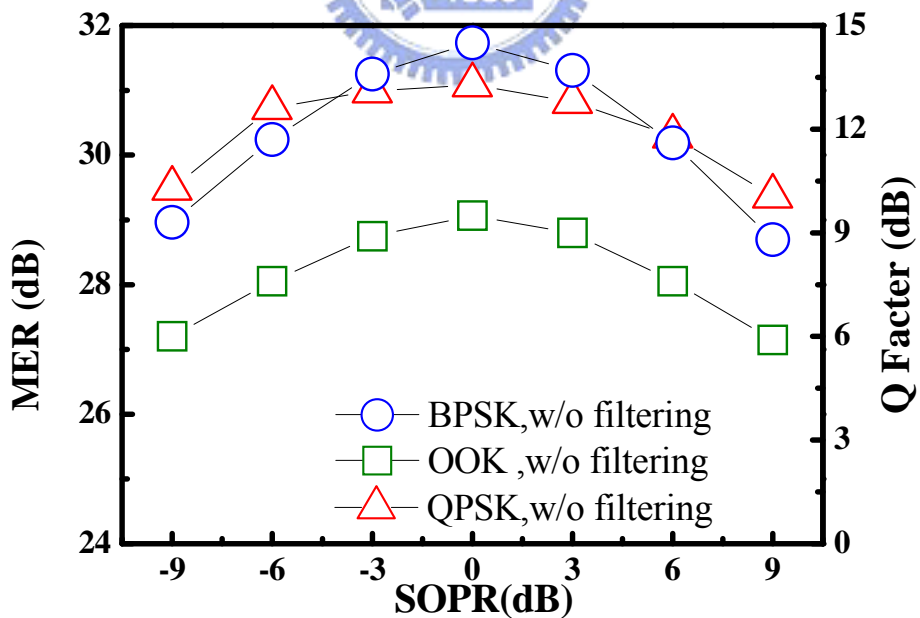


Figure 4-12 the simulation result of MER and Q factor for BPSK, OOK and QPSK.

4.3.3 Transmission results

Fig. 4-13 plots the BER curves of OOK, BPSK and QPSK signals without optical filtering using optimal SOPRs following 50-km SMF transmission. The receiver sensitivity penalty of RF signals increases with transmission length of SMF due to fiber dispersion. Fig. 4-14 and Fig. 4-15 show the eye diagrams for BPSK and OOK become smaller as transmission length increases. For QPSK signal the constellation and IQ eye diagram becomes smaller as transmission length increases is shown in Fig. 4-16.

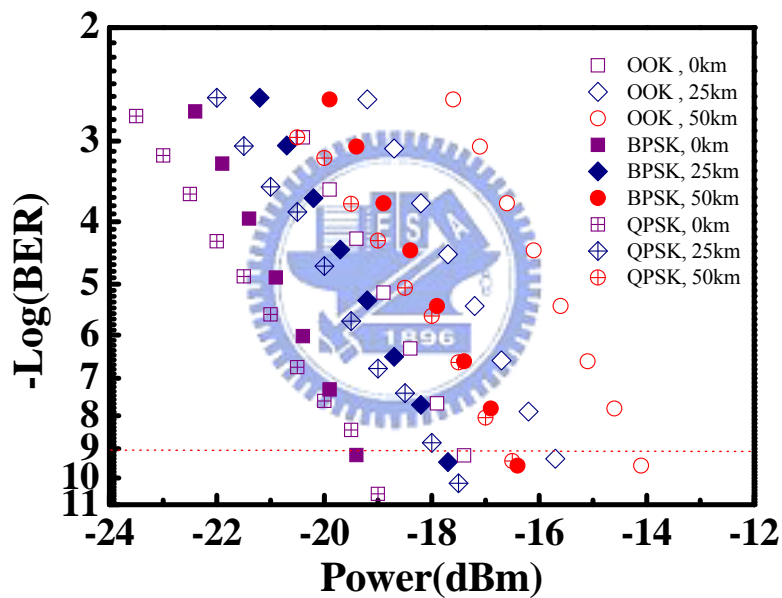


Figure 4-13 the BER curves of OOK, BPSK and QPSK signals.

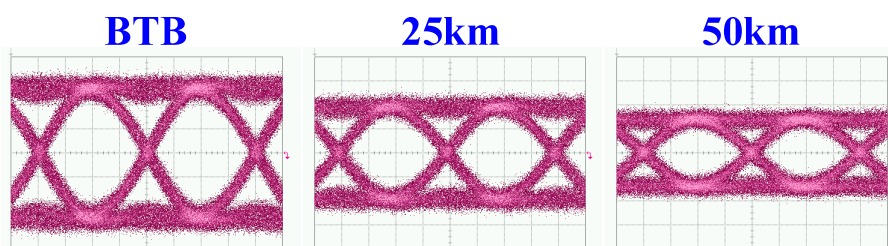


Figure 4-14 the eye diagrams for BPSK signal w/o filtering.

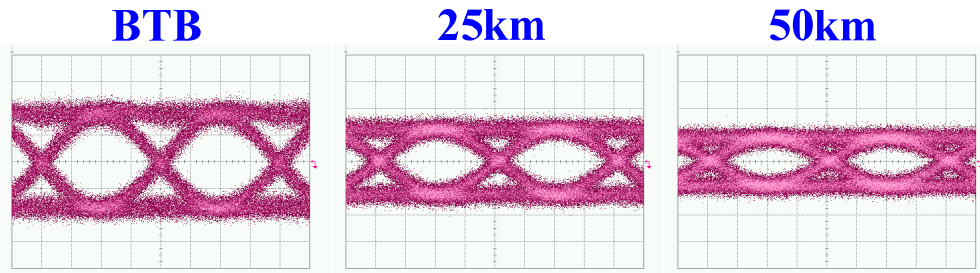


Figure 4-15 the eye diagrams for OOK signal w/o filtering.

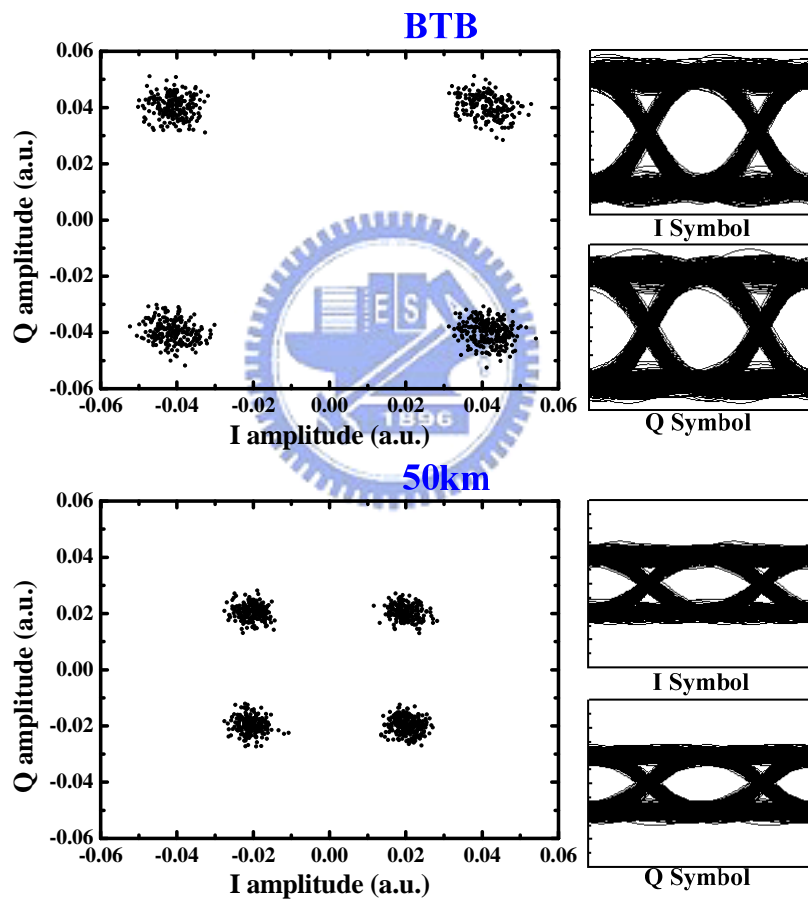
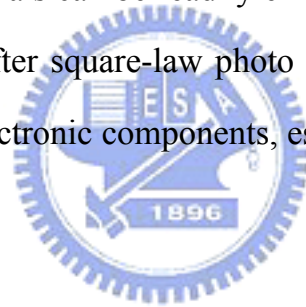


Figure 4-16 the constellations and I/Q eye diagram for QPSK signal.

4.4 Experimental setup for optical signal with optical filtering

The generated optical spectrum that has two upper-wavelength sidebands and two lower-wavelength sidebands with carrier suppression. After square-law photo detection, the optical RF signals have RF fading problem. The reason is that there are two sources for the generated 5-GHz or 15-GHz RF signal. For the 15-GHz RF signal, the cross terms of $USB2*LSB1$ and $USB1*LSB2$ will contribute the power of that. After standard single mode fiber (SMF) transmission, the relative phase of the two cross-term signal will change with transmitted length, resulting in performance fading. If an optical filter is utilized to remove anyone of the four optical subcarriers, the fading of both 5-GHz and 15-GHz RF signals can be readily eliminated. Notably, a frequency multiplication (1.5 times after square-law photo detection) scheme is adopted to reduce the cost of the electronic components, especially for RF signals in the millimeter-wave range.



4.4.1 Experiment setup

Fig. 4-17 displays the experimental setup for optical vector signal generation and transmission using a single-electrode MZM. At the remote node, a fiber Bragg grating filter removes the $LSB2$ or $LSB1$. After the photo receiver, the optical signal generates two RF signals with a difference frequency of 5 GHz (f_2-f_1) and a sum frequency of 15 GHz (f_1+f_2), respectively. In this study, we only consider the generated RF signal at 15 GHz. Insets (i) and (ii) of Fig. 4-17 show the receiver architectures of RF OOK/BPSK and QPSK signals, respectively.

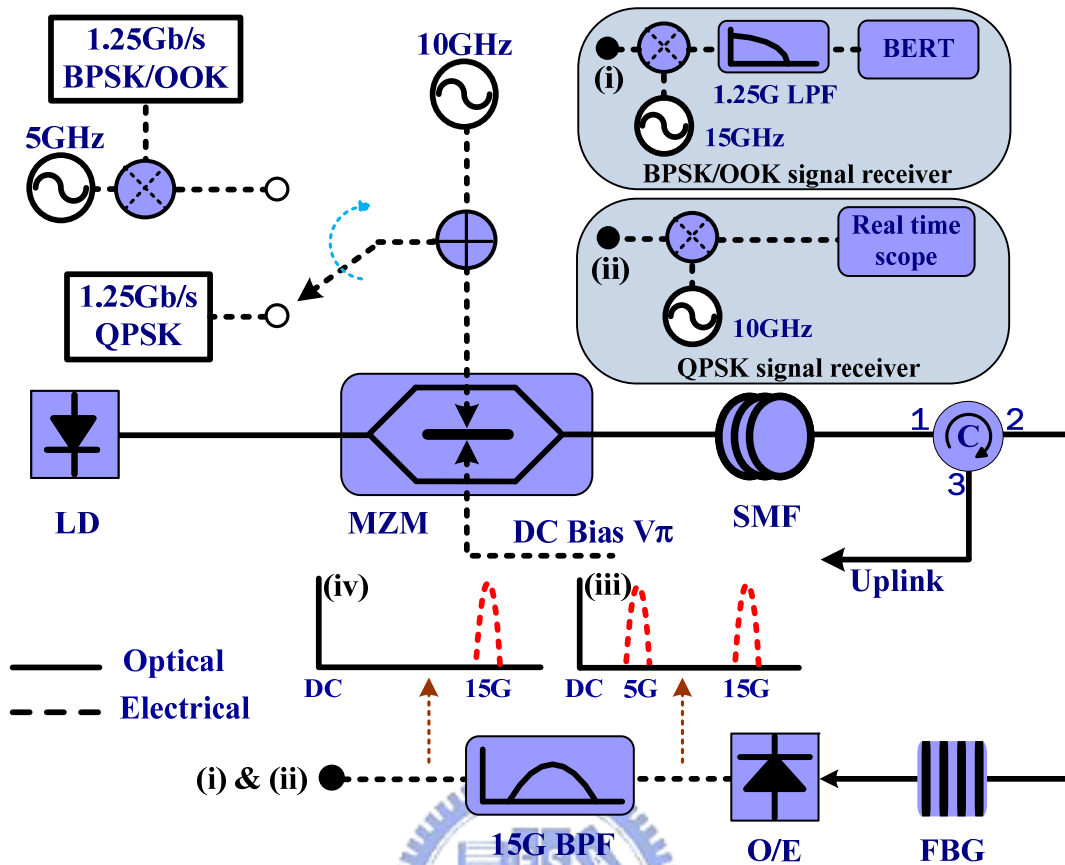


Figure 4-17 shows the experiment setup w/ optical filtering.

4.4.2 RF signals at sum frequency

Fig. 4-18 plots the optical spectrums for BPSK signals with filter out LSB2. Fig. 4-19 shows the simulation result of MER and Q factor for BPSK OOK and QPSK signals with optical filter out LSB2. The optimal SOPR is 3 dB. Fig. 4-20 shows the experimental results of receiver sensitivity at BER of 10^{-9} . Fig. 4-21 display the eye diagrams of BPSK signal with optical filter out LSB2. Fig. 4-22 plots the optical spectrums for BPSK signals with filter out LSB1. Fig. 4-23 shows the experimental results of receiver sensitivity at BER of 10^{-9} . Fig. 4-24 display the eye diagrams of BPSK signal with optical filter out LSB1. The experimental result is consistent with simulation.

Fig. 4-25 shows BER curves for optical signal when LSB2 is filtering out. The RF fading issue is overcome for all three signals. Fig. 4-26 shows the LSB2 is filter out, for QPSK signal the constellation and I/Q eye diagram is very clear after transmission. Fig. 4-27 shows the LSB1 is filter out, after 50km SMF transmission the constellation and I/Q eye diagram is still very clear.

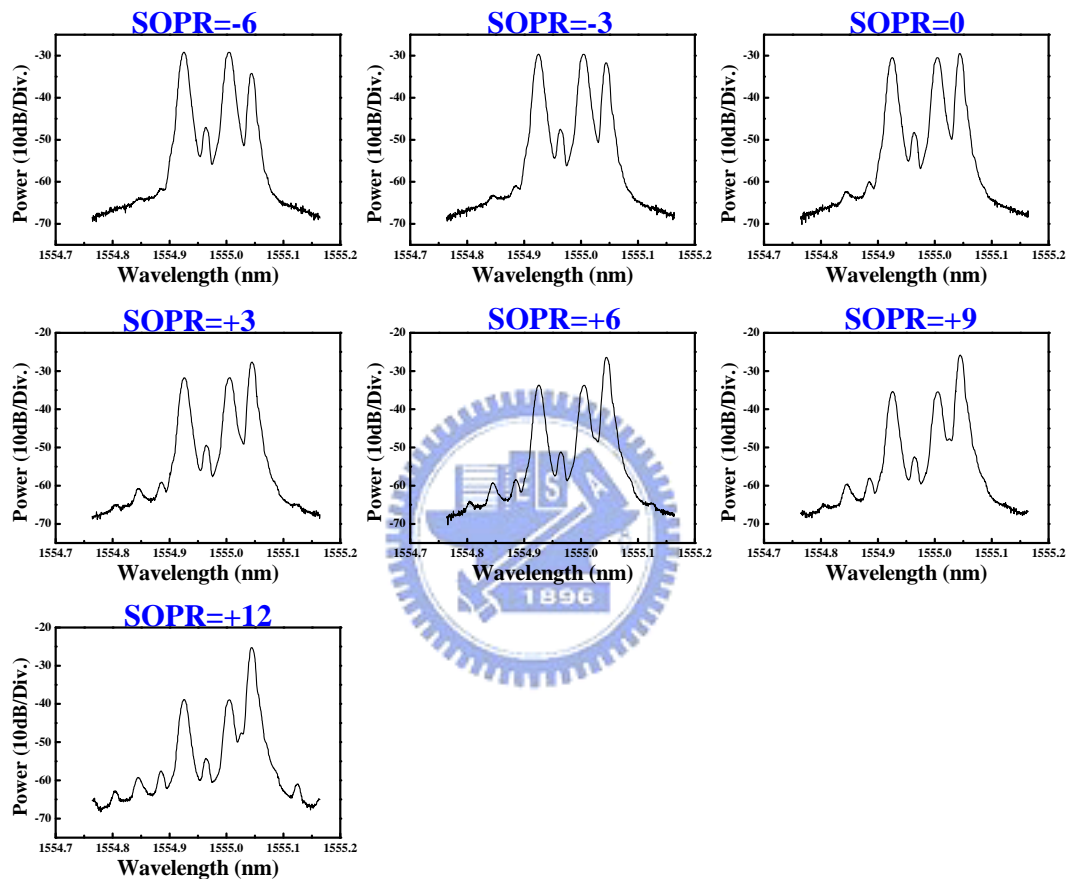


Figure 4-18 the optical spectrum w/ filter out LSB2.

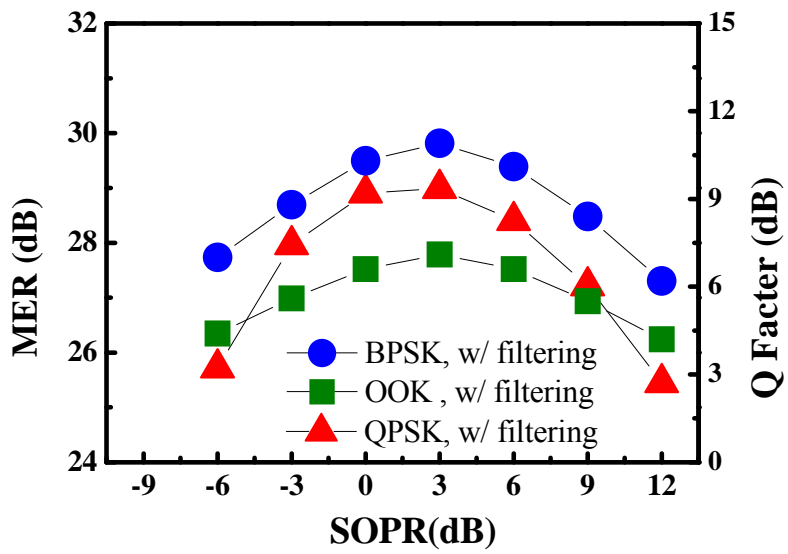


Figure 4-19 the simulation result of MER and Q factor for BPSK, OOK and QPSK.

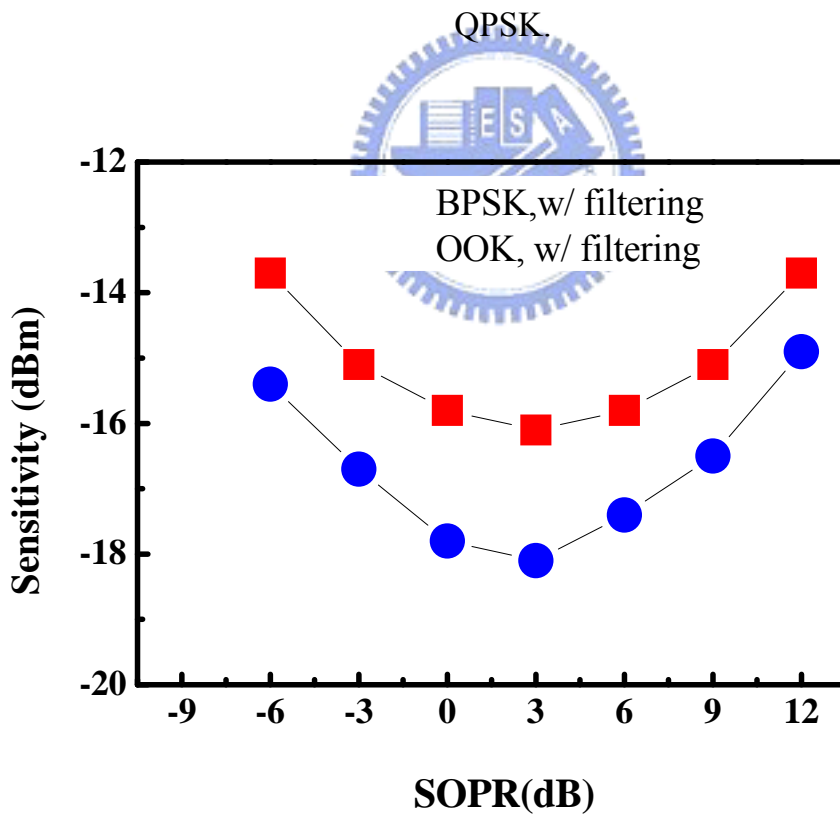


Figure 4-20 measured receiving sensitivity at BER=10⁻⁹ of OOK and BPSK signals versus SOPR.

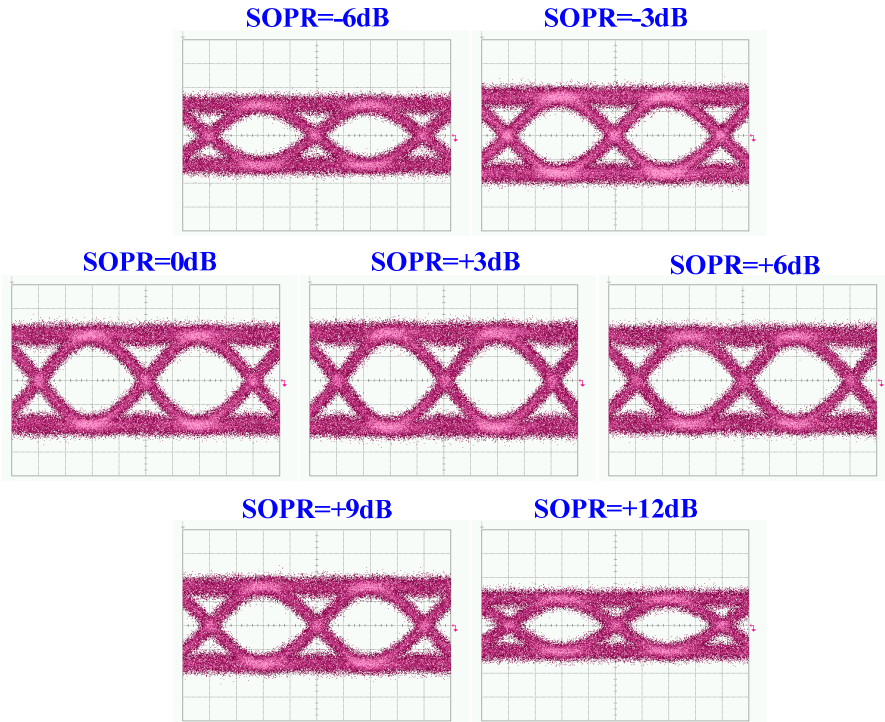


Figure 4-21 shows eye diagrams when the LSB2 is filter out.

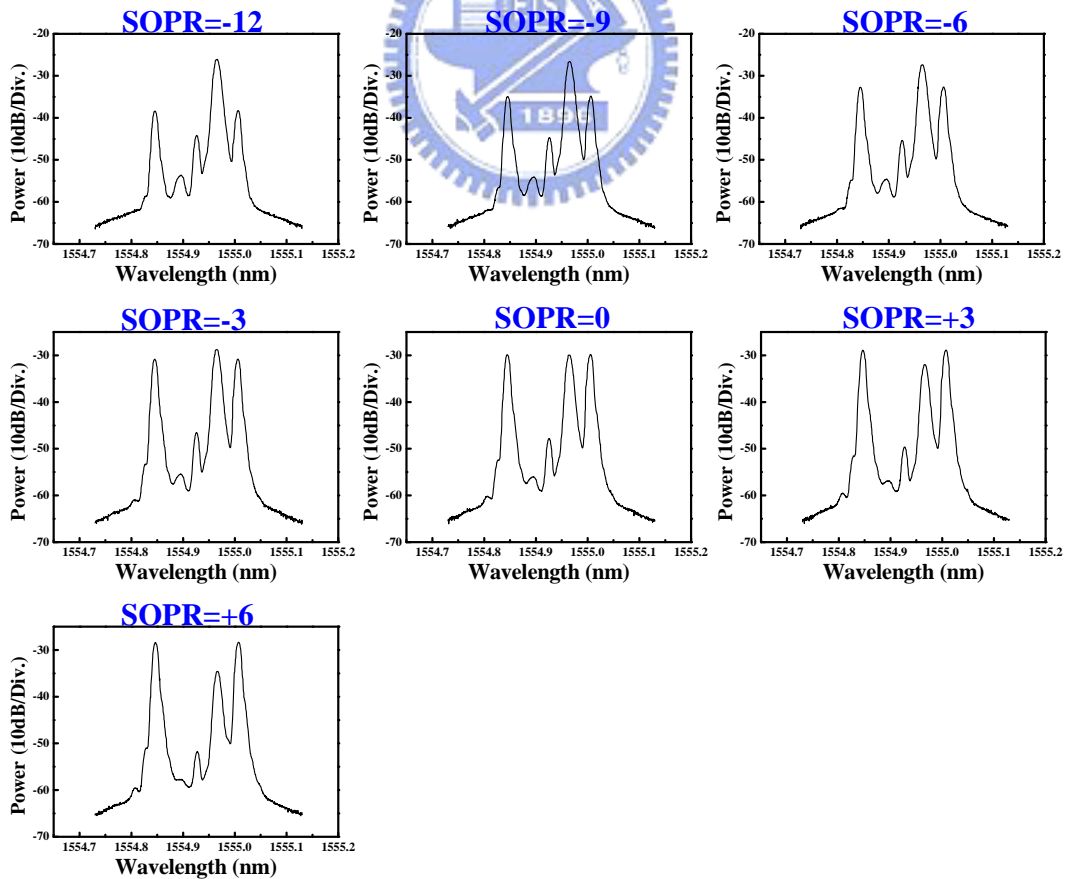


Figure 4-22 the optical spectrum w/ filter out LSB1.

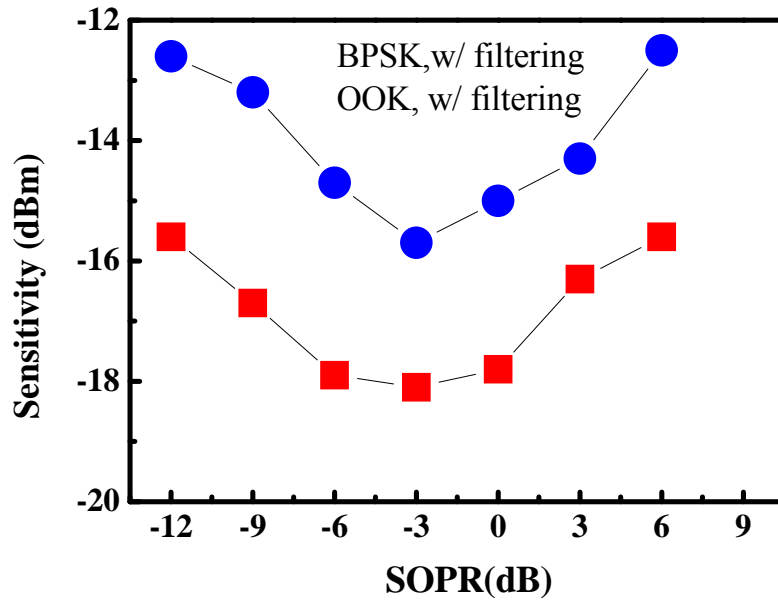


Figure 4-23 measured receiving sensitivity at BER=10⁻⁹ of OOK and BPSK signals versus SOPR w/ filter out LSB1.

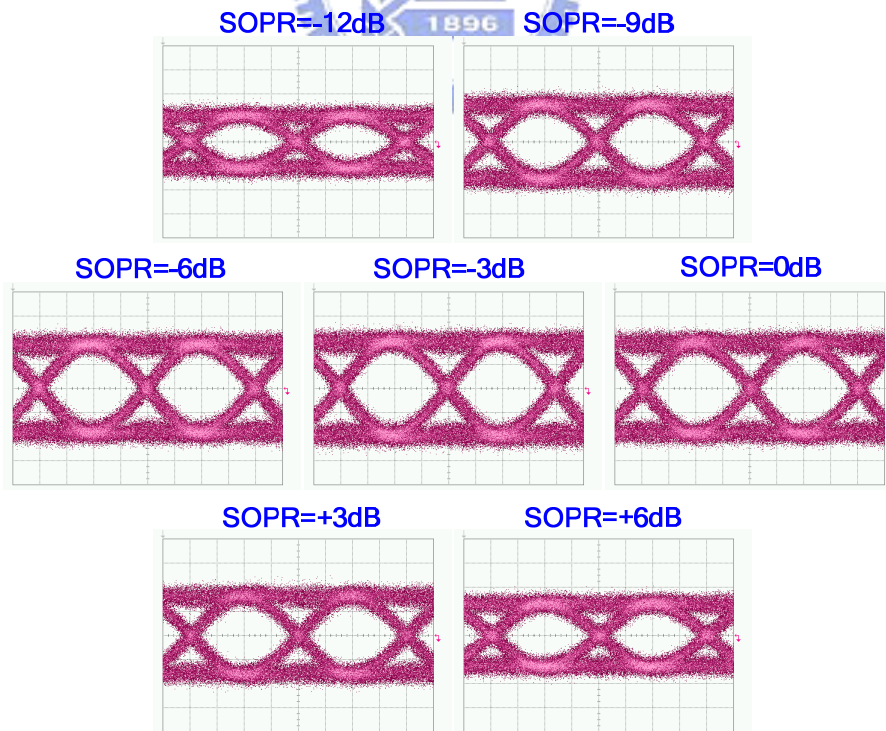


Figure 4-24 shows eye diagrams when the LSB1 is filter out.

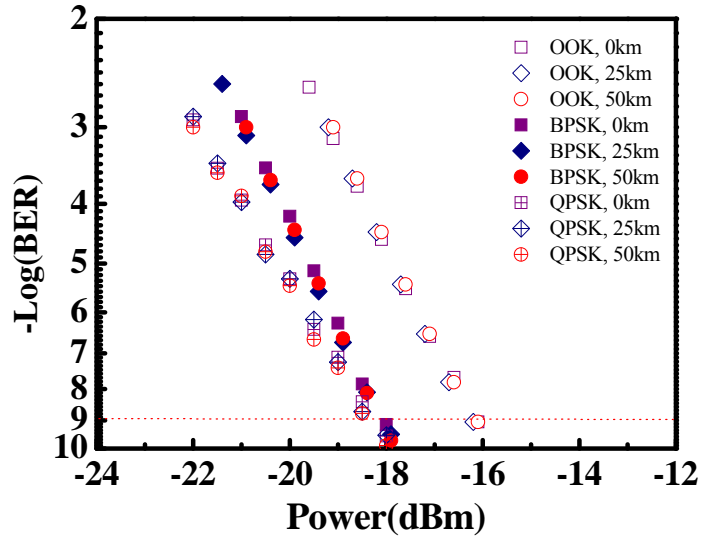


Figure 4-25 the BER curves of OOK, BPSK and QPSK signals.

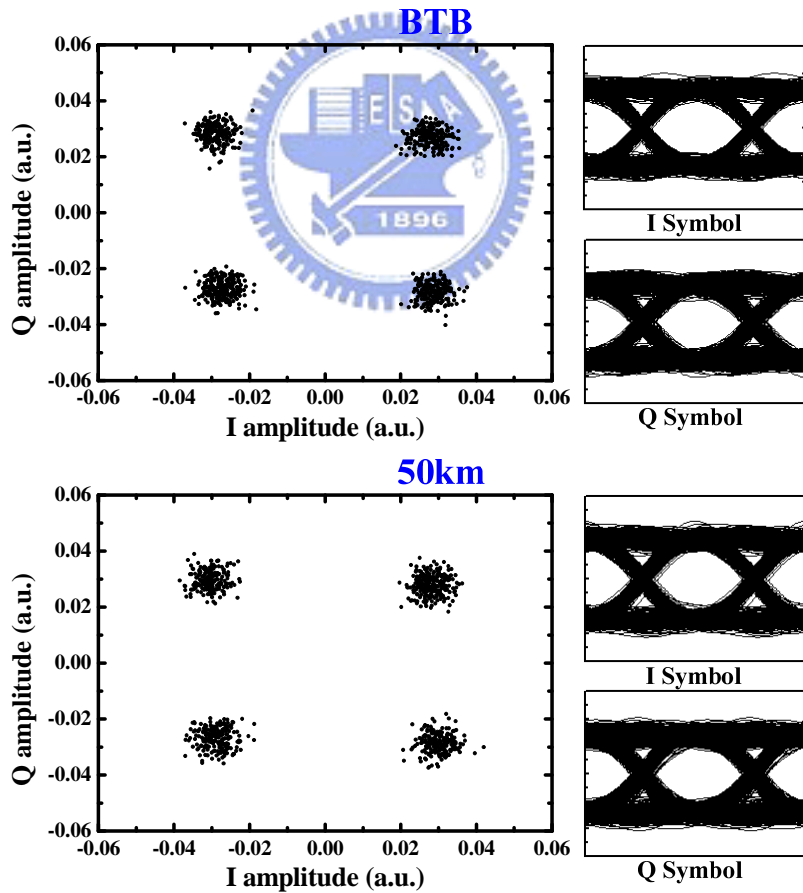


Figure 4-26 the constellations and I/Q eye diagram for QPSK signal w/ filter out LSB2.

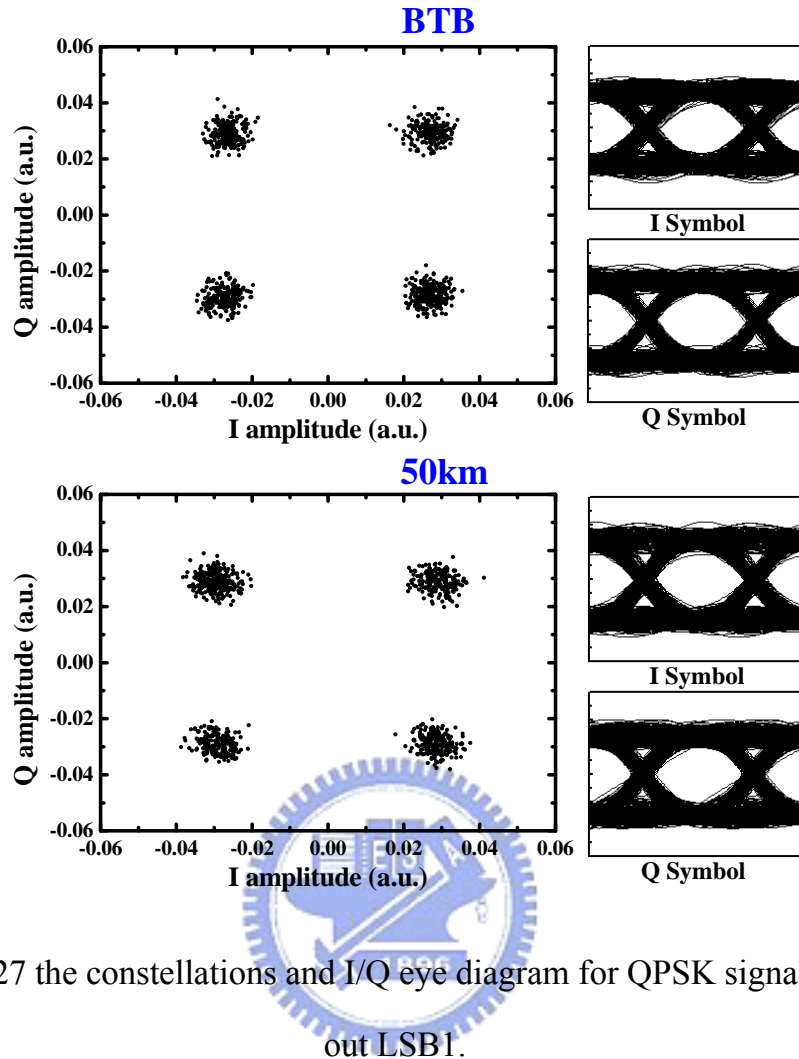


Figure 4-27 the constellations and I/Q eye diagram for QPSK signal w/ filter out LSB1.

4.4.4 RF signal at different modulation index

In chapter 3, the theoretical calculation results showed that the modulation index ($MI = V_{p-p} / 2V_{\pi}$, V_{p-p} is the peak-to-peak voltage of the MZM driving signal) for driving MZM increases, the optical power ratio and electrical power ratio will be reduced. We also demonstrated experimental results for the different modulation index for driving MZM. Fig. 4-28 shows the optical spectrum for BPSK and OOK RF signal when the LSB2 is filtered out. Fig. 4-29 shows the optical spectrum for BPSK and OOK RF signal when the LSB2 is filtered out. Fig. 4-30 shows the MZM driving RF PSK signal at 0.1, 0.2 and

0.3 modulation index when the LSB2 is filtering. And we also measured the RF OOK signal at different modulation index shown in Fig. 4-31. Fig. 4-32 shows the MZM driving RF PSK signal at 0.1, 0.2 and 0.3 modulation index when the LSB1 is filtering. And we also measured the RF OOK signal at different modulation index shown in Fig. 4-33. The same result with theoretical calculation is observed.

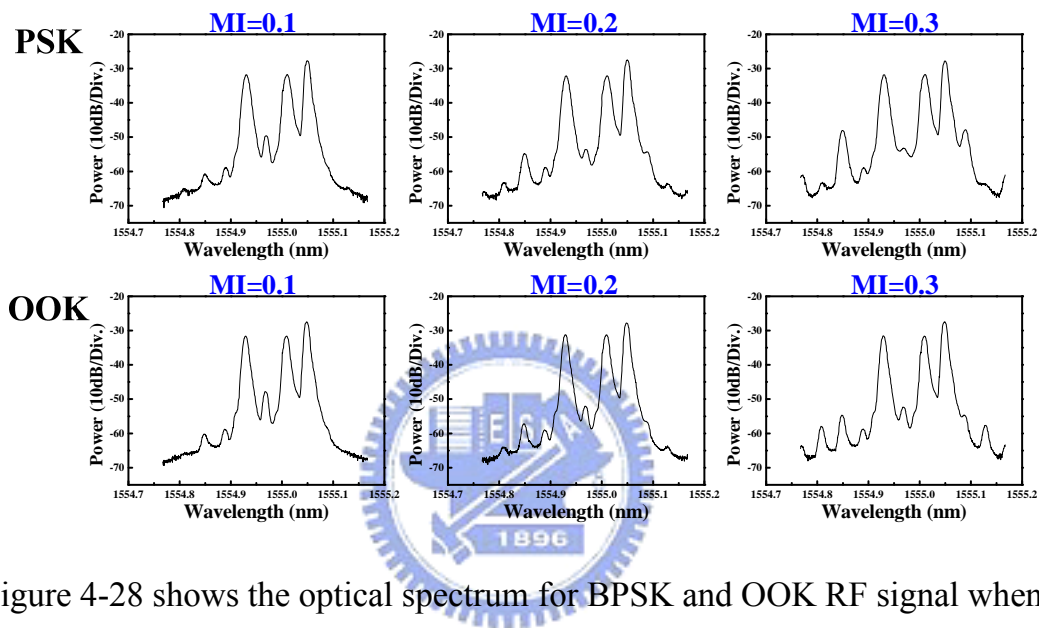


Figure 4-28 shows the optical spectrum for BPSK and OOK RF signal when the LSB2 is filter out.

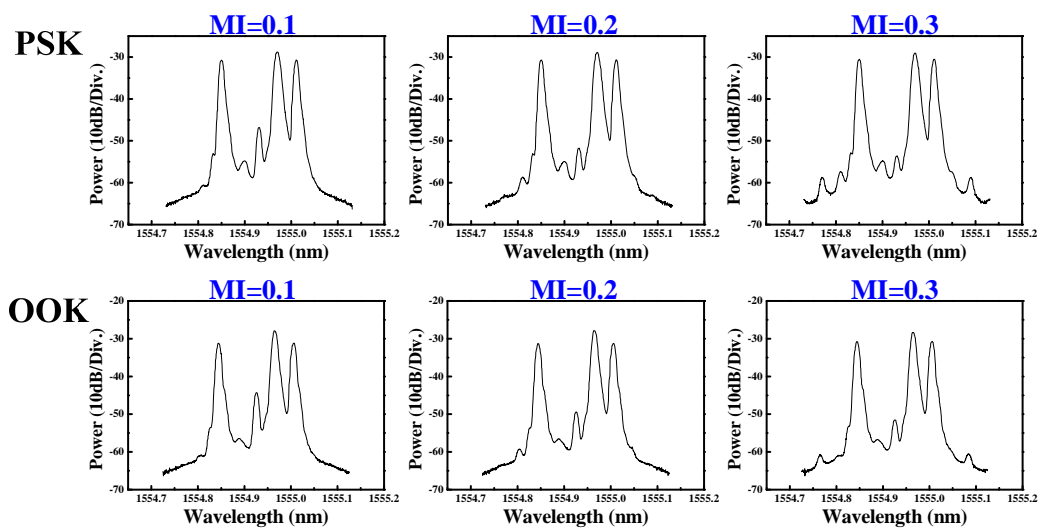


Figure 4-29 shows the optical spectrum for BPSK and OOK RF signal when the LSB1 is filter out.

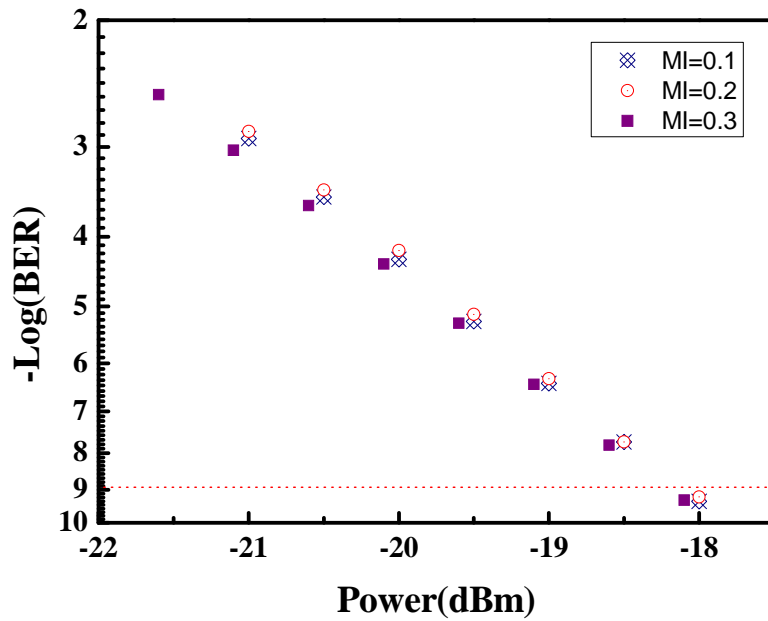


Figure 4-30 shows the BER curves for PSK signal in different MI when the LSB2 is filter out.

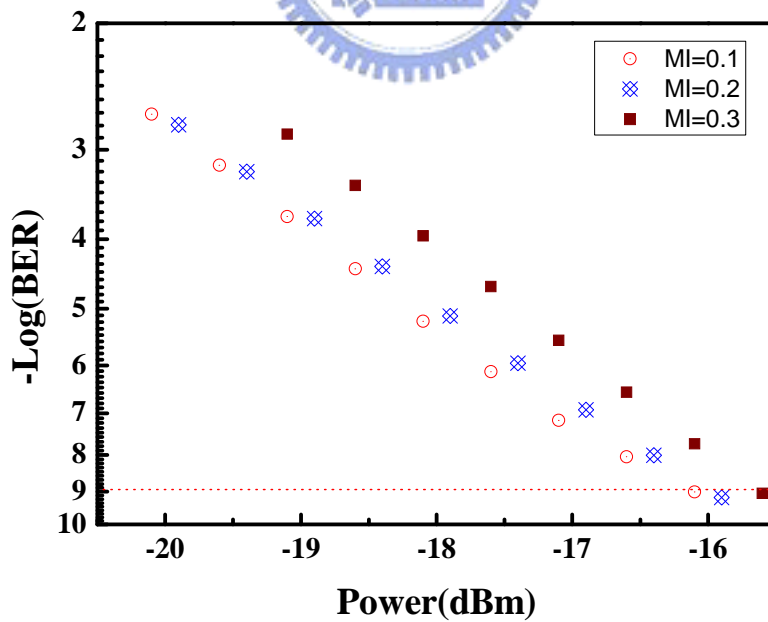


Figure 4-31 shows the BER curves for OOK signal in different MI when the LSB2 is filter out.

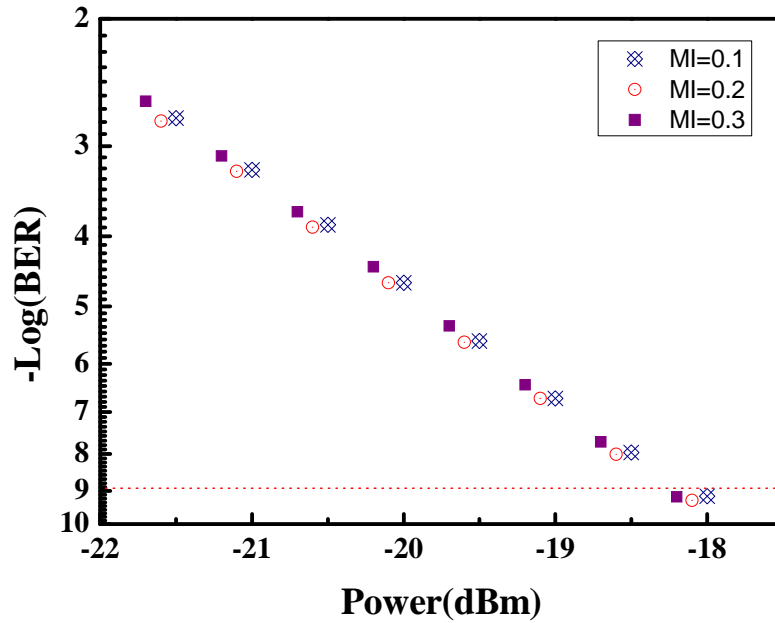


Figure 4-32 shows the BER curves for PSK signal in different MI when the LSB1 is filter out.

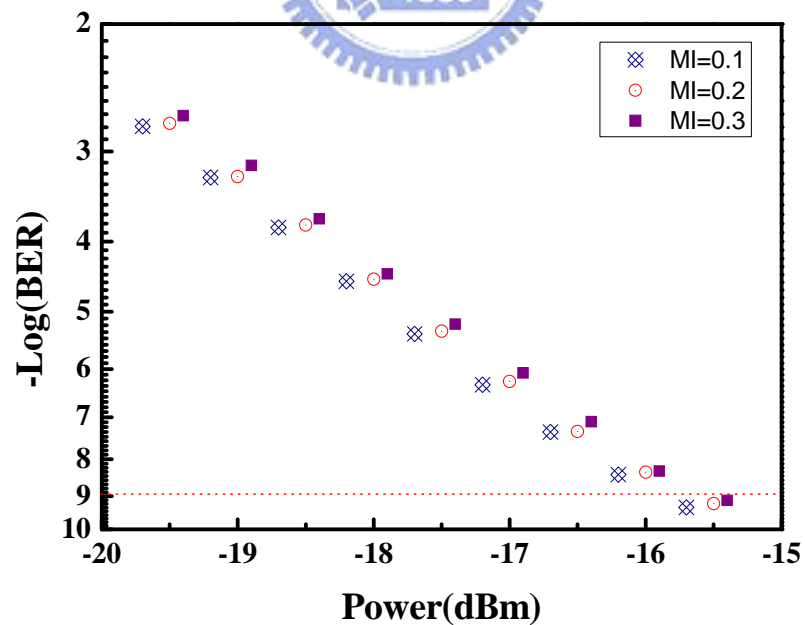


Figure 4-33 shows the BER curves for OOK signal in different MI when the LSB1 is filter out.

Chapter 5

Experimental Demonstration of OFDM Signal Generation

5.1 Introduction OFDM generation system

The combination of orthogonal frequency-division multiplexing (OFDM) and radio-over-fiber (RoF) systems (OFDM-RoF) has attracted considerable attention for future gigabit broadband wireless communication. The high peak to average power ratio (PAPR) and the nonlinear distortion of the optical transmitter are the main issues raised by OFDM and RoF systems, respectively. The optical radio frequency (RF) signal generation using an external Mach-Zehnder modulator (MZM) based on double-sideband (DSB), single-sideband (SSB), and double-sideband with optical carrier suppression (DSBCS) modulation schemes have been demonstrated. Since the optical RF signals are weakly modulated because of the narrow linear region of MZM, those that have undergone DSB and SSB modulation suffer from inferior sensitivities due to limited optical modulation index (OMI). Hence, an optical filter is needed to improve the performance. Furthermore, the DSB signal experiences the problem of performance fading because of fiber dispersion. Among these modulation schemes, DSBCS modulation has been demonstrated to be effective in the millimeter-wave range with excellent spectral efficiency, a low bandwidth requirement for electrical components, and superior receiver sensitivity following transmission over a long distance. However, all of the proposed DSBCS schemes can only support on-off keying (OOK) format, and none can transmit vector modulation formats, such as phase shift keying (PSK), quadrature amplitude modulation (QAM), or OFDM signals, which are of

utmost importance for wireless applications.

On the other hand, optical RF signal generations using remote heterodyne detection (RHD) have been also demonstrated. The advantage of RHD systems is that the vector signal can be modulated at baseband. Therefore, the bandwidth requirement of the transmitter is low. However, the drawback is that phase noise and wavelength stability of the lasers at both transmitter and receiver should be carefully controlled.

This work presents a novel method for optical RF signal generation using the DSBCS modulation scheme that can carry vector signals. Both 5-Gb/s 16-QAM OFDM signal using proposed transmitter for ROF downstream link and 1.25-Gb/s on-off-keying signal via reflective semiconductor optical amplifier (RSOA) for upstream link are demonstrated. Negligible penalty is observed after 25-km single mode fiber (SMF) transmission.

5.2 Experimental Concept and Setup

Fig. 5-1 schematically depicts the concept of the proposed optical OFDM signal generation using a single-electrode MZM. The MZM driving signal consists of an OFMD signal at a frequency f_1 modulated and a sinusoidal signal with a frequency of f_2 , as indicated in insets (i)-(iii) of Fig. 5-1, respectively. To realize the DSBCS modulation scheme, the MZM is biased at the null point. Inset (iv) in Fig. 5-1 presents the generated optical OFDM spectrum that has two upper-wavelength sidebands (USB1, USB2) and two lower-wavelength sidebands (LSB1, LSB2) with carrier suppression. At the remote node, the LSB2 subcarrier is filtered out for the upstream data link, and the rest of the signal is sent to local users. After square-law photo detection, the optical signal generates two electrical RF signals at the difference frequency

(f_2-f_1) and the sum frequency (f_2+f_1) . Notably, a frequency multiplication (a sum frequency) scheme is achieved to reduce the bandwidth requirement of the OFDM transmitter, which is important for RF OFDM signals at millimeter-wave range. Therefore, we only consider the generated RF OFDM signal at the sum frequency (f_2+f_1) in this paper. Furthermore, the OFDM can be modulated at lower frequency to obtain higher signal-to-noise ratio due to lower noise figure (NF) of electrical MZM amplifier.

Note that the filtering out of LSB2 subcarrier not only provides an upstream light source but also eliminates performance fading due to fiber dispersion. As presented in Fig. 5-2, f_1 and f_2 at frequencies of 3.7 GHz and 16.3 GHz are used to simulate the performance fading. The generated RF signals at the sum frequencies of 20 GHz suffer performance fading before filtering. The reason is that there are two sources for the generated 20-GHz RF signal. The cross terms of $USB_2 \times LSB_1$ and $USB_1 \times LSB_2$ will contribute the power of the generated 20-GHz RF signal. After standard single mode fiber (SMF) transmission, the relative phase of the two generated cross-term signal will change with transmitted length, resulting in performance fading. If an optical filter is utilized to remove anyone of the four optical subcarriers, 20-GHz RF signal fading can be eliminated.

Fig. 5-3 depicts the experimental setup of the proposed OFDM signal generation. The block diagram of the typical OFDM transmitter is shown in Fig. 5-4(a). The OFDM signals are generated by a Tektronix AWG7102 arbitrary waveform generator (AWG) using a Matlab program. The sample rate and digital-to-analogue converter resolution of the AWG are 20 Gb/s and 8 bits, respectively. The IFFT length is 512. A 39.0625-MSym/s 16-QAM symbol is encoded at channel 80 to 111 (i.e. in the subcarrier center frequency range from

3.125 to 4.3359375 GHz.) with the remaining 480 channels set to zero. A sinusoidal subcarrier with a frequency of 16.3 GHz is utilized. Therefore, an optical 5-Gb/s 16-QAM OFDM signal that has 32 subcarriers and occupies a total bandwidth of 1.25 GHz can be generated at a center frequency of 20 GHz. The cyclic prefix is set to 1/256 symbol time to combat fiber dispersion.

At base station, a fiber Bragg grating filter removes the LSB2 for the upstream data link and LSB2 is modulated with a 1.25-Gb/s OOK signal via RSOA. Note that LSB2 filtering can overcome the RF fading and the generated OFDM spectrum and constellation are clearly observed as shown in insets (i) and (iii) of Fig. 5-2. After square-law photo detection, a 5-Gb/s 16-QAM OFDM signal at a sum frequency of 20 GHz is generated. In RoF applications, this signal can be directly utilized for wireless transmission. For intermediate frequency (IF) demodulation, the OFDM signal is down-converted to 3.7GHz by a 16.3GHz oscillator and a mixer and the waveform is captured by a Tektronix DPO 71254 with a 50-Gb/s sample rate and a 3-dB bandwidth of 12.5 GHz. The block diagram of the typical OFDM receiver is shown in Fig. 5-4(b). The off-line DSP program using matlab is employed to demodulate the OFDM signal. The demodulation process includes synchronization, Fast Fourier Transform (FFT), one-tap equalization, and QAM symbol decoding. The bit error rate (BER) performance is calculated from the measured error vector magnitude (EVM)

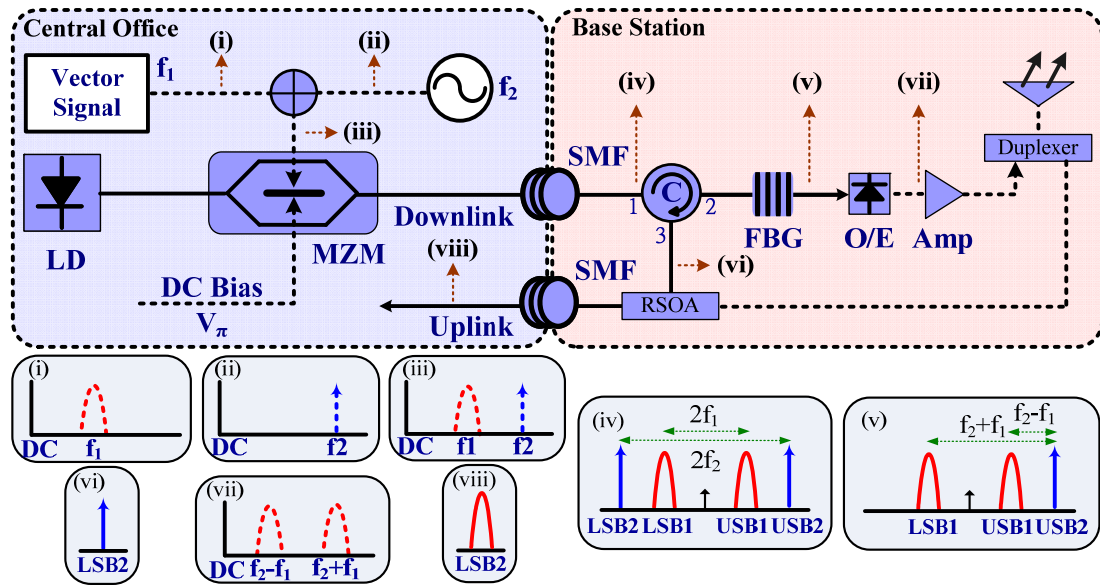


Figure 5-1 Conceptual diagram of generating optical OFDM-RoF signals.

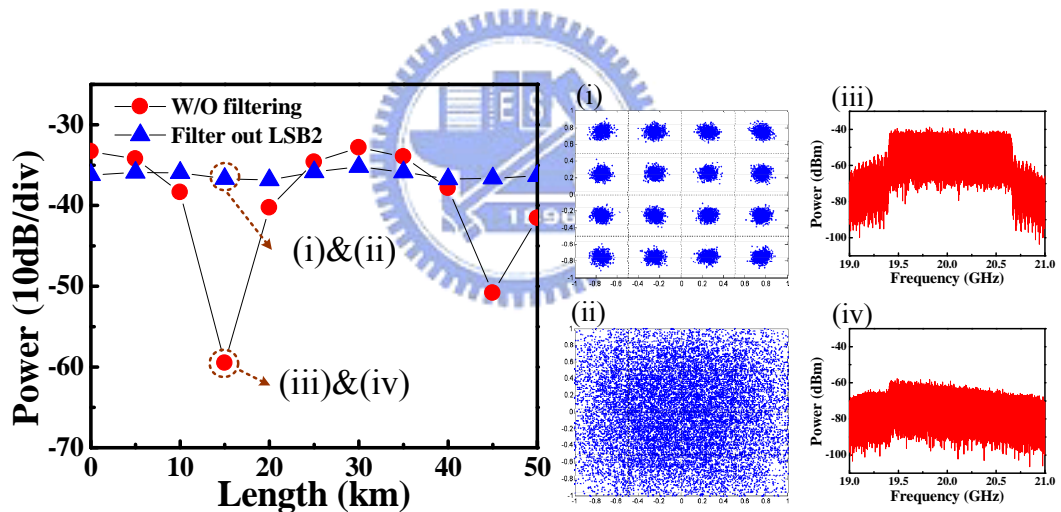


Figure 5-2 Simulation of RF performance fading versus SMF transmission length.

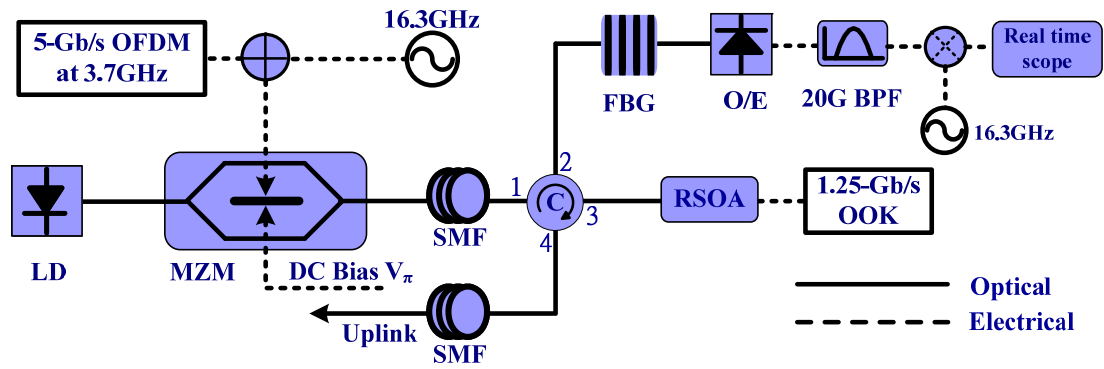


Figure 5-3 Experimental setup of optical RF OFDM signal generation.

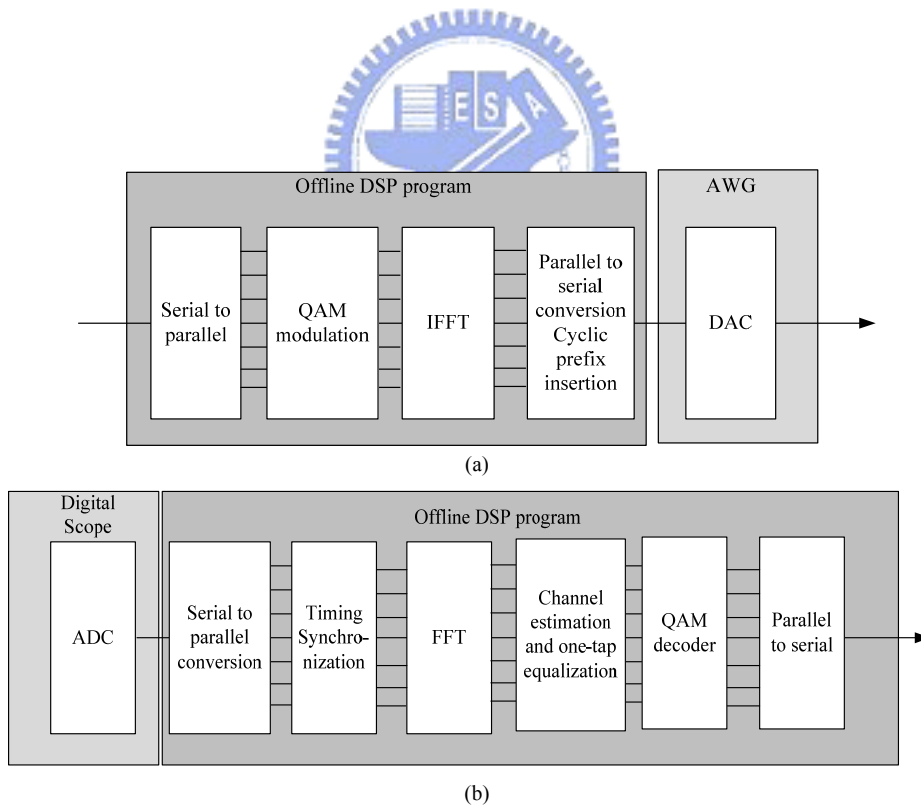


Figure 5-4 Block diagrams of OFDM transmitter (a) and receiver (b).

5.3 Experimental Results and Discussions

The optical power ratio (OPR) of the optical subcarrier to the optical OFDM-modulated subcarrier strongly influences the performance of the optical OFDM signals [4]. One of the advantages of the proposed OFDM transmitter is that the relative intensity between optical subcarrier and OFDM-modulated subcarrier can be easily tuned by adjusting the individual amplitude of the sinusoidal signal and the OFDM signal to optimize the OFDM performance. Fig. 5-5 illustrates the receiver sensitivity of the OFDM signals versus different OPRs. For OFDM signals without filtering out LSB2, the optimal OPR is 1 dB. As LSB2 is filtered out, the optimal OPR is 4 dB. As LSB1 is filtered out, the optimal OPR is -3 dB. Fig. 5-6(a) shows the optical spectrum without filtering. Fig. 5-6(b) and Fig. 5-6(c) show the optical spectrum with filter out LSB2 and LSB1, respectively. At the Base station, the LSB2 subcarrier is filtered out for the upstream data link and the rest of the signal is sent to local users. After fiber bragg grating, the optical spectrum is shown in Fig. 5-6(d). The optical carrier to noise ratio for wavelength reuse is 20dB. And then the LSB2 provides wavelength reuse for uplink via RSOA. After RSOA, the optical spectrum is shown in Fig. 5-6(e). The optical reuse signal to noise ratio is 15dB. Fig. 5-7(a) shows the electrical spectrum after AWG. This driving RF OFDM signal includes vector signal combined with a sinusoidal signal shown in Fig. 5-7(b). Fig. 5-7(c) shows the electrical spectrum after photo receiver. In order to demodulator the RF OFDM signal, the signal is down-converted to 3.7GHz by a mixer, as shown in Fig. 5-7(d). Fig. 5-8 shows OFDM constellation diagrams before and after the one-tap equalizer in back-to-back (BTB)

and following 25-km SMF transmission cases. After equalizer, a clear constellation can be achieved. Fig. 5-8(a)(b)(c) shows the constellation diagrams without optical filtering. Fig. 5-8(d)(e)(f) and Fig. 5-8(g)(h)(i) show the constellation diagrams with filter out LSB2 and LSB1, respectively. After filtering out LSB2 or LSB1, the generated OFDM signals do not suffer RF periodic fading issue due to fiber dispersion. Only in-band distortion of the OFDM-encoded subcarrier caused by fiber dispersion is considered. Since the symbol rate of each subcarrier is only 39.0625 MSym/s, the fiber chromatic penalty can be ignored. Fig. 5-9 shows the BER curves of the downstream 5-Gb/s 16-QAM OFDM signal using optimal OPRs and the upstream 1.25-Gb/s OOK signal after transmission over 25 km SMF. For optical downstream signal, when any optical subcarrier is filter out the sensitivity penalties are negligible. If the optical signal without filtering the sensitivity penalties is 0.5dB. We also measure the BER curves of uplink 1.25-Gb/s OOK signal. After transmission over 25 km SMF, the sensitivity penalty is 0.5 dB. And the eye diagraph little change for BTB and after transmission over 25km SMF is shown in inset (i)(ii).

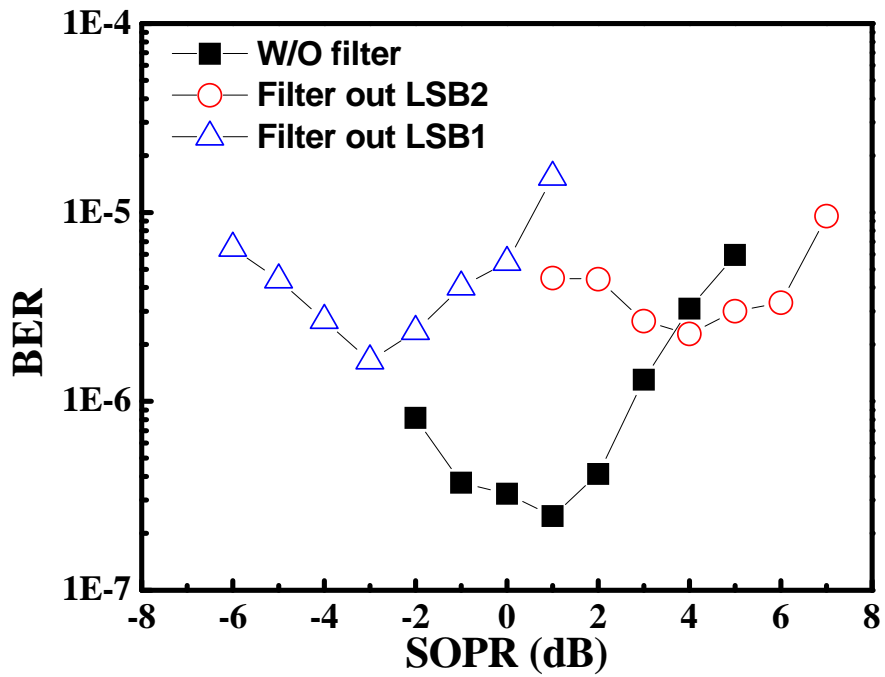


Figure 5-5 BER versus different OPRs.

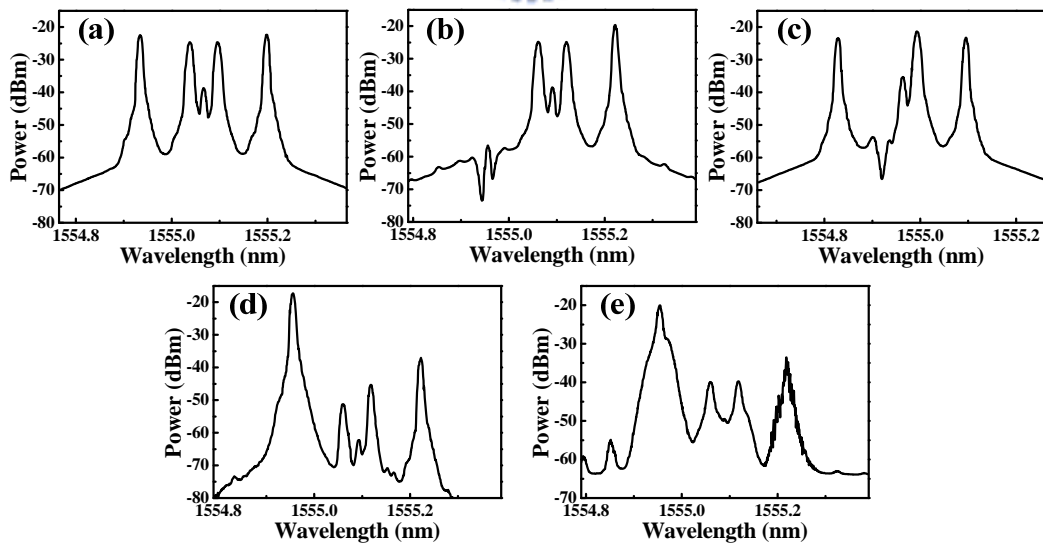


Figure 5-6 Optical spectra of RF signals.

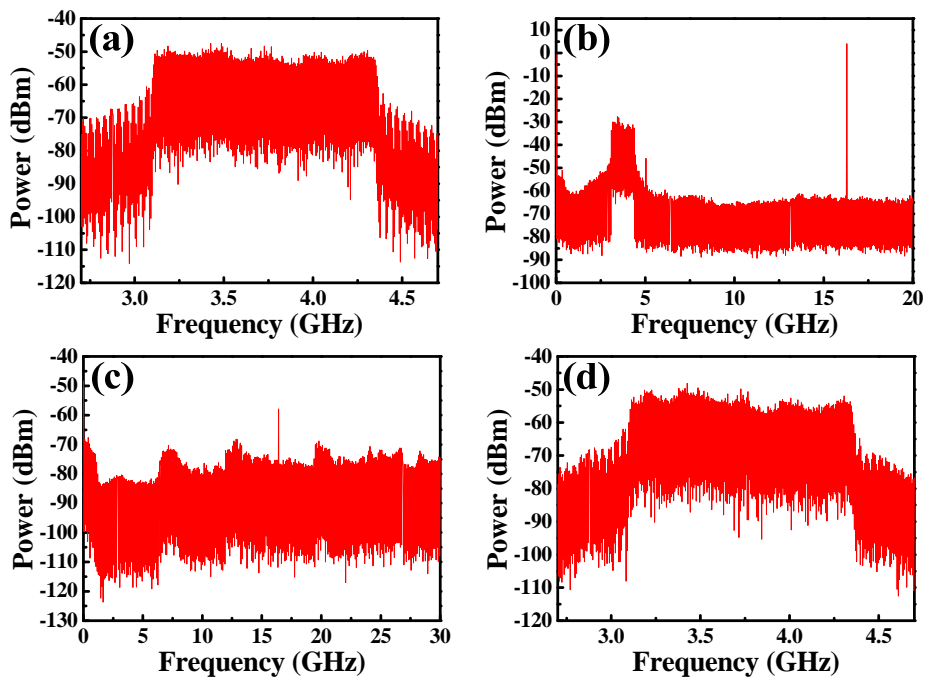


Figure 5-7 Electrical spectra of OFDM signals.



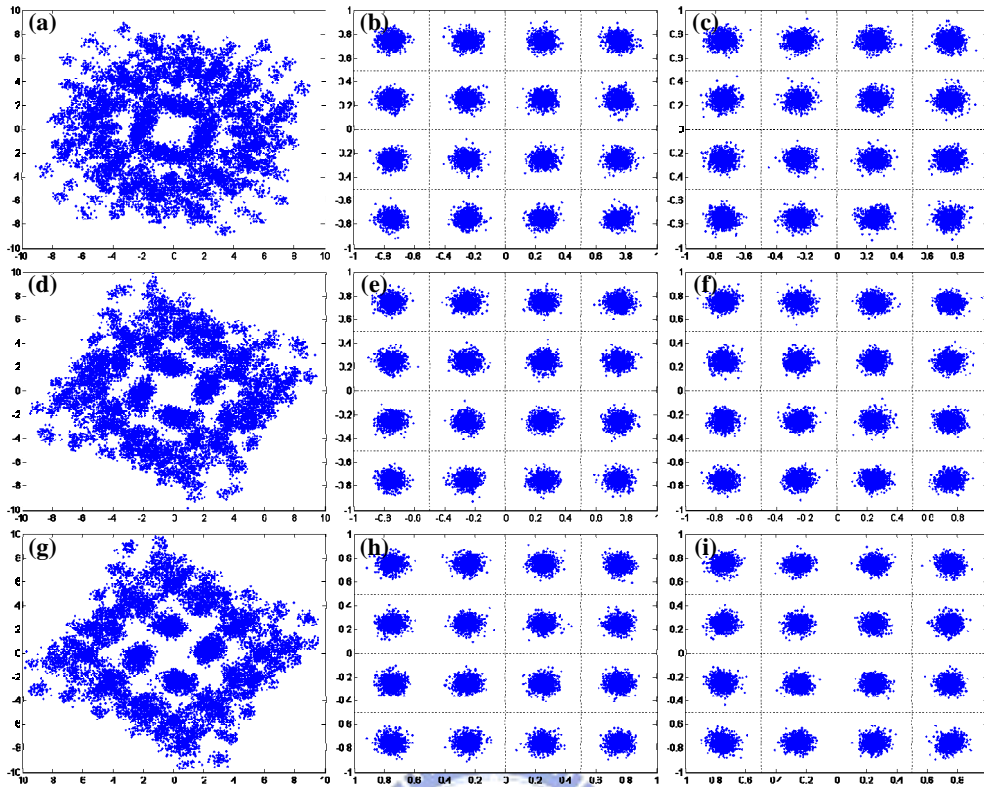


Figure 5-8 Constellations of OFDM signal

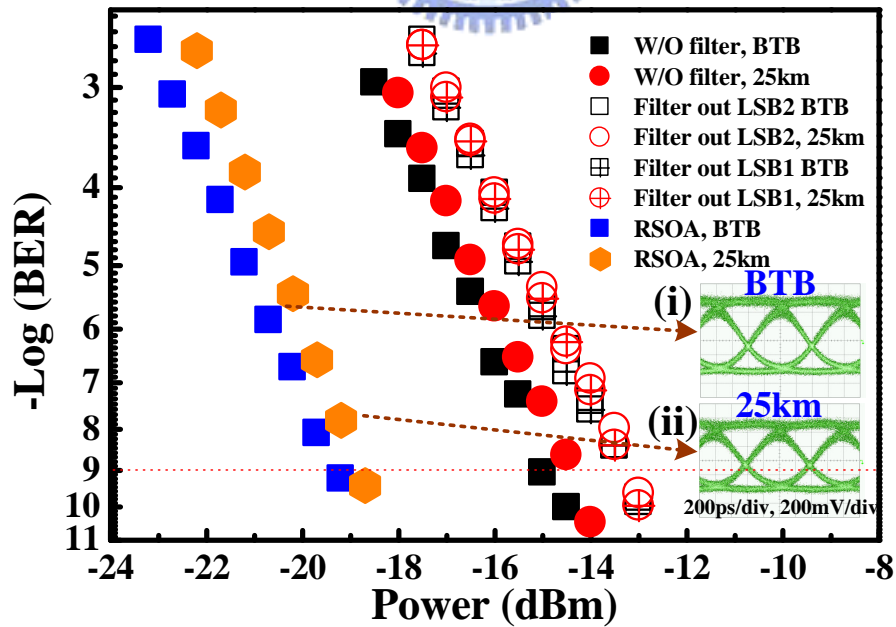


Figure 5-9 BER curves of the downstream and the upstream signal.

Chapter 6

Conclusion

This work presents a new modulation approach to generate optical vector signals by frequency multiplication based on a DSBCS scheme. Compared with conventional DSBCS modulation using MZM which can support vector signals, the proposed modulation using single-electrode MZM needs lower bandwidth requirement and also support vector signal.

First, we provide the theoretical calculations, including optical nonlinear distortion, electrical nonlinear distortion and optical power ratio. When the modulation index increased, optical and electrical nonlinear distortion of the results is become worse. When the optical signal without filtering, the optimal optical power ratio is 0dB. When the optical signal filters out LSB1 and LSB2 the optimal power ratio is 3dB and -3dB, respectively. Second, we experimental demonstrate three different modulation formats of 1.25-Gb/s OOK, 1.25-Gb/s BPSK and 625-MSym/s QPSK signals are adopted to determine the system performance. For RF signal generation without filtering out any subcarrier, the optimal SOPR of both BPSK and OOK RF signals is 0 dB. When LSB2 is filtered out, the optimal SOPR of both BPSK and OOK RF signals is 3 dB. When LSB1 is filtered out, the optimal SOPR is shifted to -3 dB. After transmission over 50 km SMF, the power penalty of all three modulation formats is less than 0.2 dB. QPSK format has twice the spectral efficiency and approximately 2-dB better receiving sensitivity than the OOK format. Final, we apply this system to transmit OFDM signal. ROF systems supporting OFDM signals that have been widely utilized in RF-wireless communication are of utmost importance to extent transmission distance over

fiber and air links. The data rate of 16-QAM OFDM signal is 5-Gb/s and the center frequency is about 3.7GHz and the sinusoidal signal frequency is 16.3GHz. For the downstream OFDM signal after transmission over 25km SMF, the sensitivity penalty is less than 0.1 dB. We also demonstrate wavelength reuse via reflective semiconductor optical amplifier for 1.25-Gb/s OOK signal upstream data link. After transmission over 25 km SMF, the sensitivity penalty is 0.5 dB.



REFERENCES

- [1] A. J. Lowery and J. Armstrong, "Orthogonal-frequency-division multiplexing for dispersion compensation of long-haul optical systems," *Opt. Express* 14, 2079-2084 (2006).
- [2] I. B. Djordjevic and B. Vasic, "Orthogonal frequency division multiplexing for high-speed optical transmission," *Opt. Express* 14, 3767-3775 (2006).
- [3] H. Bao and W. Shieh, "Transmission simulation of coherent optical OFDM signals in WDM systems," *Opt. Express* 15, 4410-4418 (2007).
- [4] W. H. Chen, and W. I. Way, "Multichannel Single-Sideband SCM/DWDM Transmission System," *J. Lightwave Technol* 22, 1697-1693 (2004).
- [5] C. Wu, and X. Zhang, "Impact of Nonlinear Distortion in Radio Over Fiber Systems with Single-Sideband and Tandem Single-Sideband Subcarrier Modulations," *J. Lightwave Technol.* 24, 2076-2090 (2006).
- [6] J. Yu, Z. Jia, L. Yi, G. K. Chang, and T. Wang, "Optical millimeter wave generation or up-conversion using external modulators," *IEEE Photon. Technol. Lett.* 18, 265-267 (2006).
- [7] J. J. O'Reilly, P. M. Lane, R. Heidemann, and R. Hofstetter, "Optical generation of very narrow linewidth millimeter wave signals," *Electron. Lett.* 28, 2309-2311 (1992).
- [8] C. Lim, M. Attygalle, A. Nirmalathas, D. Novak, and R. Waterhouse, "Analysis of Optical Carrier-to-Sideband Ratio for Improving Transmission Performance in Fiber-Radio Links," *IEEE Trans. Microwave Theory Technol.* 54, 2181-2187 (2006).
- [9] L. N. Langey, M. D. Elkin, C. Edge, M. J. Wale, U. Gliese, X. Huang, and A. J. Seeds, "Packaged semiconductor laser optical phase-locked loop (OPLL) for photonic generation, processing and transmission of microwave signals," *IEEE Trans. Microwave Theory Technol.* 47, 1257-1264 (1999).

- [10] C. S. Choi, Y. Shoji, and H. Ogawa, "Millimeter-wave fiber-fed wireless access system based on dense wavelength-division-multiplexing networks," *IEEE Trans. Microwave Theory Technol.* 56, 232-241 (2008).
- [11] T. Sakamoto, T. Kawanishi, and M. Izutsu, "Continuous-phase frequency-shift keying with external modulation," *IEEE J. Sel. Top. Quantum Electron.* 12, 589–595 (2006).
- [12] W. Shieh, X. Yi, and Y. Tang, "Experimental Demonstration of Transmission of Coherent Optical OFDM Systems," *OFC/NFOEC 2007, OMP2*, March, 2007.
- [13] V. J. Urick, J. X. Qiu, and F. Bucholtz, "Wide-band QAM-over-fiber using phase modulation and interferometric demodulation," *IEEE Photon. Technol. Lett.*, 16, pp.2374-2376, October 2004.
- [14] M. Kavehrad and E. Savov, "Fiber-Optic Transmission of Microwave 64-QAM Signals," *IEEE J. Sel. Areas in Commun.* 8, 1320-1326 (1990).
- [15] Z. Jia, J. Yu, A. Chowdhury, G. Ellinas, and G. K. Chang, "Simultaneous Generation of Independent Wired and Wireless Services Using a Single Modulator in Millimeter-Wave-Band Radio-Over-Fiber Systems", *IEEE Photon. Technol. Lett.*, vol. 19, pp. 1691-1693, 2007.
- [16] Z. Xu, X. Zhang, and J. Yu, "Frequency upconversion of multiple RF signals using optical carrier suppression for radio over fiber downlinks", *Opt. Express*, vol. 15, pp. 16737-16747, 2007.
- [17] Q. Chang, H. Fu, and Y. Su, "A Radio over Fiber System for Simultaneous Generation and Transmission of Multiband Signals", *IEEE Photon. Technol. Lett.*, vol. 20, pp. 181-183, 2008.
- [18] J. L. Corral, J. Marti, and J. M. Fuster, "General Expressions for IM/DD Dispersive Analog Optical Links with External Modulation or Optical Up-Conversion in a Mach-Zender Electrooptical Modulator," *IEEE Trans. Microwave Theory Tech.*, vol. 49, pp. 1968–1976, Oct. 2001.
- [19] J. Park, W. V. Sorin and K. Y. Lau "Elimination of the fiber chromatic dispersion penalty on 1550 nm millimeter-wave optical transmission," *Electron. Lett.*, vol. 33, pp. 512, 1997.

Publications

International journals (SCI journal paper)

1. P. C. Peng, C. T. Lin, **W. J. Jiang**, J. Chen, F. M. Wu, P. T. Shih, and S. Chi, "Improvement of Transmission in Fiber Wireless System Using Semiconductor Laser Amplifier," *IEE Electronics Letters*, vol. 44, no. 4, pp. 298-299, Feb 2008.
2. C. T. Lin, P. T. Shih, J. Chen, P. C. Peng, S. P. Dai, **W. J. Jiang**, W. Q. Xue, and S. Chi, "Cost-Effective Multi-Services Hybrid Access Networks with no Optical Filter at Remote Nodes," *IEEE Photonics Technology Letters*, vol. 20, issue 10, pp. 812-814, May 15, 2008.
3. P. C. Peng, F. M. Wu, C. T. Lin, J. H. Chen, W. C. Kao, P. T. Shih, **W. J. Jiang**, H. C. Kuo, and S. Chi, "40 GHz Phase Shifter based on Semiconductor Laser," *Accepted by IEE Electronics Letters*.
4. Chun-Ting Lin, **Wen-Jr Jiang**, Jason (Jyehong) Chen, Peng-Chun Peng, Er-Zih Wong, and Sien Chi, "Novel Optical Vector Signal Generation with Carrier Suppression and Frequency Multiplication Based on Single-Electrode Mach-Zehnder Modulator," *Accepted by IEEE Photonics Technology Letters*.

International conferences papers

1. Chun-Ting Lin, **Wen- Jr Jiang**, Jason(Jyehong) Chen, Er-Zih Wong, Sheng-Peng Dai, Yu-Min Lin, Po Tsung Shih, Peng-Chun Peng, and Sien Chi, "Experimental Demonstration of Optical 5-Gb/s 16-QAM OFDM Signal Generation and Wavelength Reuse for 1.25-Gbit/s Uplink Signal" *34th European Conference and Exhibition on Optical Communication Conference (ECOC 2008)*, Mo.3.E.1, Brussels, Belgium, September 21-25, 2008.

2. Chun-Ting Lin, Sheng-Peng Dai, Wen- Jr Jiang, Jason(Jyehong) Chen, Yu-Min Lin, Po Tsung Shih, Peng-Chun Peng, and Sien Chi, "Experimental Demonstration of Optical Colorless Direct-Detection OFDM Signals with 16- and 64-QAM Formats beyond 15 Gb/s" *34th European Conference and Exhibition on Optical Communication Conference (ECOC 2008)*, We.1.F.3, Brussels, Belgium, September 21-25, 2008.
3. P. C. Peng, F. M. Wu, W. J. Jiang, C. T. Lin, J. H. Chen, P. T. Shih, W. C. Kao, S. Chi, "Slow Light in Distributed Feedback Laser for All-Optical Inverter" *2008 OSA Slow and Fast Light Topical Meeting (SL 2008)*, JMB29, Boston, Massachusetts, July 13-16, 2008.
4. C. T. Lin, W. J. Jiang, E. Z. Wong, J. Chen, P. T. Shih, P. C. Peng, and S. Chi, "Optical Vector Signal Generation Using Double Sideband with Carrier Suppression and Frequency Multiplication," *IEEE/OSA Conference on Lasers and Electro-Optics (CLEO/QELS 2008)*, CThR5, San Jose, California, May 4-9, 2008.
5. P. C. Peng, F. M. Wu, C. T. Lin, J. Chen, P. T. Shih, W. C. Kao, W. J. Jiang, H. C. Kuo, and S. Chi, "Tunable Slow Light in Quantum Well Vertical-Cavity Surface-Emitting Laser at 40 GHz," *IEEE/OSA Conference on Lasers and Electro-Optics (CLEO/QELS 2008)*, JThA2, San Jose, California, May 4-9, 2008.
6. P. C. Peng, C. T. Lin, W. J. Jiang, J. Chen, P. T. Shih, F. M. Wu, and S. Chi, "Transmission Improvement in Fiber Radio Links Using Semiconductor Laser," *2008 Optical Fiber Communication Conference (OFC 2008)*, JThA68, San Diego, California, Feb. 24-28, 2008.

Local conference papers

1. Wen-Jr Jiang, Peng-Chun Peng, Chun-Ting Lin, Jason (Jyehong) Chen, Po Tsung Shih, Fang-Ming Wu, Sien Chi, "PERFORMANCE IMPROVEMENT IN RADIO-OVER-FIBER SYSTEM BY USING SEMICONDUCTOR LASER AMPLIFIER," BO-043, presented at *OPT2007 (Optics and Photonics Taiwan)*, Nov. 30-Dec.1, 2007, Taichung, Taiwan.

2. Ching-Wei Chen, Wen-Jr Jiang and Ci-Ling Pan, “Phase Retrieval Of Ultrafast Optical Pulses From Interferometric Autocorrelation Measurement By Population-Split Genetic Algorithm (PSGA) ,” C-FR-V2-7, presented at *OPT2005 (Optics and Photonics Taiwan)*, Dec. 9-10, 2005, Tainan, Taiwan.(2005 年光電科技研討會學生論文獎)
3. Wen-Jr Jiang, Ching-Wei Chen , and Ci-Ling Pan, “Pulse Reconstruction From Frequency-Resolved Optical Gating Measurement By Use Of Population-Split Genetic Algorithm (PSGA),” PC-FR2-05, presented at *OPT2005 (Optics and Photonics Taiwan)*, Dec. 9-10, 2005, Tainan, Taiwan.

Patents

1. “一種光調變系統(An Optical Modulation System) ,” 台灣與美國專利申請中

